UNIVERSITÄT ZU LÜBECK

Aus der Klinik für Augenheilkunde
der Universität zu Lübeck
Direktor: Prof. Dr. med. Salvatore Grisanti

Correlation of the SD-OCT staging system for glaucoma severity with intraocular and systemic endothelin-1 concentration and ocular blood flow impairment measured by OCT-angiography

Inauguraldissertation
zur
Erlangung der Doktorwürde
der Universität zu Lübeck
- Aus der Sektion Medizin -

Vorgelegt von
Lasse Schopmeyer
aus Münster

Lübeck 2025

1. Berichterstatter/Berichterstatterin: PD Dr. med. Claudia Lommatzsch

Ko-Betreuer*in: Prof. Dr. med. Harald Langer

2. Berichterstatter/Berichterstatterin: PD Dr. med. Dr. med. dent. Corinna Zimmermann

Tag der mündlichen Prüfung: 29.04.2025

Zum Druck genehmigt. Lübeck, den 30.04.2025

Promotionskommission der Sektion Medizin

Table of Contents

List of abbreviations

Abbreviation	Definition
ACE	Angiotensin-converting-enzyme
ADP	Adenosine diphosphate
AI	Acircularity index
AqH	Aqueous humour
A-scan	Amplitude-scan
ATP	Adenosine triphosphate
AUROC	Area under the receiver operating characteristics
BBB	Blood brain barrier
BRB	Blood retina barrier
BSA	Bovine serum albumin
B-scan	Brightness-scan
CA	Carbonic anhydrase
Ca^{2+}	Calcium ions
cAMP	Cyclic adenosine monophosphate
CBBG	Coomassie brilliant blue G-250
CC	Choriocapillaris
CDI	Colour doppler imaging
CDR	Cup-to-disc ratio
cGMP	Cyclic guanosine monophosphate
CL	PD Dr. med. Claudia Lommatzsch
CNS	Central nervous system
CO_2	Carbon dioxide
COX	Cyclooxygenase
CVA	Cerebrovascular accident
dB	Decibel
dpt	dioptres
DVP	Deep vascular plexus
DVT	Deep vein thrombosis
ECE	Endothelin-converting enzyme
ELISA	Enzyme-linked immunosorbent assay
ET	Endothelin
ET-A-R	Endothelin-A-receptor
ET-B-R	Endothelin-B-receptor
FAZ	Foveal avascular zone
FD-300µm	Foveal density 300µm
FLV	Focal loss volume
FS	Flammer Syndrome
GCC	Ganglion cell complex
GCC	Ganglion cell complex
GLV	Global loss volume
GSS	Glaucoma staging system
GTP	Guanosine triphosphate
H_2CO_3	Carbonic acid
H_2SO_4	Sulfuric acid
HRP	Horseradish peroxidase
ICP	Intracranial pressure
i.e.	Id est
IL	Interleukin

ILM	Internal limiting membrane
IOP	Intraocular pressure
IPL	Inner plexiform layer
IQR	Interquartile range
kPa	Kilopascal
KR	Kai Rothaus
LCS	Lamina cribrosa sclerae
LED	Light emitting diode
LGN	Lateral geniculate nucleus
LogMAR	Logarithm of the minimum angle of resolution visual acuity
KR	Kai Rothaus
LSFG	Laser speckle flowgraphy
MAP	Mean arterial pressure
MD	Mean deviation
MI	Myocardial infarction
MK	Dr. rer. nat. Maren Kasper
ml	Millilitre
mm	Millimetre
mmHg	Millimetre of mercury
MOPP	Mean ocular perfusion pressure
NADPH	Nicotinamide adenine dinucleotide phosphate (reduced form)
Nd:YAG	Neodymium-doped yttrium aluminum garnet
NMDA	N-Methyl-D-Aspartate
NO	Nitric oxide
NTG	Normal tension glaucoma
OBF	Ocular blood flow
OCT	Optical coherence tomography
OCT-A	Optical coherence tomography angiography
OCT-GSS	Optical coherence tomography glaucoma staging system
ONH	Optic nerve head
ONS	Optic nerve subarachnoid space
OPL	Outer plexiform layer
OPP	Ocular perfusion pressure
OR	Odds ratio
PACG	Primary angle-closure glaucoma
$PaCO_2$	Partial pressure of CO_2
PE	Pulmonary embolism
PG	Prostaglandin
pg	Picogram (10−12 grams)
POAG	Primary open-angle glaucoma
PVD	Primary vascular dysregulation syndrome
QALY	Quality-adjusted life years
R^2	Coefficient of determination
RGC	Retinal ganglion cells
RNFL	Retinal nerve fiber layer
ROS	Reactive oxygen species
RPC	Radial peripapillary capillary
RPE	Retinal pigment epithelium
RPM	Rounds per minute
SBP	Systemic blood pressure
SD	Standard deviation
SD-OCT	Spectral domain optical coherence tomography

sGC	Soluble guanylyl cyclase
SQ	Scan quality
SS-OCT	Swept-source optical coherence tomography
SSBP	Systolic systemic blood pressure
SSI	Signal strength index
SVP	Superficial vascular plexus
TD-OCT	Time-domain optical coherence tomography
TE	Trabeculectomy
TM	Trabecular meshwork
TMB	3,3′,5,5′-Tetramethylbenzidine
TNF-α	Tissue necrosis factor alpha
VCDR	Vertical cup-to-disc ratio
VD	Vessel density
α-agonists	α-adrenergic receptor agonists
β-blockers	β-adrenergic receptor blockers
µl	Microlitre

List of figures

List of tables

1. Introduction - Glaucoma

Glaucoma describes a group of heterogenous ocular diseases that all eventually damage the retinal ganglion cells (RGC) and optic nerve head (ONH). If left untreated, the disease causes progressive visual field loss. In the final stage, irreversible blindness may result.

1.1 Epidemiology

Globally, glaucomas present the leading cause of irreversible blindness with a rapidly increasing incidence[2,3]. Of the global population aged between 40 and 80 years, approximately 3.55% are affected by one form of primary glaucoma[2–4]. When separating into the two most prevalent forms of primary glaucoma, globally 3.05% are affected by primary open angle-glaucoma (POAG) and 0.5% are affected by primary angle-closure glaucoma (PACG)[3]. The prevalence of POAG is 36% higher in men than in females (Odds Ratio [OR] 1.36)[3]. Within the ethnic groups the highest prevalence of POAG can be found in people of African ancestry with 5.40% compared to 2.37% and 2.29% in people of European and Asian ancestry respectively[3]. This is believed to be caused by a combination of genetic susceptibility, environmental factors and limited access to early diagnosis and treatment[5].

People of Asian ancestry have the highest incidence of PACG with 1.2%, compared to a prevalence of 0.4% in people of European ancestry. The high prevalence of PACG in Asians is attributed to anatomical variations like a shallow anterior chamber that reduce the drainage angle and therefore lead to occludable angles and iridotrabecular contact[6–8]. Despite the differences in prevalence, the worldwide numbers of bilaterally blind people by POAG and PACG in 2020 were almost identical (5.9 and 5.3 million respectively), illustrating PACG's devastating impact if left untreated[2].

While the global number of people with glaucoma in 2013 was estimated to be around 64.3 million people, it has increased to 76 million in 2020 and is expected to reach 112 million by 2040[3,9]. In 2020, 53 to 66 million of these people had POAG[10]. The POAG prevalence in the United States is currently growing by approximately 28% per decade[11].The sharp increase in numbers can in part be explained by the

increasing life expectancy and the resulting older population as well as population growth, as the global odds ratio (OR) for POAG prevalence was calculated to be 1.73 per 10 years increase in age[3]. In 2010, 10% of people with POAG and 25% of people with PACG were assumed to be blind on both eyes [2]. A significant proportion of POAG patients do not have elevated intraocular pressure (IOP), which is called normal tension glaucoma (NTG)[12].

The prevalence of NTG within the POAG population varies greatly among ethnic groups, with around 30% in the Italian population, 39% in the Dutch population, 30% to 50% in the United States and 57% in the predominantly black South African population[13]. The highest rates of NTG within the POAG patients have consistently been reported in Asia, where on average 76% of all POAG cases have NTG. Japan has reported the highest percentage with up to 92%, followed by 79% to 84% in China, 82% in southern India and 77% in South Korea[4,13,14].

Previous research indicated that only about 10-50% of affected people globally are aware of having glaucoma[15,16]. It is thought that of people who become blind due to glaucoma, one third is not diagnosed at all, one third is not treated properly and one third is non-compliant to therapy[17].

1.2 Socioeconomic Impact

Besides the tremendous impact on the patient's functioning and quality of life, glaucoma also leads to significant socioeconomic impact, that is vastly increasing due to the ageing population and previously mentioned population growth. In the United States, the average annual treatment of POAG was estimated to be approximately €592 for the early defect stage up to €2387 for the end-stage defect stage as classified by the Hodapp-Parrish-Anderson criteria[18]. The treatment costs in the EU and UK appear to be somewhat lower[19]. It is important to realize that these costs are only related to direct healthcare, including medication, possibly surgery, use of medical facilities as well as workforce and administration costs of health care workers. The potentially tremendous financial and economic impact of disability, incapacitation for work and related additional health care expenditures are not included in these numbers. Beside the economic considerations, the effects of progressing glaucomatous damage and loss of vision can lead to declines in

psychological well-being and social isolation, and can contribute to further deterioration of general health, for example by reduction of physical activity[20].

A recent cost-utility analysis based in the United States analysed the socioeconomic effects of adherence to non-adherence to glaucoma medication. It was found that the total healthcare costs for adherent patients, measured from age 40 for 60 years until death or age 100, were approximately €59.000 while the total healthcare costs for non-adherent patients approximated €49.500, while these patients lost an average of 0.34 quality-adjusted life years (QALY), equalling a cost-effectiveness ratio of around €28.500 per gained QALY[21]. The study concluded that the treatment regimens, that often include applying eye drops several times daily, only have a persistently good adherence in around 15% of patients[21]. Considering that the commonly accepted threshold of willingness-to-pay per QALY in western countries ranges from €50.000 to €150.000, it was concluded that there is plenty of room to introduce programs to improve patient adherence[21]. These numbers illustrate the importance of early diagnosis and adequate follow-up of glaucoma.

1.3 Clinical Presentation

1.3.1 Primary open angle glaucoma (POAG)

The most common form of glaucoma, POAG, usually develops slowly progressive and painless over a period of many years[9]. Most patients do not experience symptoms until the disease has far progressed and mostly irreversible damage to about 30-50% of the RGCs has occurred, which is also known as pre-perimetric primary open-angle glaucoma (pre-POAG)[22–24]. The typical visual field defects begin peripherally and are commonly caused by an initial decrease of retinal nerve fiber layer (RNFL) in the inferior quadrant, resulting in visual field loss in the upper hemifield[22,25,26]. The typical area of early defects are arcuate, nasal and paracentral step defects, which are tied to the anatomic course of the nerve fiber bundles from the optic nerve into the peripheral retina, representing separate visual fields (see Figure 1 & 2)[26,27]. Because the inferior-temporal area of the optic nerve is anatomically particularly susceptible to damage, these defects more commonly occur in the superior hemisphere of the visual field. The macula lutea and thereby the visual field center is usually spared in early stages of the disease, limiting defects

to the peripheral vision, further contributing to a delayed diagnosis[25]. Since glaucoma normally does not develop homonymous in both eyes, many defects can initially be compensated by the brain, which can also lead to reduced or absent awareness of the defects. Subjectively, many patients report needing more light to see, experiencing blurry vision and loss of contrast sensitivity[28]. In the further progression of the disease the defects progress centripetally, eventually resulting in tunnel vision and in the worst case causing complete blindness[25].

It should be noted that the retinal nerve fibers do not cross the horizontal raphe in the anatomic course through the lamina cribrosa sclerae (LCS), a mesh-like tissue of collagen fibers that the ganglion cell axons pass while exiting the sclera into the optic nerve. Because of that, the visual field defects usually respect the horizontal midline[9,22]. Visual field defects that early in the disease rather respect the vertical midline of the visual field should therefore rather be suspected to be of central neurologic origin, whereas spread across the horizontal meridian is more commonly seen in late-stage glaucoma[9,27].

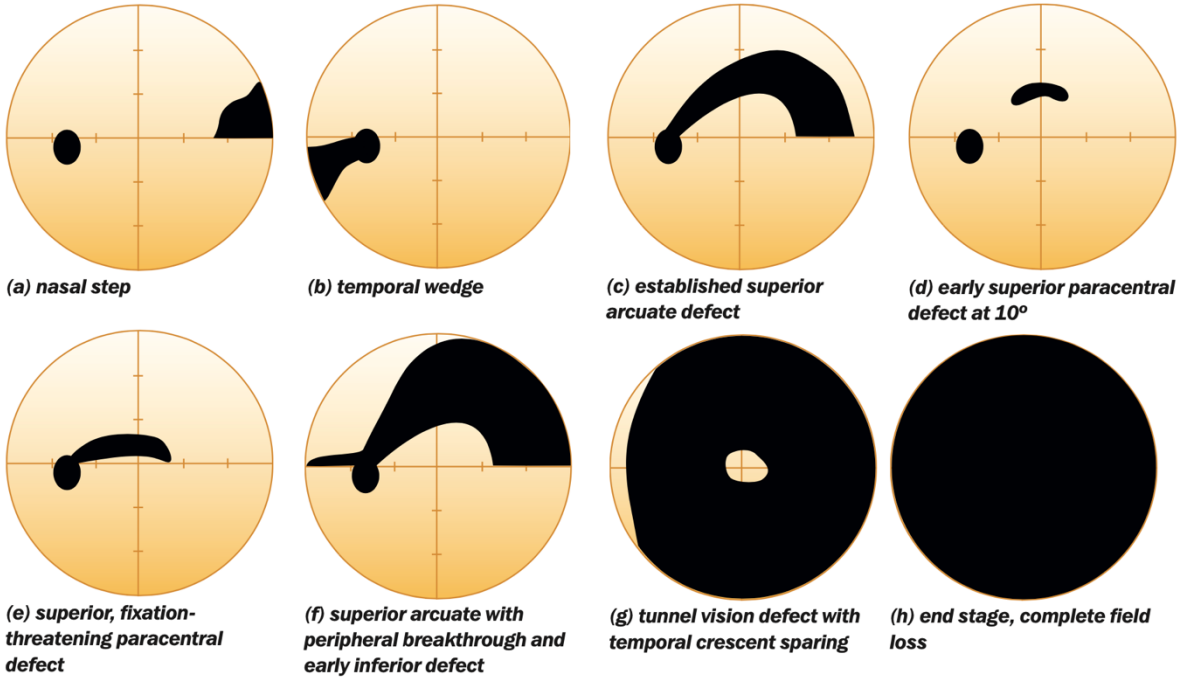

Figure 1 Common progression of glaucomatous field defects in the left eye. Figure adapted from Broadway, 2012, Community Eye Health[26]

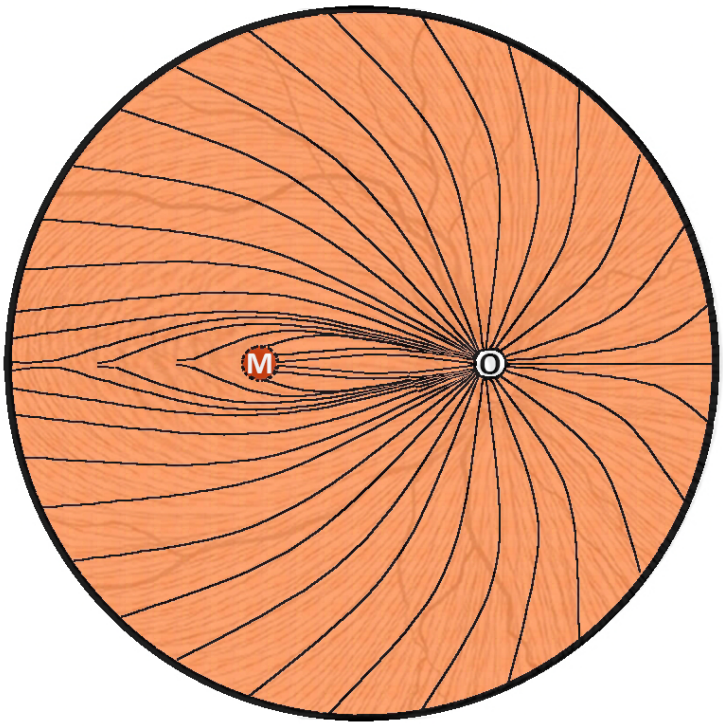

Figure 2 Pattern of retinal nerve fiber anatomy of the right eye. M - Macula, O - Optic nerve head. Figure modified from Nudeldorf, 1998, Creative Commons License

1.3.2 Primary angle-closure glaucoma (PACG)

PACG can present itself chronically and acutely. The acute form of angle closure glaucoma usually presents with severe ocular pain, a red conjunctiva, blurred to severely diminished vision on the affected eye, often accompanied by nausea and vomiting[29]. Clinical examination often reveals conjunctival edema and a mid-dilated, unresponsive pupil and a flat anterior chamber[4]. Gonioscopy reveals partial or complete iridotrabecular contact. IOP often surpasses 40 millimetres of mercury (mmHg), can reach 80 mmHg and higher (normal range per definition 10-21 mmHg) and raises rapidly due to outflow obstruction of the trabecular meshwork (TM)[26,29]. The chronic form develops gradually with a progressive increase in IOP because of initially incomplete or intermittent outflow obstruction and is often painless and silent[29].

1.4 Physiology and Pathophysiology

1.4.1 General

The general pathophysiologic mechanism that eventually leads to loss of vision and blindness is damage of RGCs resulting decrease of the retinal nerve fiber layer (RNFL) and changes of the ONH, which normally ranges from 1.2 millimetres (mm) to 2.0 mm in diameter and is observable during fundoscopy (see chapter diagnosis - 1.5)[24]. The RGCs are a specific type of retinal neuron that transmit visual information generated by the photoreceptors, the rods and cones, via the intermediate amacrine and bipolar cells. RGCs are third order neurons with a long axon that terminate in the visual cortex of the brain and are therefore part of the central nervous system (CNS)[30]. The retinal part of RGCs is not myelinated, whereas the extraocular parts are. The density and number of photoreceptors transmitting input to one RGC varies according to the eccentricity of the eye, meaning that the distance between, as well as the number of receptors that send information to a single RGC, increase towards the peripheral vison. This causes a lower resolution and lower visual acuity peripherally. On average, the retina of each eye contains around 90 to 120 million rods and 4.5 to 6 million cones, connecting to 0.7 to 1.5 million RGCs, resulting in an average ratio of one hundred photoreceptors per RGC, ranging from five in the foveal area up to several thousand in the periphery[31]. Even though the fovea makes up only around 2% of the retinal surface, it contains more than 30% of all RGCs[32]. Currently there are at least 18 different types of RGCs known in humans, which differ in function and morphology[30]. It appears that different types of RGCs transmit separate characteristics of the image to distinct areas within the cerebral visual centers. The different characteristics range from colour, intensity of light, motion to the separate qualities of textures and contrast[30]. The RGCs within the retina are directed towards the optic nerve head (ONH), where they bend, pass the sclera and the LCS, a specialized mesh-like area made by collagen fibers that allow the axons and arteria and vena centralis retinae to pass into the optic nerve (Figure 3). Since the LCS provides less structural stability than the sclera, it easily impresses in states of elevated IOP, leading to shear stress and damage of the traversing RGC axons[9]. Increased IOP can also induce mitochondrial dysfunction leading to metabolic insufficiency and eventually

apoptosis[9]. Progressive loss of RGCs leads to thinning of the RNFL and results in thinning of the neuroretinal rim (NRR) and deepening of the optic disc. The damage to the RGCs is irreversible. Eventually, the LCS also undergoes irreversible structural changes that further impede action potential transmission and retrograde transport of neurotropic factors from the brain, which are essential for survival of the intraocular cell bodies, leading to further deterioration of the RGCs[24] (Figure 3). The LCS is also thinner in all types of glaucoma compared to healthy controls[33]. As the long axons reach into the lateral geniculate nucleus and visual cortex, the loss of cells is not limited to the intraocular parts but takes place along the entire pathway[4]. Typically, the damage is most pronounced in the inferior, followed by the superior quadrants, which becomes clinically obvious in defects in the superior and inferior VF, respectively (Figure 1). Because the RNFL bundles travel in arches that generally do not cross the midline from the fovea towards the ONH (Figure 2), the bundles entering the NRR are particularly thick in the inferior and superior quadrant, making them particularly vulnerable to damage. One possible explanation is differences in the structural composition of the LCS. The pores of the LCS in the usually less affected nasal and temporal quadrants are known to have a smaller diameter and have less connective tissue, probably providing more structural stability against increased IOP than the inferior and superior quadrants[32]. This theory is also commonly known as the mechanical hypothesis of glaucoma pathophysiology[34].

Since significant amounts of POAG patients globally suffer from NTG (see 1.1) and therefore have a per definition normal IOP below 22 mmHg, there must be mechanisms beside elevated IOP that lead to the characteristic glaucomatous damage[4,13,24]. In recent years, numerous other factors that contribute to the pathophysiology of glaucoma have been identified and will be discussed in the following chapters.

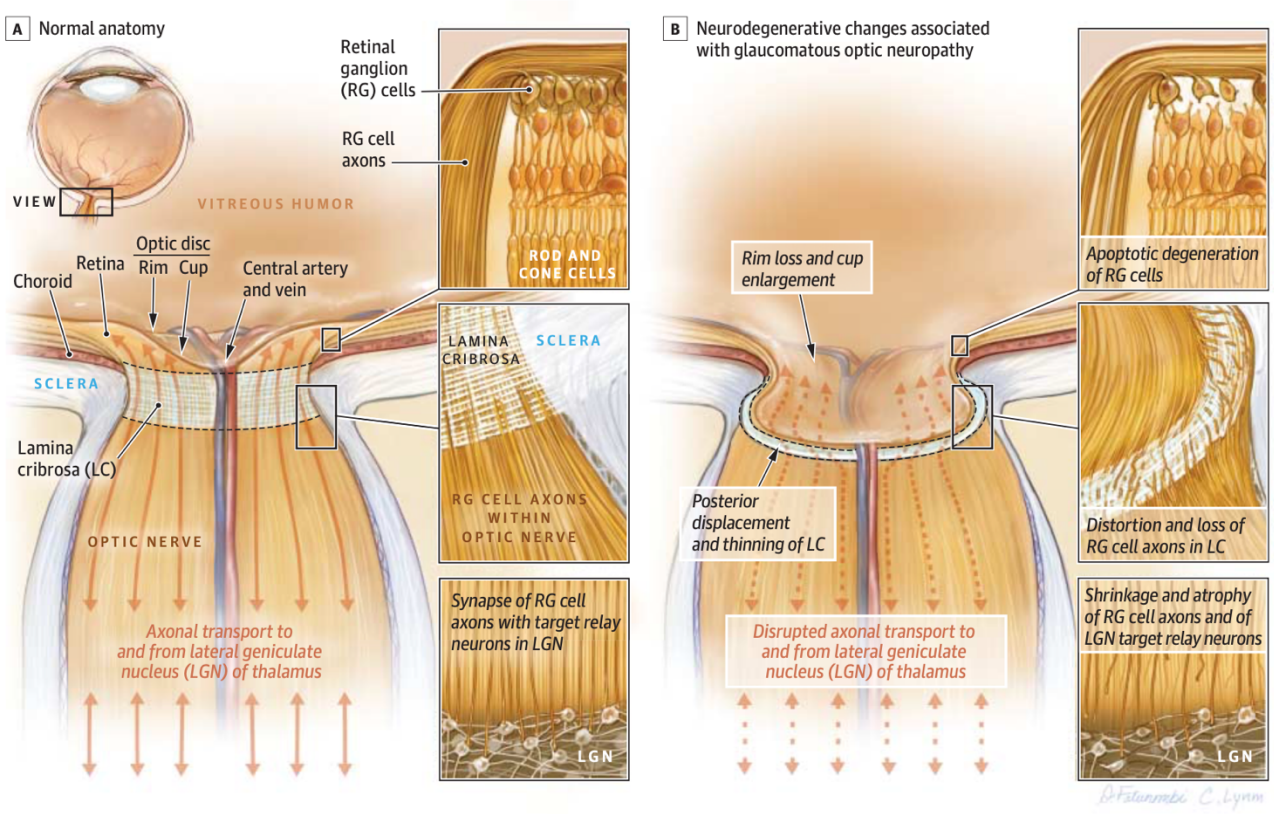

Figure 3 Normal optic nerve head anatomy compared to glaucomatous optic neuropathy. A – Bending of retinal ganglion cells' (RGCs) axons towards optic nerve and lateral geniculate nucleus (LGN) forms neuroretinal ring above optic cup and lamina cribrosa (LC). B – Increased intraocular pressure and other degenerative processes cause posterior LC displacement and impression. Shear stress damages RGCs and supportive cells, causing atrophy and apoptosis. Figure modified from Weinreb et al., 2014, JAMA[23]

1.4.2 Angle Closure Glaucoma

As mentioned in the previous chapter, PACG can present itself acutely and chronically. In both cases there is progressive angle closure, manifested by anterior apposition of the peripheral iris against the TM and cornea of the anterior chamber of the eye[23]. The TM lies in the angle that is formed anteriorly of the iris before the beginning of the cornea. It consists of a spongy structure that drains the majority (around 80%) of the aqueous humour (AqH) towards Schlemm's canal in order to transport it into the extraocular circulation[35]. When obstructed, the amount of drained AqH decreases. As the production of AqH primarily takes places in the non-pigmented part of the ciliary body, which is located posteriorly of the iris in the posterior chamber of the eye, it takes place mostly independently of the drainage in the TM. The majority of AqH, which is essential for nutrient- and oxygen-supply, as well as waste removal of the avascular lens and cornea, is produced by diffusion of

water from the blood perfusing the ciliary body due to an osmotic gradient generated by active sodium-potassium pumps[36]. A smaller fraction is produced by blood ultrafiltration. It is therefore understandable that reduced drainage with unaltered production leads to an imbalance that eventually causes increased IOP, followed by the characteristic glaucomatous optic neuropathy. Classically, a closure of at least 180° of the angle together with elevated IOP or the presence of peripheral anterior synechiae (development of adhesions of the iris to the TM) during gonioscopy fulfils the diagnosis of primary angle closure. If primary angle closure occurs together with glaucomatous nerve damage of the RGCs, PACG can be diagnosed[37]. As the AqH needs to pass the opening of the pupil to reach to anterior chamber for drainage, there is a continuous flow, leading to a small pressure gradient. If the TM is partly occluded and the IOP begins to raise, the increasing pressure gradient can cause the iris to bow anteriorly in a convex fashion, possibly activating a vicious cycle by blocking even more TM[37]. Besides obstruction of the TM, the bending of the iris can also lead to contact of the iris and the lens at the opening of the pupil, called pupillary block. As previously mentioned, anatomic variations like a shallow anterior chamber can predispose to pupillary block[7]. Secondary angle closure glaucoma (SACG) is caused by other (ophthalmologic) diseases. For example, a rather thick and anteriorly positioned cataract lens can push the iris anteriorly and lead to a pupillary block. Inflammations that result in swelling, growth of epithelial or fibrous tissue, as well as obstruction by blood, pus or tumours are other possible causes.

In acute PACG, the IOP raises quickly and progressively to commonly 40 to 80 mmHg, accompanied by edema of the cornea, a fixed mid-sized pupil, hyperaemia of the conjunctiva, visual disturbances of the affected eye and severe pain and nausea[23]. Acute PACG is an emergency often seen at the emergency room and requires immediate treatment to preserve vision.

1.4.3 Open Angle Glaucoma

In contrast to PACG, in POAG, the angle is not blocked, hence the term open angle glaucoma. Nevertheless, many POAG patients have increased resistance to AqH outflow, leading to a disbalance between production and drainage and raising IOP, eventually leading to loss of RGCs. The pathophysiology of POAG is not entirely

understood, as there appear to be many factors that contribute, and new research is continuously providing new insight into the complex pathophysiology of POAG.

Most of the increased drainage resistance at the TM is thought to be generated close to the endothelial layer of Schlemm's canal (SC), where the AqH drains into before reaching the episcleral blood vessels. The increased resistance is in part thought to be caused by insufficient function of mitochondria in the endothelium of the TM and SC, which are required to supply the energy dependent processes of active AqH drainage[10]. Further structural changes of the epithelium and the extracellular spaces can amplify this effect, such as the progressive reduction in endothelial cells of the TM which occurs in aging. Other factors and theories for elevated IOP in POAG consider the accumulation of microscopic material such as mucopolysaccharides that accumulate at the TM and reduce drainage capacity. Reduced numbers of trabecular pores and giant vacuoles in the endothelium of SC are also thought to contribute[24,38].

Several genes have been identified that are related to an increased incidence of POAG[4].

NTG is sub form of POAG where IOP is consistently below 21 mmHg and more than half of all POAG cases are actually NTG cases[39]. It is evident that several factors beyond IOP contribute to POAG, with particular significance in NTG. However, currently, reducing IOP stands as the sole clinically demonstrated intervention that significantly retards the progression of POAG and can be effectively modulated through medication[4,10,23,24].

Other important contributors of POAG and NTG will be discussed in the following sections.

In POAG, no visible outflow obstruction is observable or identifiable. Secondary open-angle glaucoma (SOAG), on the other hand, refers to OAG in which an identifiable medical condition contributes to the previously described increased drainage resistance. Common forms of SOAG are exfoliation glaucoma (XFG) and pigmentary glaucoma (PG). XFG results from the systemic exfoliation syndrome (XFS) and its specific cause is unknown, yet there is some evidence for a genetic component[40]. In the eye, XFS leads to small white and grey granular protein flakes that are most likely produced by abnormal basement membrane epithelial cells of the lens and other structures. They can, among other locations, accumulate in the

anterior chamber[40,41]. Ophthalmologic examination can detect build-ups in the iridocorneal angle. If the accumulated exfoliative material obstructs the TM, outflow of AqH gets reduced and IOP rises[41,42]. When these findings are concomitant with glaucomatous optic neuropathy, the term used is exfoliative glaucoma (XFG).

In PG, mechanical outflow obstruction at the TM parallels the process observed in XFG. However, in PG, the obstructing substance consists of pigment particles, which are liberated from the iris due to repeated contact between the posterior peripheral iris and the zonular fibers of the lens during accommodation and pupil movement[43]. The dislodged pigment gets transported to the TM by physiologic AqH flow and accumulates, eventually leading to an increase of IOP.

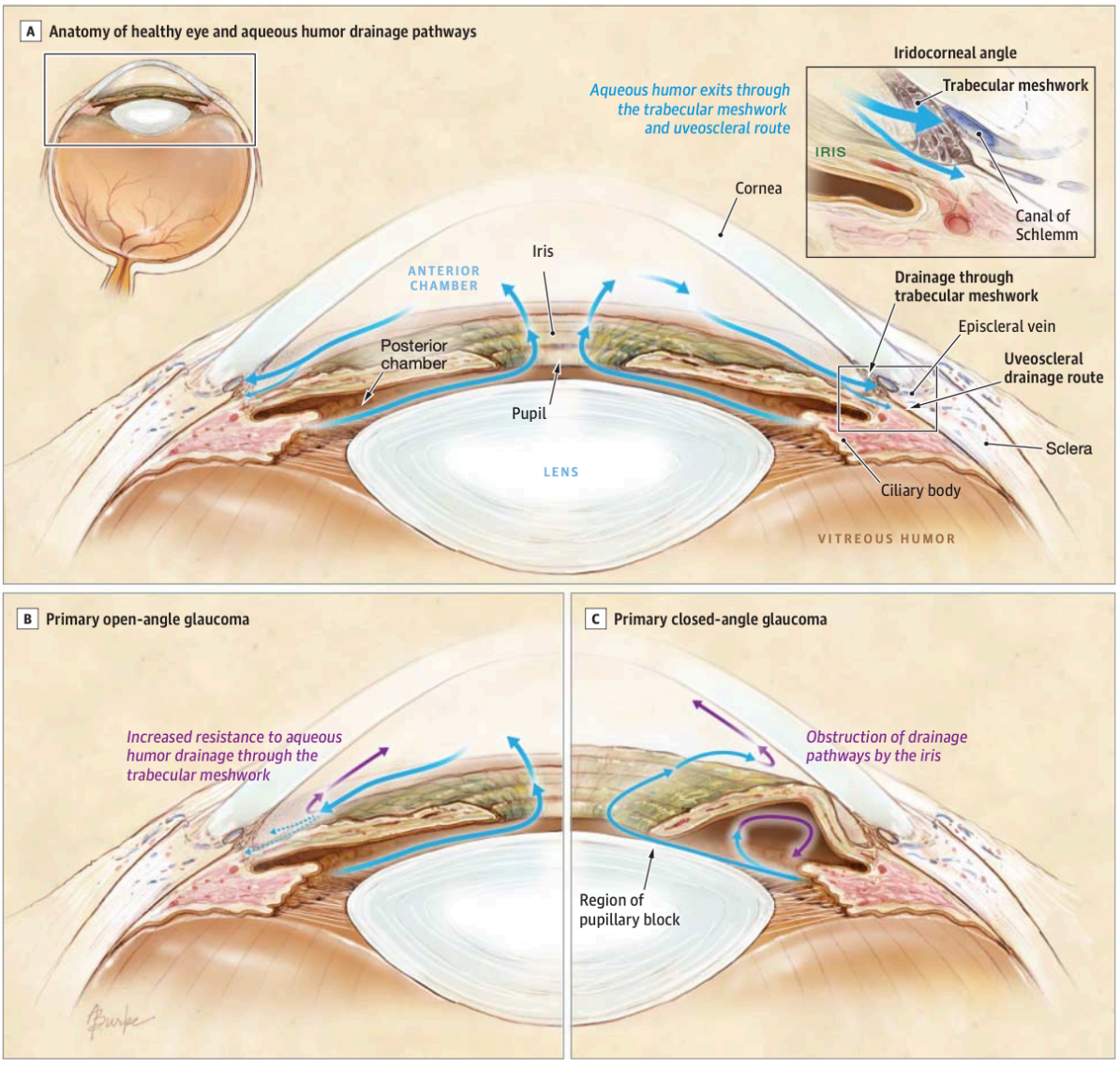

Figure 4 Aqueous Humor (AqH) drainage in healthy eye compared to primary open angle glaucoma (POAG) and primary angle closure glaucoma (PACG). A. – Drainage pathway anatomy of healthy eye, the AqH can drain freely via the trabecular meshwork into Schelmm's canal, production and drainage are in balance. B. – Reduced AqH drainage in POAG, pressure is increasing. C. – Obstruction of trabecular meshwork because of angle closure, pressure is increasing. Figure modified from Weinreb et al., 2014, JAMA[23]

1.4.4 Vascular considerations

The retina and RGCs have a high rate of metabolism and are therefore highly susceptible to ischaemic damage and alterations of blood flow. In fact, the retina exhibits the highest oxygen consumption relative to its weight among all tissues in the human body, highlighting its extreme vulnerability to metabolic injury[44].
The mean ocular perfusion pressure (MOPP) is calculated by multiplying ⅔ with the mean arterial pressure (MAP) and then subtracting the IOP. Because of the complex metabolic demands of the ONH and retina, the ONH perfusion is tightly regulated under normal circumstances.

1.4.4.1 Vascular anatomy

The arterial supply of the eye begins with the arteria ophthalmica, which branches off the arteria carotis interna, following the optic canal[45]. The arteria centralis retinae is the first branch and travels within the nervus opticus, next to the vein into the eye, arriving in the ONH. It supplies the inner 75% of the retina and therefore all RGCs that form the optic nerve and is therefore crucial to vision, occlusion usually leads to blindness. The arteria centralis retinae represents the system of the retinal blood circulation and accounts for approximately 15% of the eye's blood flow[46]. However, there is an anatomical variation in 10-40% of people, called cilioretinal arteries, where parts of the posterior ciliary artery system, which represents the second branch, divert off and supply parts of the retina, often temporally of the optic disc, including the macula and thereby the central vision[47]. The other 85% of blood supply to the eye takes place via the choroidal system[46]. The arteriae ciliares posteriores branch off the arteria ophthalmica and can be divided in short and long arteries which supply the uveal circulation system of the eye. The short arteries pierce the sclera close to the optic nerve and supply the ONH and the proximal choroid, including the outer part of the retina and Bruch's membrane and are therefore also critical for vision. The superficial layer of the ONH however, is supplied by the arteria centralis retinae[46]. Some of the short arteries form an anastomotic ring known as the circle of Zinn-Haller in the ONH region. The ONH is therefore supplied by a combination of the retinal and choroidal systems. The long arteries pierce the sclera close to the optic nerve and travel anteriorly to supply the distal choroid, the iris and

the ciliary body of the iris[45]. More distally, the arteria ophthalmica branches into the medial and lateral muscular branch, supplying the extraocular muscles. From these muscular arteries, the arteriae ciliares anteriores divert anteriorly to supply blood to the conjunctiva, sclera, and iris. This vascular arrangement forms the circulus arteriosus major, also known as the arterial circle of the iris[45].

Within the retinal blood circulation, the retinal capillaries that are formed by the terminal arterioles before going over into the venules can be distinguished into a superficial layer, located close to the RGCs, and a deep layer, close to the inner nuclear layer[48]. Around the fovea, the foveal avascular zone (FAZ, mm^2) lacks vessels and capillaries to facilitate maximally unobscured vision[49]. The vena centralis retinae runs through the nervus opticus parallel to the arteria and drains into the sinus cavernosus[48].

1.4.4.2 Blood Retina Barrier

Similar to the blood brain barrier (BBB), the eye possesses the blood ocular or blood retina barrier (BRB), consisting of a layer of vascular endothelial cells connected by tight junctions, preventing many drugs and substances to pass. The BRB is susceptible to damage and of pathophysiological interest in glaucoma[50]. The inner BRB, lining the intraretinal vessels, is next to the vascular endothelium, supported by different types of cells. The vessels are surrounded by glial cells, which can be grouped into macroglia and microglia[51]. The macroglia consist of astrocytes and Müller cells, which take part in the homeostasis and functionality of the BRB and many metabolic processes. While Müller cells can be found throughout the entire retina, astrocytes are usually confined to the optic nerve and RGCs[48]. The macroglial cells are essential for metabolism and transport of various molecules. For example, they are responsible for the aerobic metabolization of glucose to lactate, which is then released towards the RGCs, to serve as their primary source of energy[51]. The macroglia are also involved in the uptake and enzymatic conversion of extracellular glutamate in order to avoid neurotoxicity for RGCs. They also fulfil important functions in the synthesis of D-serine, an essential cofactor of N-Methyl-D-Aspartate (NMDA) receptor activation by glutamate[51]. Dysfunction of the glial cells has been identified as a contributor in the pathogenesis of glaucoma[51]. The

outer BRB on the other hand is located at the level of retinal pigment epithelium (RPE) and Bruch's membrane. The endothelium of the choroidal vessel is fairly permeable but the tighter Bruch's membrane and mostly the RPE, which are located in between the choroidal vessels and the retinal structures, form the effective outer BRB. The RPE consists of a single layer of tight junction epithelium with specialized transcellular transport systems which facilitate the complex metabolic demands of the retina. Next to transport of nutrients and vitamins from the circulation towards the retina, the RPE is specialized in back-transporting metabolites and extracellular fluid that is generated during aerobic metabolization. It also organizes the daily phagocytosis and removal of shed outer segments of photoreceptors, which is necessary for their survival[44].

Under normal circumstances the BRB should not allow circulating immune cells to enter. It has however been demonstrated that circulating T cells are involved in RGC degeneration in glaucoma with elevated IOP, suggesting that the BRB can be directly damaged by increased IOP[50]. However, an intact BRB is essential for the delicate metabolism and homeostasis of the RGCs. Common risk factors for glaucoma like aging, hyper- as well as hypotension and diabetes mellitus and diabetic retinopathy lead to breakdown of the BRB. Nevertheless, the exact pathophysiology of BRB breakdown in glaucoma and its clinical importance, for example whether BRB occurs secondary to RGC damage and resulting inflammatory processes or whether it is the primary starting point that facilitates the RGC decline, remain largely unknown at this point of time[50]. As an exemption, the capillaries of ONH region appear to be lacking a functional BRB, while all other parts of the retina, under normal circumstances, are protected by the BRB[46]. Additionally, because of the previously mentioned combination of retinal and choroidal blood flow in the ONH, the rather fenestrated characteristics of the choroidal capillaries facilitate the diffusion of various molecules in the ONH[52]. This makes the ONH region of special interest for the pathophysiology of glaucoma. Compared to the BBB, the endothelial cells of the BRB contain lower levels of the enzyme superoxide dismutase, which is essential for the breakdown of superoxide radicals that occur during oxygen metabolism[48]. This renders the BRB and thereby the retina and RGCs more sensitive to oxidative damage, highlighting the importance of a constant and controlled blood supply.

1.4.4.3 Autoregulation

Like the cerebral autoregulation of blood flow, the eye is known to autoregulate the retinal and optic nerve blood flow independent of systemic blood pressure (SBP) and adapted to the complex metabolic demands of the eye[53]. Most of the autoregulatory mechanics take place via changes in retinal vascular resistance. The pressure-flow autoregulatory system can react well to changes in systemic blood pressure, allowing the ocular perfusion pressure (OPP) to remain within tight limits. If the MAP decreases or increases within MAP limits between 60 to 150 mmHg, the smooth muscle cells in the retinal vasculature will dilate or constrict, respectively. For example, stretch of the mentioned smooth muscle cells leads to activation of specific channels that eventually result in the influx of calcium ions (Ca^{2+}), causing constriction of muscle cells. Next to the vascular smooth muscle cells, the retinal capillaries and venules are rich in pericytes below the endothelial layer and embedded in the basement membrane. These pericytes also fulfil essential tasks in myogenic autoregulation as they contain contractile smooth muscle actin and myosin[48]. Moreover, the pericytes express various receptors for metabolic vasoactive substances, as will be discussed below. It is thought that after autoregulation mechanisms, about 5% of systolic systemic blood pressure (SSBP) variation are reflected in IOP changes, estimating that each SSBP increment of 10 mmHg explains 0.3 – 0.5 mmHg increase in IOP[54].

Elevated IOP is known to severely disturb correct functioning of autoregulation, possibly leading to reduced ocular blood flow (OBF) and resulting ischemic damage of retinal cells[53,55]. Although atherosclerosis in optic and retinal blood vessel is, especially in the aging population, known to be a risk factor contributing to glaucoma, it seems that disturbed autoregulation and insufficient blood supply is the main problem within the vascular theory of glaucoma pathophysiology[46]. The blood circulation of the choroidal vessels is sympathetically innervated and its blood flow therefore responsive to the autonomic nervous system, next to known autoregulatory substances. However, the retinal and ONH vascular system is not innervated[55]. Besides the previously described mechanical autoregulation mechanisms, there are various compounds known to be involved in the retinal and choroidal autoregulation.

1.4.4.4 Metabolic blood flow mediators

One of the strongest metabolic vasomotor mediators is carbon dioxide (CO_2). It acts indirectly via the acidity of the blood, causing increased concentrations of hydrogen ions with a lower pH, which intracellularly leads to a reduction of Ca^{2+} and vasodilatation[56]. To a lesser extent, the vasoactive functions of the partial pressure of CO_2 ($PaCO_2$) are also mediated by nitric oxide (NO) and adenosine pathways[53]. In endothelial cells, NO is synthesized by NO synthase enzymes from L-arginine and oxygen, with the help of nicotinamide adenine dinucleotide phosphate (NADPH, reduced form)[57]. NO works on smooth muscle tone by diffusing into the cell and activating the enzyme soluble guanylyl cyclase (sGC), which causes increased formation of cyclic guanosine monophosphate (cGMP) by conversion of guanosine triphosphate (GTP)[58]. cGMP in turn activates certain calcium channels in the vascular muscle cell, causing Ca^{2+} to leave the cell, resulting in vasodilatation[58]. NO is very short-lived with a half-life of less than 15 seconds and is quickly metabolized to nitrite and nitrate[58].

Hypercapnia with increased acidity (hydrogen ion concentration) therefore leads to retinal vasodilation and can, above certain thresholds, even overrule the mechanical autoregulation mechanisms. For cerebral autoregulation of patients under general anaesthesia the limit for overruling was found to be approximately above 60 mmHg (8 kilopascal [kPa]) $PaCO_2$[59]. The arterial oxygen (PaO_2) level is also known to impact the cerebral and retinal autoregulation, however these effects usually only become apparent once PaO_2 falls below 50 mmHg (6,6 kPa). Once this threshold is passed, the effects of hypoxia on the autoregulation can be very potent, reaching up to a four-fold increase in resting cerebral and ocular blood flow[60]. As PaO_2 does not significantly influence the pH, this mechanism is facilitated by opening of potassium channels in the arteriole's smooth muscle cells due to a hypoxic adenosine triphosphate (ATP) breakdown to adenosine diphosphate (ADP) and others because of the inability to perform sufficient oxidative phosphorylation to maintain the ATP levels. This leads to opening of specific ATP/ADP-sensitive potassium channels and subsequent efflux of potassium out of the cell, resulting in hyperpolarization and reduced intracellular Ca^{2+}, ultimately causing vasodilatation[60]. As a secondary effect of hypoxia and low PaO_2, NO is increasingly released, leading to further vasodilatation.

Other endothelium-derived and metabolic vasoactive substances in the process of autoregulation have been identified. For example, increased levels of extracellular lactate have also been shown to cause vasodilatation in hypoxic conditions. The prostaglandins are a group of lipid compounds of physiological importance in the vascular autoregulation and are synthesized from arachidonic acid by cyclooxygenases 1 and 2 (COX-1 and COX-2). Prostacyclin, also known as prostaglandin I2 (PGI2), is the most important endothelium-derived prostaglandin. Via its own G-protein coupled receptor it upregulates the second messenger cyclic adenosine monophosphate (cAMP) as well as the earlier described cGMP pathway and thereby activates channels to lower the intracellular Ca^{2+}, resulting in dilatation[61]. It also possesses platelet inhibitory and pro-inflammatory functions. Other prostaglandins, like prostaglandin H2 (PGH2), which acts a precursor for several further prostaglandins, exhibit dose dependent, mostly vasodilatory vascular effects. Besides the vascular effects, prostaglandins produce various effects throughout the human body. Of specific interest in glaucoma are prostaglandins of the F2 group. They increase the AqH outflow via the uveoscleral pathway, which occurs independently of the TM and usually comprises a significantly smaller fraction of total AqH drainge[62]. This route encompasses drainage via the sclera, choroidal vessels, ciliary muscles and the subarachnoid space. This happens in part by relaxation of ciliary muscle cells and the stimulation of the production matrix metalloproteinases in the ciliary muscle, leading to subsequent extracellular matrix remodelling and loosening, allowing faster AqH drainage[62].

1.4.4.5 Endothelin

Since their discovery, endothelin (ET) peptides consisting of 21 amino acids, have received increasing attention in ocular autoregulation and specifically the pathogenesis of glaucoma. The three isoforms ET-1, -2 and -3 are known, with ET-1 being the most prevalent and most studied in mammals[63,64]. ET-1 has been shown to be the most potent human vasoconstrictor known[65].

Most of the ET-1 is produced by endothelial cells, and to a lesser extent by cardiomyocytes, macrophages, leukocytes, mast cells, neurons, the renal medulla, airway epithelium and vascular smooth muscles cells themselves[61,63].

During the synthesis of ET-1, after transcription of the according gene, the precursor protein pre-pro ET-1 is synthesized. A furin-type convertase then cleaves the protein, resulting in the direct, but inactive precursor of ET-1, Big ET-1[64,66]. In a final step, Big ET-1 is cleaved by endothelin-converting enzyme (ECE) into active ET-1, resulting in a more than 140-fold increased vasoconstrictive potency of ET-1 compared to the precursor Big ET-1[67]. Because of the high biologic activity of ET-1, it is known to be quickly cleared out of the systemic and local circulation[66,68]. Big ET-1 appears to be resistant to proteolytic cleavage by enzymes other than ECE[64]. It is known that Big ET-1 remains in the tissue and circulation for a longer period than ET-1 and is therefore thought to be measurable for a longer period. Therefore, Big ET-1 is increasingly seen as an important substance of ET-1 research[66,69].

One of the active sites of ET-1 is the G-protein coupled ET-A-receptor (ET-A-R), which is abundant in vascular smooth muscle cells as well as cardiomyocytes, and causes vasoconstriction upon activation via the following cascade.

The transmembrane receptor binds to the agonist, in this case ET-1, and activates the intracellular production of the second messengers inositol 1,4,5-triphosphat and diacylglycerol. This activates specific calcium channels that cause a Ca^{2+} release from the sarcoplasmic reticulum into the cell, as well as an influx of extracellular Ca^{2+} into the cell, leading to vasoconstriction[61].

On the other hand, activation of ET-B-receptor (ET-B-R) appears to partly counteract some of the effects of ET-A-R and supports clearance of ET-1 to avoid ET-A-R overstimulation. ET-B-R activation causes a certain degree of vasodilatation via a NO pathway and G-protein coupled prostacyclin release, while another subtype of ET-B-R was found to result in vasoconstriction of vascular smooth muscle. In contrast to ET-A-R, which is mainly located on the vascular smooth muscle cells, ET-B-R is mostly present in endothelial cells, which are also the main producer of ET-1. When bound to ET-B-R, ET-1 is endocytosed and eventually degraded by lysosomes[61]. One of the chronic effects of ET-A-R activation are induction of vascular smooth muscle proliferation[61].

The ET receptors can, next to the mentioned vascular cells, be found in many tissues, including neurons, heart, liver, kidneys and lungs. ET-1 has been shown to be involved in different diseases like essential hypertension and pulmonary hypertension but also in glaucoma.

Recently, the interest in ET-1 as important influencer of glaucoma has increased. Several studies have found elevated plasma ET-1 levels in patients with various stages of POAG, many of whom present with normal IOP, possibly identifying another important risk factor besides IOP[70]. In patients with stable POAG without recent visual field deterioration, plasma ET-1 tended to be lower[71]. Various animal models have demonstrated that local application of ET-1 to the anterior optic nerve vasculature induces an optic neuropathy resembling that observed in glaucoma, independent of elevated IOP[72,73]. It has also been shown that glaucoma leads to overexpression of ET-A-R and ET-B-R, thereby promoting cell death[74].

POAG patients appear to respond differently to ET-A-R antagonism. Studies have shown less pronounced vasodilatory effects after administration of ET-A-R antagonists in POAG patients compared to healthy controls. It is hypothesized that, in these patients, ET-B-R-mediated vasodilatory effects due to NO release are reduced[75].

Several studies have indicated that elevated ET-1 levels in glaucoma, as well as in other diseases such as diabetic retinopathy, are associated with reduced ocular blood flow (OBF), as measured by various, generally low-resolution imaging techniques, such as colour Doppler imaging (CDI).

A newer imaging technique, optical coherence tomography angiography (OCT-A), is a further development of optical coherence tomography (OCT) and enables detailed visualization of retinal vessel density (VD) (see chapter 1.5.1). Several studies have shown that VD, as measured by OCT-A, is reduced around the optic disc and macula in glaucomatous eyes[76,77].

Additionally, increasing evidence suggests that VD changes in glaucoma can be detected earlier than RNFL changes as measured by OCT, highlighting OCT-A as a promising tool for early glaucoma diagnosis [78].

To date, no studies have investigated the effects of ET-1 levels on retinal VD as assessed by OCT-A [66,68].

1.4.4.6 Systemic blood pressure

It has been found that a low systolic OPP (SOPP) of below 98 mmHg doubled the risk for development of POAG, while a mean OPP of below 40 mmHg even caused

a 2.5-fold increase in risk[79]. Likewise, another study determined that the progression of POAG occurred almost 1.5-fold faster when the SOPP was below 125 mmHg[54]. These findings also illustrate how for example treatment of systemic hypertension, which commonly occurs in the ageing population, can possibly have detrimental effects on the onset and progression of glaucoma. Lowering of the MAP by means of antihypertensives does not lower the IOP and therefore leads to a reduced OPP, despite autoregulatory adaptions. It appears that chronic systemic hypertension can lead to thickening of the retinal vascular smooth muscle cells because of chronic adaptive constriction. If the SBP is following artificially lowered by medications, the adapted retinal smooth muscle cells lose some of their ability to dilate and thereby to increase the OPP. Also, it seems that idiopathic systemic hypotension elevates glaucoma risk for the same reasons[33].

It has further been postulated that especially temporal spikes and dips in OPP like for example during sleeping, are detrimental for RGCs because of temporary ischemia followed by oxidative stress due to reperfusion injury[46]. Therefore, not only permanently reduced OBF contributes to the development of POAG but also temporary OBF fluctuations, which might be even more difficult to register and to monitor. Concluding, dysfunctions of the autoregulatory and vascular systems have been proven to be important contributors to the development and progression of POAG, particularly NTG.

1.4.5 Intracranial Pressure

Another factor in the pathogenesis of POAG is intracranial pressure (ICP)[33]. As mentioned earlier, the LCS is the mesh-like collagenous structure at the ONH where the axons of the RGCs pass through into the nervus opticus towards the brain and is impermeable to the vitreous body as well as cerebrospinal fluid (CSF) (see 1.4.1). CSF is present on the other side of the LCS, surrounding the optic nerve, being part of the CNS, filling the so-called optic nerve subarachnoid space (ONS), towards the subarachnoid space of the brain. On the inside of the eye the pressure is the IOP, while the pressure on the other side is the ICP. As the normal range for ICP (5 – 15 mmHg) is below the normal IOP range (10 – 21 mmHg), it becomes apparent that a pressure gradient exists because of the impermeability[80].

There is some evidence that the ICP in the ONS is not always equal to the actual cerebral ICP because of septa within the ONS that can influence the flow of CSF. This appears to be the case if the ICP drops below 3 mmHg, because the orbital pressure of 3 mmHg collapses the ONS and prevents further CSF drainage. This is for example the case when a person stands up from a supine position, leading to an ICP fluctuation and decrease of up to – 10 mmHg at eye level, as the CSF displaces vertically within the subarachnoid space due to gravity[33]. However, the IOP only drops by a maximum of 4 mmHg, illustrating the pressure gradient that builds up at the LCS[33]. It is also obvious that elevated IOP, which occurs in many glaucoma patients, further increases the pressure gradient at the fragile LCS. The same previously explained mechanism, which leads to damage of RGC axons due to shear stress at the LCS, can therefore also be elicited by changes in ICP. Especially a low ICP eventually leads to more outward deformation of the LCS and increased mechanical stress on the axons. Several studies have shown lower ICP in glaucoma patients than in healthy controls. Particularly in NTG patients, a lower ICP was found than in POAG patients with elevated IOP, suggesting a possible risk factor for the pathogenesis of NTG[33]. Additional studies have shown a lower blood flow of the arteria centralis retinae at the level of the ONH when the ICP was lower than 8 mmHg[33].

1.5 Diagnosis and Imaging

Traditionally, it was thought that glaucoma is inevitably connected to elevated IOP. It has however been shown that many POAG patients suffer from NTG with a normal IOP and that many treated POAG patients exhibit disease progression even when their IOP remains within the normal range because of medication.

It has become evident that IOP monitoring has limitations in detecting glaucoma progression[4,24]. Nevertheless, monitoring of IOP, usually done with the Goldmann applanation tonometer, remains important in the diagnosis and follow-up of glaucoma. Static, computer-assisted visual field measurement (perimetry) is still considered the diagnostic gold standard today, despite its test-retest variability[81]. This involves testing the light difference sensitivity at different retinal locations with an achromatic stimulus. The functional parameters derived from this psychophysical

examination exhibit limitations due to their reliance on subjective factors such as patient attention, motivation, and reaction speed. As mentioned previously, it is assumed that 30% to 50% of RGCs have already been irreversibly lost before changes in perimetry can be detected[22–24]. Therefore, it appears obvious that neither IOP measurement nor perimetry analysis are the ideal tools for early and reliable detection of glaucoma related changes. Consequently, it is crucial to prioritize diagnostic tools capable of early disease detection, as they can facilitate earlier initiation of therapy, potentially slowing down or halting further disease progression. The most important physical examinations in the early diagnosis of glaucoma as well as follow-up examinations are inspection of the ONH and the RNFL. The ONH, also known as optic disc or the blind spot, is traditionally assessed with ophthalmoscopy but can also be analysed with newer imaging techniques like OCT (see chapter 1.5.1). During ophthalmoscopy it appears as yellow area medially of the fovea with the arteria centralis retinae entering the eye through its center. The optic cup is the central excavation within the ONH and usually appears brighter than the region outside of the ONH[82]. Compared to a normal ONH, where a cup-to-disc ratio (CDR) of one to three is considered to be normal, the glaucomatous ONH shows progressive enlargement and excavation of the optic cup. Under normal circumstances the NRR follows the ISNT rule, saying that the thickness of the NRR gradually decreases from inferior to superior to nasal to temporal (inferior ≥ superior ≥ nasal ≥ temporal)[83]. In glaucoma, the ISNT rule is commonly violated, especially in the inferior and superior poles [83]. Typically, a larger vertical CDR than horizontal CDR, can be observed in glaucoma, whereas the horizontal ratio is usually greater in healthy eyes[4,22–24,83]. This corresponds to the glaucomatous visual field defects that are often initially observed in supero- and infero-temporal areas of the ONH. A CDR above 0.6 is only found in around 5% of individuals without glaucoma[83]. Additionally, an CDR asymmetry greater than 0.2 between the two eyes is very uncommon and should raise suspicion, as glaucoma usually does not develop symmetrically in both eyes. Because of the optic disc cupping and excavation, the arteries originating from the retinal artery can shift nasally and appear somewhat kinked, also called bayonetting. Simultaneously, optic disc haemorrhages or splinter haemorrhages, which are detectable during funduscopy, may arise[83]. However, this examination has a large observer variance[84].

1.5.1 Optic coherence tomography (OCT) & OCT-Angiography (OCT-A)

OCT is a non-invasive imaging technology that was first clinically introduced in 1996, but only started its revolutionary implementation as a standard of care for retinal pathology in ophthalmology in 2006[85]. OCT allows to create two- and three-dimensional high-resolution images of the retina up to a depth of approximately three mm. Due to its high resolution, the different layers of the retina, including the RNFL and ganglion cell complex (GCC) can be visualized and measured, making it the ideal tool for early diagnosis and follow up of glaucoma. In ophthalmology, infrared light with wavelengths of 800 to 1400 nm is commonly used[86]. The technology makes use of inferometry to measure and visualize the different structures of the retina. The infrared light with a short coherence length is split up, where one part is directed towards the tissue, in this case the retina, and measures the properties of the reflected light waves. The other part is directed towards a reference track with a predefined length. The reflections returning to the highly sensitive sensors on both arms are subsequently analysed and compared using interferometry. Interferometry involves examining the phase differences resulting from the overlapping of reflected light waves[85]. Software then calculates depths and distances and translates the measurements into an image. Like in ultrasonography, amplitude-scans (A-scans) are one dimensional, measuring along the axis of a single point. Multiple A-scans, scanned laterally along the beam of the OCT device, create a two-dimensional, cross-sectional scan (Brightness-scan - B-scan) of the retina. Several successive B-scans along the desired scanning area, which are usually defined regions like the macula or the optic disc, allow to generate 3-dimensional (3D) images of the entire study area (Composition-scans).

Early OCT versions like the time-domain OCT (TD-OCT) were slow and therefore resulted in a lower image resolution and artifacts because of involuntary eye movement. The more recent and widely distributed further development is the spectral domain OCT (SD-OCT), which mostly overcomes these problems. Previously, mechanical adjustments of the reference arm length were required in earlier versions to achieve the desired depth range for each scan, allowing for interference checks. However, SD-OCT employs a spectrometer and a super-luminescent diode with a wavelength of 840 nm. This configuration spatially separates the distinct wavelengths of the detected signal, enabling simultaneous

signal collection across the entire depth range[87]. The by the spectrometer separated wavelengths can be processed by the Fourier transformation without adjustment of the reference arm[87]. Therefore, SD-OCT allows to conduct significantly more scans, up to 70.000 per second, as compared to around 400 scans per second with TD-OCT, resulting in a higher resolution and less distortion due to eye movement[85].
Most SD-OCT systems nowadays are capable of scanning an area of at least 6 mm x 6 mm with a depth of at least 2 mm, and axial in-tissue resolution of at least 5 µm axially and 20 µm laterally[86].
A more recent development is the swept-source OCT (SS-OCT). Partly due to its high price it is not yet widely implemented. SS-OCT uses a tuneable laser which divides the spectrum of the light during measuring and therefore makes the spectrometer redundant. The technology uses a longer wavelength of 1060nm that allows a deeper penetration and can clearly visualize deeper structures like the vasculature of the choroid or the RPE, as well as the vitreous body[88]. Due to the tuneable laser technology, even higher scanning speeds of up to twice the speed of SD-OCT are available[86].
The increased speed, resolution and field of view have allowed to eventually expand the imaging from imaging stationary anatomic structures to the ocular vasculature and the flow of blood within. This technology is called OCT-angiography (OCT-A) and has first been clinically used in 2014[85]. Using the high speed of modern SD-OCT and SS-OCT machines, OCT-A performs numerous sequential B-scans of exactly the same area during a predefined short amount of time. Due to the motion of blood and its contents such as erythrocytes, the reflected signals along even very small capillaries vary in the passage of time because differently positioned erythrocytes produce different backscattering signals that are detected in the OCT-A machine[89]. Since the stationary structure's signal remains unchanged, specialized software can calculate and visualize the pathways of different sizes of ocular blood vessels, up to very small capillaries and areas of neovascularization. OCT-A thereby provides a powerful new tool for assessment of the retinal microvasculature and perfusion in many retinal diseases, including glaucoma[86,89].
OCT-A scans usually differentiate between the superficial and deep vascular plexus and sometimes also the outer retina and choroid layer and are in state of measuring the retinal VD[89].

1.5.2 Glaucoma Staging Systems

Several tools and formulas for the classification and grading of glaucoma have been developed.

One of the first widely used methods was proposed by Aulhorn et al. in 1977 and evaluated visual field defects as registered with a manual Tübingen perimeter. The registered defects are then compared with a large sample of glaucoma patients, allocating patients to one of five severity stages[90].

A method that is still commonly used nowadays are the Hodapp-Parrish-Anderson (H-P-A) criteria, that were introduced in 1993[91]. Using standard automated perimetry, considered the gold standard for evaluating a patient's visual field, the mean deviation (MD) is quantified. MD represents the deviation of all measured illuminated visual field points in each eye when compared to a reference database of healthy subjects of similar age and ethnicity. Typically, MD values fall within the range of -30 decibels (dB) to +2 dB. Together with the number of defects within Humphrey's Statpac-2 pattern deviation probability map, the overall extent of damage of the entire visual field is calculated[90,92]. Additionally, the defect proximity to the fixation point is used as a criterion. Based on these criteria, the system classifies the glaucomatous damage within early, moderate and severe defects[92]. Disadvantages are the broad stages, the need for accurate and time-consuming analyses of every perimetry test and the lack of the specification of the location of the glaucomatous damage[91].

In 1996, Brusini et al. introduced the Glaucoma Staging System (GSS)[93]. The GSS also uses standard automated perimetry. Firstly, the mean deviation of the patient's visual field is compared to a healthy reference. Secondly, the pattern standard deviation assesses the variations in individually measured sensitivity values at each point within the visual field. This metric enables the identification of highly irregular and localized visual field defects, which are frequently observed in glaucoma cases[93]. These values are then, individually for each eye, filled into a specialized diagram on the X and Y axis. The intersection of both axes identifies the disease stage within six stages, where stage zero is a normal visual field and stage five stands for very small remnants of visual sensitivity. Additionally, it subdivides each result into either generalized field defects, mixed effects or localized effects[90,93]. Several studies have confirmed the GSS as accurate and easy to use tool,

explaining its quick implementation as one of the most used glaucoma staging and follow-up tools. Because of several limitations, an updated version, the Enhanced Glaucoma Staging System (GSS 2) was introduced in 2006[90,94]. It introduced a seventh stage, namely the borderline stage between stage zero and one, in order to avoid the abrupt differentiation between normal visual field and early defects and to refine the important area of early diagnosis[94]. It also defined clear mathematical formulas for the calculation, allowing the system to be used in computer software instead of exclusively on paper.

As mentioned earlier, the OCT has become the most common technique in visualizing glaucomatous damage to the retina and is superior in identifying early damage as compared to perimetry. In response to this development, Brusini et al. introduced the OCT Glaucoma Staging System (OCT-GSS) in 2018[95]. The OCT-GSS was designed and validated to classify within the same stages as the GSS 2, with a subdivision into superior, diffuse and inferior defects, but based on SD-OCT derived measurements (Figure 5). As mentioned earlier, the superior and inferior quadrant appear to be most commonly affected in glaucoma. The formulas of the OCT-GSS consider the physiological age related RNFL thickness decrease and use the average superior quadrant thickness on the X-axis, while using the average inferior quadrant thickness on the Y-axis.

Validation tests resulted in a sensitivity of 95% and specificity of 92% in differentiating between normal and glaucomatous (Borderline – Stage 5) eyes and thereby performs better than the GSS 2 based on perimetry[95]. Because the different SD-OCT machines produce slightly different images and have specific normal reference ranges for each retinal layer that have been defined by the manufacturer, it is impossible to directly compare RNFL thickness values of different SD-OCT machines. Brusini et al. therefore created an online tool for the OCT-GSS that, when entering the measurements and the used device, automatically corrects the RNFL thickness values for correct use within the OCT-GSS, based on the manufacturer's reference data[95]. This makes the OCT-GSS simple and quick to use.

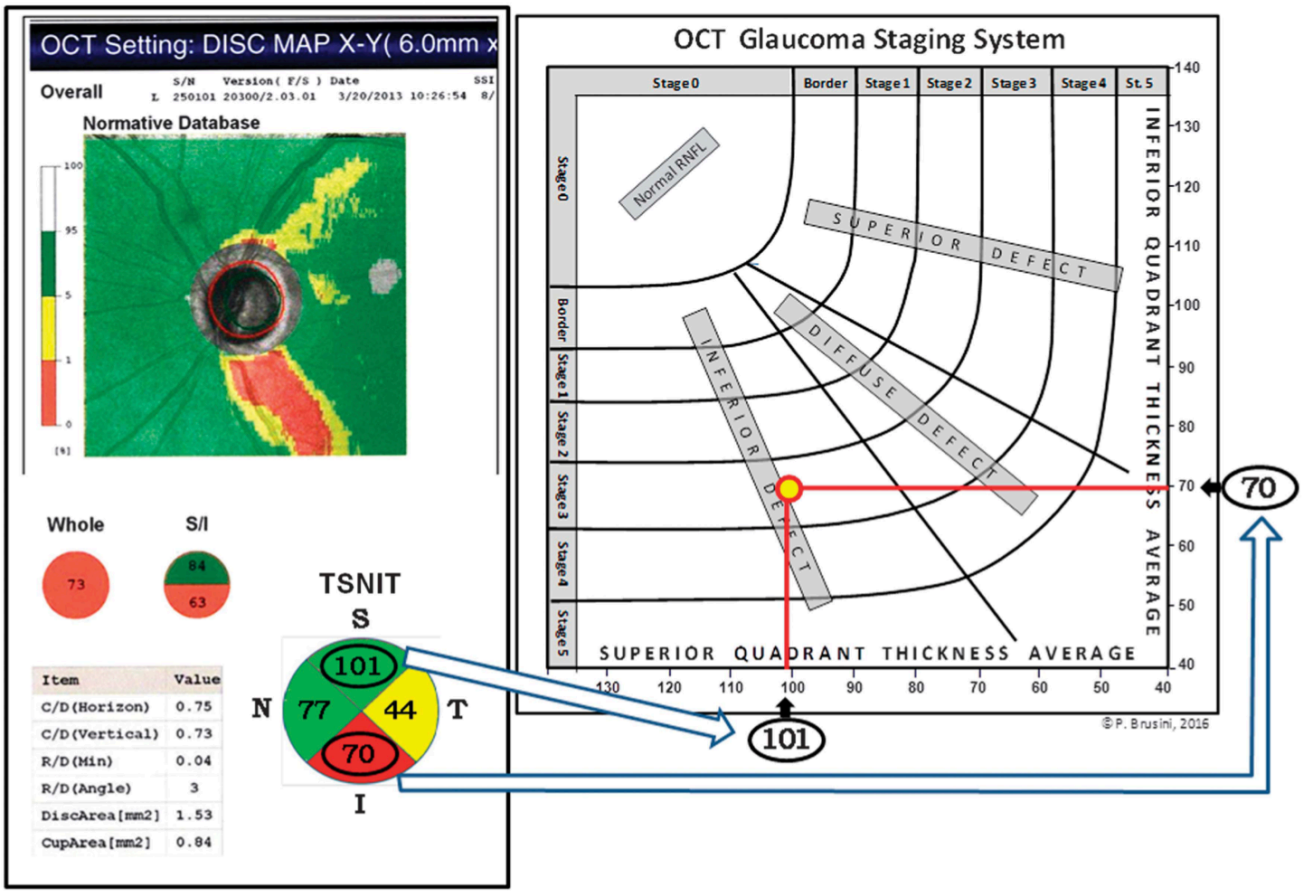

Figure 5 Example of OCT Glaucoma Staging System. The retinal nerve fiber layer (RNFL) thickness of the superior quadrant is entered on the X-axis, while the RNFL thickness of the inferior quadrant is entered into Y-axis. The intersection represents staging and localization. Figure modified from Brusini., 2018, Eye[95]

1.6 Management

1.6.1 Pharmacological Management

The pharmacological treatment of POAG and PACG is similar. The mainstay of drug treatment are drugs that lower the IOP. There are several groups of drugs that are commonly used and usually applied topically. The first group is the prostaglandin analogues, which mainly increase AqH drainage via the uveoscleral pathway (see 1.4.4.4)[62]. Another group is the locally applied β-adrenergic receptor blockers (β-blockers). Even though the mechanism of action is not fully understood, it is thought that unselective beta blockers bind to mostly β-2 adrenergic receptors in the ciliary epithelium and supplying vasculature and counteract β-2 adrenergic receptor mediated vasodilatation. Thereby they lead to reduced ciliary body perfusion and to

reduced AqH formation while not influencing drainage, eventuating in a decrease of IOP[96].

The second group of adrenergic receptors, the α-adrenergic receptors, is commonly modified by α-adrenergic receptor agonists (α-agonists) in glaucoma. Most frequently α-2-selective agonists are used that result in vasoconstriction in the ciliary body and other structures and thereby cause reduced AqH production[97]. α-agonists are also known to stimulate matrix metalloproteinases and to cause degradation of the extracellular matrix, facilitating uveoscleral pathway drainage similar to prostaglandin analogues[97].

Additional commonly used topical agents are carbonic anhydrase (CA) inhibitors. The CA inhibitors inhibit the enzyme CA which catalyses the hydration of CO_2 to carbonic acid (H_2CO_3) and following to bicarbonate and protons in the ciliary body. AqH is formed by transport of molecules and resulting osmotic fluid movement through the ciliary epithelium into the posterior chamber and involves an active sodium bicarbonate co-transporter channel. Therefore, lower levels of available bicarbonate appear to slow down AqH production[98].

Of added value, especially in PACG with pupillary block, are the parasympathomimetics, which activate muscarinic receptors in the sphincter muscle of the iris, leading to miosis and opening of the angle, allowing AqH to get absorbed in the TM[37].

A relatively new class of topical antiglaucoma medications is the Rho kinase inhibitors, that is increasingly gaining attention for the treatment of glaucoma[99]. The Rho proteins are small G-proteins that can activate Rho Kinase in their active form when connected to guanosine triphosphate. Several substances can lead to this activation, including several cytokines as well as ET-1[99]. Activated Rho kinase causes increased production of cell adhesion, increased cell rigidity and proliferation by modulating the myosin light chain. At the TM, these effects lead to an increased AqH outflow resistance and can therefore contribute to the build-up of IOP. The Rho kinase inhibitors can decrease these effects, resulting in modulation of the actin cytoskeleton in the TM and thereby increasing AqH outflow[99].

Even though these medications are applied topically, certain amounts will be taken up systemically and can possibly produce side effects.

Pharmacological treatment tends to be less effective in XFG and PG because of the physical obstruction of the TM. In these cases, surgical interventions might be indicated earlier[41].

1.6.2 Surgical Interventions

If pharmacological treatment alone is not sufficient or leads to intolerances, several surgical and non-surgical interventions are available and might be indicated in conjunction with pharmacological management. The extensive array of surgical interventions is beyond the scope of this dissertation and will not be discussed in detail. The basic principle of the most performed techniques that might be of importance for this research will be briefly explained.

One of the most commonly performed interventions in (acute) PACG is iridotomy. Commonly with a laser, less commonly surgically, a perforation in the peripheral iris is created to allow AqH to flow and to relieve pupillary block[37]. The used laser is commonly a neodymium-doped yttrium aluminum garnet (Nd:YAG) laser used in a Q-switching mode with doubled frequency to achieve a wavelength of 532 nm[36,37].

The most frequently used ophthalmic surgery for the reduction of IOP in POAG is trabeculectomy (TE). It is a surgical procedure where a part of the obstructed TM is removed and a direct connection to a small cavity underneath of the conjunctiva is created, allowing AqH to flow from the anterior chamber into the subconjunctival space, where it can accumulate and is eventually absorbed[37].

An alternative IOP lowering procedure is canaloplasty, where Schlemm's canal is dilated surgically with a catheter or only by viscodilation to improve its physiological AqH drainage activity[26,100]. As this technique, in opposition to trabeculectomy, does not create an open connection of the anterior chamber to the subconjunctival space, it appears to create less complications like infections, bleeding or AqH leakage[100].

Newer techniques include the microinvasive glaucoma surgeries such as the iStent® and the XEN® Gel Stent. These are very small implantable devices that create a mechanical connection between the anterior chamber with Schlemm's canal or the subconjunctival space respectively, in order to facilitate AqH outflow[101].

The Preserflo® stent also follows the principle of subconjunctival drainage, but by definition, is not a minimally invasive glaucoma surgery. Another minimally invasive

approach is the implantation of a stent into the suprachoroidal space, for which the Miniject® implant is currently available.

1.7 Research Aim

This research will specifically target patients with open angle glaucoma. The primary objective is to further elucidate the complex vascular pathogenesis underlying the disease, with particular emphasis on ET-1, given the mounting evidence of its significance in glaucoma. The investigation will explore potential correlations of ET-1 with the retinal VD at the ONH and macula, as well as other parameters derived from OCT-A. ET-1 in plasma and AqH as well as its precursor Big ET-1 and protein concentrations in healthy controls and glaucoma patients across different disease stages are to be analysed.

Currently, no existing research investigates the precise correlation between OCT-A measurements and ET-1 levels. These insights are believed to offer valuable novel information for disease diagnosis, follow-up, and a deeper understanding of the disease's pathophysiology.

Moreover, this dissertation aims to investigate the potential utility of OCT-A in comparison to SD-OCT for early diagnosis and staging of POAG, particularly focusing on its compatibility and potential extension into existing staging tools such as the OCT-GSS. This could possibly facilitate earlier glaucoma diagnosis and prompt initiation of treatment.

2. Materials and Methods

2.1 Materials

2.1.1 Chemicals

Chemicals	Manufacturer, Location
Distilled Water	Ophtha-Lab, Münster, Germany
Isopropanol	Carl Roth®, Karlsruhe, Germany
Caustic Soda / Sodium hydroxide	Carl Roth®, Karlsruhe, Germany
Ethanol > 99.5%	Carl Roth®, Karlsruhe, Germany

2.1.2 Consumables

Consumables	Manufacturer, Location
Borosilicate glass bottle 500 ml, 1000 ml	Carl Roth®, Karlsruhe, Germany
Disposable nitrile gloves	Carl Roth®, Karlsruhe, Germany
Insulin syringe	Carl Roth®, Karlsruhe, Germany
Measuring cylinder 100ml, 500 ml	Carl Roth®, Karlsruhe, Germany
Nunc-Immuno® pate, 96-Wells (ELISA-plate)	Thermo Scientific®, Schwerte, Germany
Petri dish	Thermo Fischer®, Dreieich, Germany
Pipette tips (Clearline®) 10 µl, 200 µl, 1000 µl	Kisker Biotech®, Steinfurt, Germany
Pleated filter grade 3	Sartorius Lab®, Göttingen, Germany
Reactiontube holder	VWR International®, Darmstadt, Germany
Reactiontubes 1.5ml	Sarstedt®, Nümbrecht, Germany
S Monovette® 7.5 ml LH (heparinized blood collection tube)	Sarstedt®, Nümbrecht, Germany
Terumo® syringe 1ml	Terumo®, Eschborn, Germany
V-Bottomplate	BioLegend®, Koblenz, Germany

2.1.3 Laboratory Devices

Laboratory Devices	Manufacturer, Location
Bio-Plex® MAGPIX® Multiplex Reader	Bio-Rad Laboratories®, USA
Centrifuge Multifuge 3	Heraeus Holding®, Hanau, Germany
Clean bench laminar flow Herasafe	Heraeus Holding®, Hanau, Germany
Eight channel-pipette	Eppendorf®, Hamburg, Germany
Eppendorf Centrifuge	Heraeus Holding®, Hanau, Germany
Erlenmeyer flask 250 ml	Carl Roth®, Karlsruhe, Germany
Freezer -80°C	Heraeus Holding®, Hanau, Germany
Fridge 4°C	Heraeus Holding®, Hanau, Germany
Funnel	Carl Roth®, Karlsruhe, Germany
Horizontal shaker IKA K 130 basic	IKA-Werke®, Staufen, Germany
Icemachine Scotsman AF 80	Hibu Eismaschine®, Sprockhövel, Germany
Microplate reader MRX (8 channels)	Dynatech Laboratories®, Denkendorf, Germany
Pipette, 10-, 200-, 1000 µl	Eppendorf AG®, Hamburg, Germany
Vortex shaker	Marienfeld®, Mergentheim, Germany
Water purifying system NANOpure Diamond	Wilhelm Werner®, Leverkusen, Germany

2.1.4 Testing systems

Testing systems	Manufacturer, Location
ProcartaPlex Multiplex Immunoassay	Thermo Fisher®, Dreieich, Germany
Bradford protein assay	Bio-Rad Laboratories®, USA
Quantikine Elisa Endothelin-1 Immunoassay	Biotechne®, Wiesbaden, Germany

2.1.5 Software

Software	Manufacturer, Location
Bio-Plex Manager MP	Biorad Laboratories®, USA
G*Power (Version 3.1)	Faul, F., Erdfelder, E., Buchner, A., & Lang, A.-G., Düsseldorf, Germany
Microsoft Office Excel	Microsoft®, USA
Statistics software R (Version 4.0.2)	R Foundation, USA
ProcartaPlex Analyst Software 1.0	Thermofisher, Dreieich, Germany

2.2 Methods

2.2.1 Study design

The study was designed as prospective monocenter study and took place at the department of Ophthalmology of the St. Franziskus Hospital in Münster, Germany. The laboratory analyses were performed in the Ophtha-Lab, which is adjacent to the department of Ophthalmology at the St. Franziskus Hospital, and in the Department of Dermatology at the University Medical Center in Münster, Germany.

2.2.2 Ethical Considerations

The study was approved by the ethics committee of the Medical Association of Westfalen-Lippe, Germany (reference number 2018-331-f-S). Patient data were anonymously processed and electronically stored. All procedures were conducted in accordance with the declarations of Helsinki and Istanbul. All patients provided written informed consent prior to study commencement and were allowed to retract their consent at any moment.

2.2.3 Participants, Inclusion & Exclusion criteria

In the period of 2018 to 2020, participants were prospectively identified and included. Participants were required to be adults (≥ 18 years). All participants were scheduled for either cataract or glaucoma surgery, which allowed to gather a specified amount of AqH intraoperatively without additional invasiveness. Before the surgery, all participants underwent detailed ophthalmic examination and review of medical history by an ophthalmologist, best corrected visual acuity testing, Goldmann applanation tonometry, slit-lamp funduscopy, measurement of the SBP as well as SD-OCT and OCT-A prior to surgery.

Two groups of patients were included, glaucoma patients and a control group. The diagnosis of glaucoma in the glaucoma group, based on funduscopy and OCT measurements, had to meet at least two or more of the following criteria:

- Increased vertical cup-to-disc ratio (VCDR; ≥0.5)
- CDR asymmetry between both eyes >0.2

- Glaucomatous reduction of peripapillary RNFL thickness and/or GCC thickness at the posterior pole (as specified by normal range values of the manufacturer)

The group of controls consisted of patients planned for undergoing cataract surgery for light to moderate cataract.
Additionally, all included control subjects had to fulfil the following inclusion criteria:

- IOP of ≤ 21 mmHg at examination
- No medical history of elevated IOP
- No family history positive for elevated IOP or glaucoma
- Funduscopy showing a normal morphological appearance of the optic disc (see chapter 1.1.5), including a regular NRR respecting the ISNT rule and a CDR within the normal range (approximately 0.2–0.4)
- SD-OCT yielding RNFL and GCC measurements within the normal range for their age as specified by the manufacturer based on large and verified sample databases
- VCDR as analysed by SD-OCT within the normal range, i.e. <0.5.

General exclusion criteria for both groups consisted of the following:

- Severe cataract, as advanced lens opacites are known to significantly impair SD-OCT and OCT-A image quality
- Refractive error > ±6 dioptres (dpt) sphere and ± 2 dpt cylinder, as larger errors are known to negatively impair SD-OCT and OCT-A image quality
- Low imaging quality with OCT-A signal strength index (SSI) index <45 and/or scan quality (SQ) score <6 as calculated by the imaging device
- Previous ophthalmologic surgery, except uncomplicated posterior chamber lens implantation for cataract, selective laser trabeculoplasty or laser iridotomy longer than 6 months prior to inclusion
- Systemic vascular disease including arterial hypertension, diabetes mellitus, prior cerebrovascular accident (CVA), myocardial infarction (MI), deep vein thrombosis (DVT) and pulmonary embolism (PE)

- Blood pressure >150mmHg systolic and/or >100mmg diastolic during physical examination, seated and after 5 minutes of resting with electronic measurement system Boso® Medicus, which is certified by the German Hypertension Society
- Use of systemic vasoactive medication of any group (alpha blockers, beta blockers, angiotensin-converting-enzyme [ACE] inhibitors, angiotensin II receptor blockers, calcium channel inhibitors, vasodilators, diuretics)
- Smoking

2.2.4 SD-OCT and OCT-A imaging

For all OCT and OCT-A measurements, the SD-OCT device RTVue-XR by Optovue® (SD-OCT & AngioVue™, RTVue-XR; Optovue, Inc., Fremont, California, USA—software version 2016.2.035) was used.

During the SD-OCT imaging, the thickness of the averaged circumpapillary GCC and RNFL thickness, the focal and global loss volume (FLV/GLV), the CDR and rim volume were measured. The FLV and GLV are proprietary analysis tools by the manufacturer that measure the average amount of GCC loss focally and on average across the entire measuring area, respectively.

The same device was used for the OCT-A analysis. For this study, each participant underwent OCT-A imaging on a 6 mm by 6 mm area centered at the fovea and on a 4,5 mm by 4,5 mm area centered at the optic disc. The functional principle of SD-OCT and OCT-a can be found in chapter 1.5.1. This specific device scanned at a pace of 70.000 A-scans per second, resulting in a resolution of 400 (A scans) x 400 (A scans) across the examined area. The device features an optical axial resolution of 5 µm and transverse resolution of 15 µm[102]. The axial imaging depth was up to 3 mm and the total acquisition time per OCT-A scan was less than three seconds[102]. The OCT-A scans usually generate images for 4 distinct layers: superficial vascular plexus (SVP), deep vascular plexus (DVP), outer retina, and choriocapillaris (CC). The device features a proprietary 3D projection artifact removal algorithm to minimize artifacts in deeper layers. Projection artifacts occur in deeper layers due to the blood flow in fine vessels in the superior layers, resulting in visual shadows that can be misinterpreted as vascular structures in the deeper layers. Several studies have confirmed efficient reduction of projection artifacts, mostly in the deeper layers[103,104]. Additionally, the system features sensitive infrared cameras that

continuously track eye movements during the scan and the integrated software allows to thereby correct for artefacts that occur because of eye movement[102].
As mentioned earlier, scans with SSI scores below 45 and/or SQ scores below 6, as well as excessive motion artefacts and blurring of the vasculature by for example vitreous opacities, were excluded to prevent misinterpretation of poor-quality scans. The SSI is a score between zero and 100 and based on the brightness of the reflected signal, which is important for correct segmentation of the retinal layers[105]. The SQ score is a proprietary score that uses the SSI score as well as data about eye motion and focus to generate an objective image quality index and ranges from zero to 10. To minimize interobserver variability, every scan was co-assessed for quality and correct segmentation and positioning by the same experienced ophthalmologist (PD Dr. med. Claudia Lommatzsch [CL]).

2.2.4.1 Optic Nerve Head Segmentation

The OCT-A scans of the optic disc area were performed in the radial peripapillary capillary (RPC) network, which is a vascular plexus within the RNFL only existent in the superior pole. The RPC has been shown to be highly associated with RNFL health and associated retinal diseases like glaucoma[106]. The scanned segment reaches from the internal limiting membrane (ILM) to the distal border (as seem from the ILM). The software calculates a VD value in percent for each scanned segment, correlating to the amount of area that is occupied by structures that the OCT-A machine detects as vessels, due to moving objects, likely erythrocytes, within the structure. The VD measurements are split up in a VD value for the entire scanned ONH area (ONH Whole), intrapapillary VD (ONH Inside) and peripapillary VD (PeriONH). The peripapillary area is then further segmented into eight sectors, congruent with the Garway-Heath map:

- Nasal Superior Sector (PeriONH NasSup)
- Nasal Inferior Sector (PeriONH NasInf)
- Inferior Nasal Sector (PeriONH InfNas)
- Inferior Temporal Sector (PeriONH InfTemp)
- Temporal Inferior Sector (PeriONH TempInf)
- Temporal Superior Sector (PeriONH TempSup)

- Superior Temporal Sector (PeriONH SupTemp)
- Superior Nasal Sector (PeriONH SupNas)

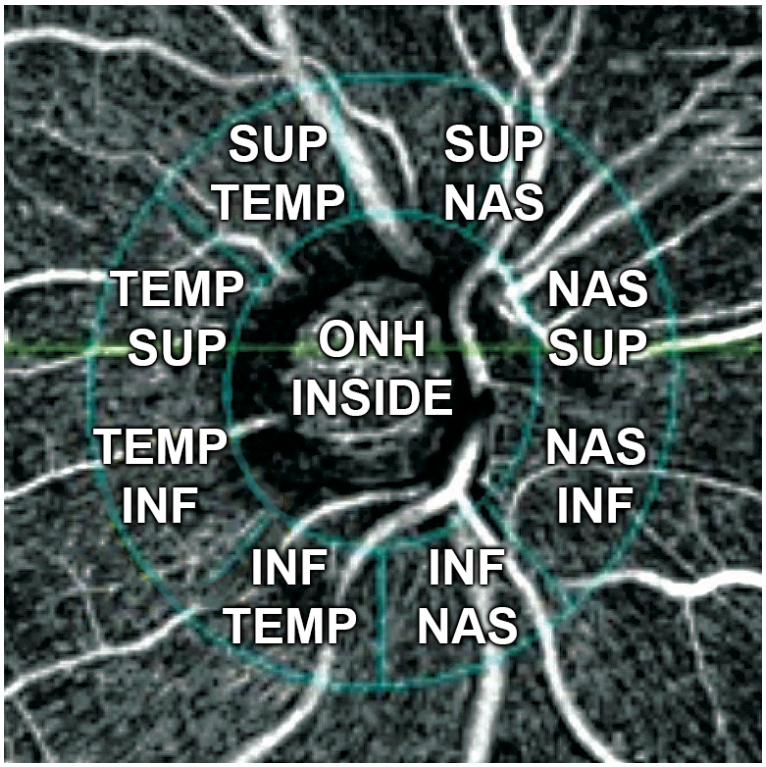

Figure 6 OCT-A of the optic nerve head (ONH) with the sectoral subdivision of the evaluated vessel density (VD) in the peripapillary area. SUP – Superior, INF – Inferior, TEMP – Temporal, NAS – Nasal

2.2.4.2 Macula Region Segmentation

The OCT-A scans of the macula region were performed in the SVP and DVP. The SVP extends from the ILM up to 10 µm proximally of the inner plexiform layer (IPL). The DVP extends from 10 µm proximally of the IPL up to 10 µm distally of the outer plexiform layer (OPL).

Similar to the ONH region, initially a VD value for the entire scanned level is generated (Macula SVP Whole and Maula DVP Whole). Then, it is separated into a foveal area, covering a 1 mm diameter area centered on the fovea (Fovea SVP and Fovea DVP), a parafoveal area, covering a diameter of 3 mm and thirdly a perifoveal region, covering a diameter of 6 mm.

The para- and peri-foveal areas are subdivided into the following quadrants in both layers:

- Temporal quadrant (ParaFovea/PeriFovea SVP/DVP Temp)
- Superior quadrant (ParaFovea/PeriFovea SVP/DVP Sup)
- Nasal quadrant (ParaFovea/PeriFovea SVP/DVP Nas)
- Inferior quadrant (ParaFovea/PeriFovea SVP/DVP Inf)

Additionally, the FAZ was determined by the manufacturer's software by overlapping the SVP and DVP scan. The software also analyses the regularity of the boundaries of the FAZ and compares it to a perfectly round circle, resulting in the so called acircularity index (AI), where one is a round circle and the index increases with a less round shape. Another value that was determined is the foveal density 300 µm (FD-300µm), which measures the VD in a 300 µm wide ring around the FAZ, ranging from the ILM to the OPL.

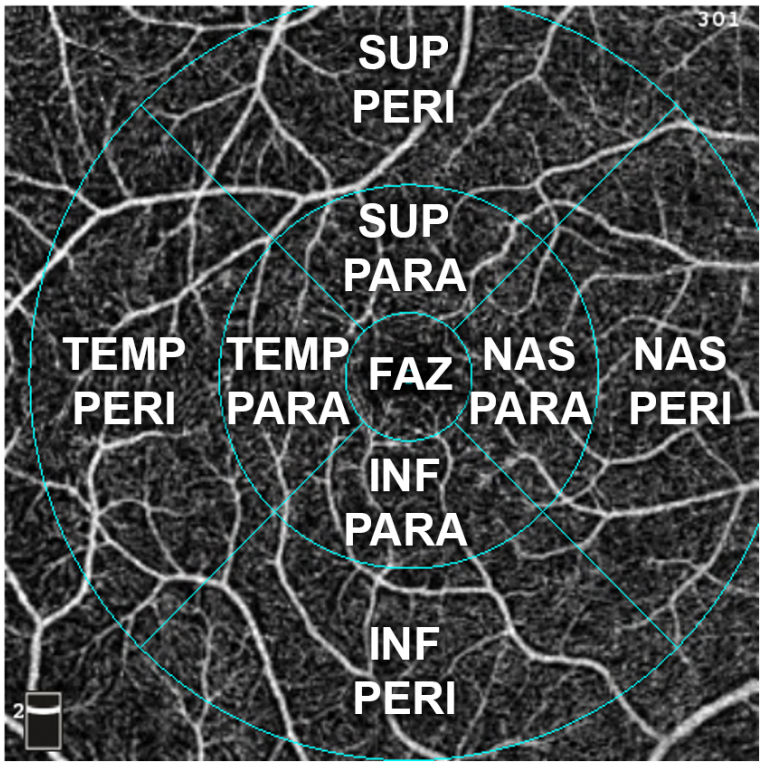

Figure 7 OCT-A of the macula region with the quadrant subdivision of the evaluated vessel density (VD). SUP – Superior, INF – Inferior, TEMP – Temporal, NAS – Nasal, PARA – parafoveal region 3 mm, PERI - perifoveal region 6 mm, FAZ - foveal avascular zone

2.2.5 OCT-GSS

The OCT-GSS by Brusini et al. has been calculated for every participant of this study[95]. The principle of the OCT-GSS has been introduced in chapter 1.5.2. Every participant therefore was classified within the seven classes of the OCT-GSS according to superior and inferior RNFL thickness and corrected for age. The results were further subdivided into superior, diffuse, and inferior defects (Figure 5):

- Healthy
- Borderline
- Stage 1 (Early damage)
- Stage 2 (Mild damage)
- Stage 3 (Moderate damage)
- Stage 4 (Advanced damage)
- Stage 5 (Terminal damage)

2.2.6 Blood and AqH sampling

Every participant got a total of 7 ml of blood and between 100 to 150 microlitres (µl) of AqH sampled during the ophthalmologic surgery.

The anaesthesiologist took the blood sample via an intravenous access into a heparinized blood collection tube before or at most 5 minutes after induction of general anaesthesia for surgery. A rest period of at least 30 minutes was ensured before collection. It was then cooled to 4°C and centrifuged for 10 minutes at 2000xg in a centrifuge (Multifuge 3®). Following, the plasma portion was pipetted into 1,5 ml reaction tubes and stored in a -80 °C freezer until further analysis.

The AqH was sampled by the ophthalmologist after opening of the anterior chamber during surgery, pipetted into a 1.5 ml reaction tube and stored in a -80 °C freezer until analysis.

2.2.7 Endothelin-1 analysis

For the quantification of ET-1 in this study, enzyme-linked-immunosorbent-assay (ELISA) was performed with the plasma and AqH, using the commercially available

ET-1 testing system “Quantikine® ELISA Endothelin-1 Immunoassay” by Bio-Techne®.

ELISA is a biochemistry immunoassay that visualizes antigen-antibody binding by enzymatic colour changes within the wells of the utilized microplate[107]. In order to detect even very small amounts of a desired substance, it makes use of specific antibodies of the antigen that is to be measured. For this study, the type sandwich ELISA was used. For this method, commercially available testing plates with wells that are coated with a specific amount of antibody that binds to a certain epitope of the desired antigen are used. The sample with the suspected antigen is then added. If the antigen matching the antibody of the coating is present in the sample, binding will occur, and the compound will remain attached to the surface allowing to be later measured by the ELISA reading device.

After a specific period of time the testing wells are washed with a washing buffer including detergent and only ET-1 proteins that are bound to the specific antibody remain. Then, another enzyme tagged antibody, binding to another specific epitope of the antigen, is added. That antibody is labelled with an enzyme, in this case horseradish peroxidase (HRP). If present in the sample, the antigen is at that point connected or “sandwiched” by two antibodies. This principle makes the sandwich ELISA very sensitive[107]. The wells are then washed again to remove unbound secondary antibody. In a next step, the enzyme-specific substrate, in this case 3,3′,5,5′-Tetramethylbenzidine (TMB) is added and in the presence of hydrogen peroxide oxidized by the HRP. The oxidation process causes the substrate to acquire a bluish colour. After 30 minutes, sulfuric acid (H_2SO_4) is added to stop the enzymatic reaction, leading to a change of colour within a yellowish spectrum[107]. The optical density of the wells is then measured at 450 nm in a plate reader (Dynatech® MRX microplate reader by Dynatech Laboratories®). Based on the measured optical density and by comparing to the predefined standard curve, the precise concentration of the examined antigen is calculated (Microsoft Excel®). To gain reliable quantification data, the ELISA standard curve is prepared in the laboratory simultaneously to the measurements of the samples. Serial dilutions of a known concentration of the desired antigen are prepared in adjacent wells and later measured by the ELISA reading device. Using this technique, the concentrations of the antigen in the samples can precisely be determined.

The correct conduction of the laboratory analysis was supervised and supported by biologist Dr. rer. nat. Maren Kasper (MK).
For this study specifically, the following steps, in accordance with the manufacturer's instructions, were performed in the Ophtha-Lab in Münster, Germany:

1. 150 µl of assay diluent RD1-105 were added to every well of the 96-Well-Plates covered with monoclonal ET-1 specific primary antibodies for rehydration
2. 75 µl [25 pg/ml, 12.5 pg/ml, 6.25 pg/ml, 3.13 pg/ml, 1.56 pg/ml, 0.78 pg/ml and 0.39 pg/ml] of standard, according to the manufacturer's instructions, were added to specified wells
3. The plasma and AqH samples were added to specified wells in duplicates
4. The wells were sealed by adhesive tape
5. The plates were incubated at room temperature for one hour on a 500 RPM horizontal shaker
6. The well's contents were aspirated
7. The wells were washed four times with 200 µl of wash buffer, remnants were beat out of the wells onto an absorbent surface
8. 200 µl of monoclonal ET-1 specific and HRP labelled secondary antibody were added
9. The plates were incubated at room temperature for three hours on a 500 RPM horizontal shaker
10. The well's contents were aspirated
11. The wells were washed four times with 200 µl of wash buffer, remnants were beat out of the wells onto an absorbent surface
12. 200 µl of chromogenic substrate (TMB) were added to the wells
13. The plates were incubated at room temperature and protected from light for thirty minutes
14. 50 µl of stop solution (H_2SO_4) were added
15. The absorbance of wells was analysed at 450 nm in the Dynatech® MRX microplate reader (Dynatech Laboratories®)

2.2.8 Big Endothelin-1 Analysis

For the quantification of Big ET-1 in this study, a Luminex® -Assay for Big ET-1 was performed with the plasma and AqH, using the commercially available Big ET-1 Luminex®-Assay by R&D Systems®.

Luminex®-Assays are a type multiplexing assays for immunoassays that measure multiple analytes simultaneously and serves as a derivate of ELISA. Microscopic magnetic beads made of polystyrene are, per designated analyte, dyed with a unique color code of two fluorescent dyes by the manufacturer, which can later be identified. Every bead is also pre-coated with the corresponding specific antibody of the antigen of interest. Theoretically, more than 100 different bead-antibody combinations can be analyzed in the same well[108]. Similar to the sandwich ELISA (see 2.2.7), after the washing cycle, another biotinylated detection antibody is added, that binds to another specific epitope of the antigen. When streptavidin, which is conjugated with the red protein complex phycoerythrin, is added, it binds strongly to the biotin area of the detection antibody.

Samples were analysed with the Bio-Plex® MAGPIX™ Multiplex Reader by Bio-Rad®, the magnetic beads can be held by a magnet in a monolayer while being illuminated by different wavelength light emitting diodes (LED) to identify the unique colour code. A charge-coupled device sensor can then determine the degree of the detected phycoerythrin, which is proportional to the amount of bound antigen. Similar to ELISA (see 2.2.7), predefined concentrations of standard are prepared in certain wells simultaneously, to create known concentrations that can be compared to the unknown concentrations in the sample. Using this technique, the concentrations of the antigen in the samples can precisely be determined.

The correct conduction of the laboratory analysis was supervised and supported by biologist MK.

For this study specifically, the following steps, in accordance with the manufacturer's instructions, were performed in the Ophtha-Lab and the Lab of Prof. Dr. Karin Loser at the Department of Dermatology at the University Medical Center in Münster, Germany:

1. 50 µl of magnetic beads with Big ET-1 specific capture antibodies were added to specified wells of the 96-Well-Plates
2. The plates were placed on the hand-held magnetic washing plate for two minutes, allowing the magnetic beads to settle on the ground
3. The plate was quickly inverted above the sink the evacuate the liquid without the beads
4. 150 µl of wash buffer were added to each well and steps 2 & 3 were repeated
5. Step 4 was repeated
6. The plate was removed from the magnetic plate
7. 25 µl of plasma or AqH sample were pipetted into specific wells
8. 25 µl [2050 pg/ml, 512.5 pg/ml, 128.13 pg/ml, 32.03 pg/ml, 2.00 pg/ml, 0.50 pg/ml] of predefined standard were added to specific wells
9. The plates were incubated at room temperature for two hours on a 500 rounds per minute (RPM) horizontal shaker
10. The washing process (Step 2-4) was repeated twice
11. 25 µl of Big ET-1 specific and biotinylated secondary antibody were added
12. The plates were incubated at room temperature for 30 minutes on a 500 RPM horizontal shaker
13. The washing process (Step 2-4) was repeated thrice
14. 50 µl of phycoerythrin-conjugated streptavidin were added to the wells
15. The plates were incubated at room temperature for 30 minutes on a 500 RPM horizontal shaker
16. The washing process (Step 2-4) was repeated twice
17. 120 µl of reading buffer were added to the wells
18. The wells were analyzed in the Bio-Plex® MAGPIX™ Multiplex Reader
19. The quantification of Big-ET-1 were done by the ProcartaPlex Analyst Software Version 1.0 (Thermo Fischer®)

2.2.9 Protein Analysis

All plasma and AqH samples were analysed for protein content using the Bradford protein assay, commercially available from Bio-Rad®. The Bradford protein assay measures the presence of protein in fluidic samples. It makes use of the fact that the

dye Coomassie brilliant blue G-250 (CBBG), in acidic environments, creates complex connections to the cationic carboxyl groups and hydrophobic pockets of proteins[109]. When this binding occurs, the structural composition of CBBG changes and causes its absorbance maximum to change from 465 nm in the unbound state to 595 nm (blue), which can be detected optically and precisely measured with a spectrophotometer. Since the amount of absorption at 595 nm is proportional to the actual protein concentration, the precise concentration can be determined with high sensitivity by the spectrophotometer[109]. In this study, bovine serum albumin (BSA) solutions were used for the standard curve, as instructed by the manufacturer. The concentration of BSA solution was adapted to commonly known normal protein concentrations of plasma and AqH. For the AqH, BSA concentrations of 1.45 µg /µl and for the plasma of 26.8 µg/µl were used.
The correct conduction of the laboratory analysis was supervised and supported by biologist MK.
For this study specifically, the following steps, in accordance with the manufacturer's instructions, were performed int the Ophtha-Lab in Münster, Germany:

1. The dye reagent (Bio-Rad®) was diluted in a ratio of one to five with distilled water, as instructed by the manufacturer
2. The reagent was, protected from light, filtered by a pleated filter
3. 5 µl of BSA standard (0, 1, 2, 3, 4, 5 µg/ml) were, according to the manufacturer, were added to specified wells of the 96 well microplate
4. 5 µl of plasma and AqH samples were, according to the manufacturer, added to specified wells
5. 200 µl of dye reagent were added to the wells
6. The wells were incubated at room temperature for five minutes
7. The absorbance of wells was analysed at 630 nm in the Dynatech® MRX microplate reader (Dynatech Laboratories®)

2.2.10 Statistical analysis

For the statistical analyses, the software R (Version 4.0.2; Dormagen, Germany) was used.

Summary statistics were obtained using conventional methods, distribution of data was checked using the Shapiro test. Normally distributed data are expressed as mean and standard deviation (SD), skewed data as medians and interquartile range (IQR). The significance level α was set to 5%. For comparison of two groups and more than two groups, a suitable T-Test or ANOVA followed by a Tukey post-hoc analysis was used respectively, if all assumptions were fulfilled.

If assumptions were not met, a non-parametric Wilcoxon test (rank test, or rank sum test) was used for the comparison of two groups, and a Kruskal–Wallis test followed by Dunn's post-hoc test was used for the comparison of more than two groups. During the post-hoc tests, p-values were corrected with the Bonferroni correction.

For the comparison of nominal data, the chi-square test was used if the value of every cell was ≥ 5, otherwise Fisher's exact test was performed.

When conducting the linear correlation analysis, Pearson's test was used for parametric data and Spearman's rank test for non-parametric data. r is the calculated correlation coefficient and situated between -1 and +1, indicating the strength and direction of the compared variable's relationship. According to Cohen's conventions of interpreting effect size r, the strength of association around 0.1 was seen as low, around 0.3 was seen as moderate, and above 0.5 was seen as strong.

Univariable regression analysis was performed. For normally distributed analysis of two variables, Pearson's correlation test was used. If the data were not normally distributed, Spearman's correlation test was used.

For the multiple regression analysis, a normally distributed and linear model was assumed. A sample size calculation was performed using the software G*Power (Version 3.1; Düsseldorf, Germany) for a two-sided linear multiple regression. Due to a lack of known studies investigating the relationship between plasma and AqH ET-1 concentration and VD measured by OCT-A, conservative estimates were used. The analysis was designed to detect a small to moderate two-sided correlation (Hypothesis ρ=0.2) versus the null hypothesis of no correlation (Alternative ρ=0.0). The assumed significance level α was 0.05 and the used power was 0.8. The required sample size was calculated to be n=44 per study group. Accounting for a 10% dropout, it was aimed to include 50 patients per study group.

To determine the minimally required number of subjects in relation to the number of predictors for the multiple regression analysis and sub-analysis, Cohen's two-step-rule using lambda was used[110,111].

The resulting p-values of the independent variable allowed to identify variables with significant influence in the multivariable regression model.

The statistical analyses were supported and supervised by mathematician Kai Rothaus (KR).

3. Results

3.1 Study Participants – Baseline characteristics

The baseline characteristics are presented in Table 1. The patient population consisted of a total of 98 eyes, composed of 30 controls and 68 glaucomatous eyes. The mean age of the control group was 66.8 (±9 SD) years with 33.3% males, while the mean age of the glaucoma group was 64.5 (±9 SD) years with 39.7% males. There was no significant difference in sex, age, and MAP between the two groups. The group of glaucoma patients registered significantly higher IOPs (18.00mmHg [15.00 - 21.25] vs. 14.00 [12.00 - 14.00]; $p<0.001$), significantly higher logarithm of the minimum angle of resolution visual acuity (LogMAR) (0.10 [0.10 - 0.30] vs. 0.40 [0.30 - 0.60]; $p<0.001$), and significantly more pseudophakic lenses (n=10 vs. n= 0; p=0.0291) as compared with the control group. The patient population included POAG (N=49), 5 confirmed NTG cases (i.e. uncorrected IOP ≤ 21mmHg), XFG (N=9), PACG (N=3), and PG (N=2) patients. Due to the limited sample size of the NTG, XFG, PACG, and PG group, separate sub-analyses on these groups were not performed.

Included surgeries were cataract surgery with posterior chamber lens implantation, trabeculotomy, canaloplasty, trabecular micro-bypass stent (iStent®) and transscleral microsurgical devices (XEN gel stent®). The control group consisted entirely of patients receiving cataract surgery with posterior chamber lens implantation, whereas the glaucoma group consisted of a combination of cataract and glaucoma surgeries (see Table 1).

Table 1 Baseline characteristics.

Parameter	Control, mean ± SD or median with IQR	Glaucoma, mean ± SD or median with IQR	P-value
Eye	OD:19|OS:11	OD:30|OS:38	0.13[2]
Age (years)	66.77 ± 9.01	64.51 ± 12.18	0.37[1]
Sex	Female:20|Male:10	Female:41|Male:27	0.71[2]
Glaucoma Entity	POAG:0|XFG:0|NTG:0|PG:0|ACG:0	POAG:49|XFG:9|NTG:5|PG:2|ACG:3	N/A[5]
First Diagnosis of Glaucoma (months)	N.A.	72.00 [29.75 - 120.00]	N/A[5]
Refractive Error (dpt)	0.07 ± 2.88	0.00 [-1.38 - 0.50]	0.29[4]
Axis Length IOLMaster (mm)	23.91 ± 1.54	24.05 ± 1.28	0.75[1]
Visual Acuity	0.40 [0.25 - 0.50]	0.75 [0.50 - 1.00]	< 0.00001[4]
Visual Acuity (LogMar)	0.40 [0.30 - 0.60]	0.12 [0.10 - 0.30]	< 0.00001[4]
IOP (mmHg)	14.00 [12.00 - 14.00]	18.00 [15.00 - 21.25]	< 0.00001[4]
Pseudophakia	phacic:30|pseudophacic:0	phacic:58|pseudophacic:10	< 0.05[3]
Mean Arterial Pressure (mmHg)	95.00 [92.50 - 99.50]	93.33 [91.67 - 101.67]	0.76[4]
Operation Technique	TE:0|Canaloplasty:0|iStent:0|XEN:0| Cataract + iStent:0|Cataract:30	TE:40|Canaloplasty:8|iStent:0|XEN:5| Cataract + iStent:2|Cataract:13	<0.001[3]
Number of topical Antiglaucomatosa	0	3.00 [2.00 - 4.00]	N/A[5]
Topical Beta-Blocker n (%)	0	43 (74.1%)	N/A[5]
Topical Carbonic Anhydrase Inhibitor n (%)	0	47 (81.0%)	N/A[5]
Topical Prostaglandin Analogue n (%)	0	51 (87.9%)	N/A[5]
Topical Alpha Adrenergic Agonist n (%)	0	23 (39.7%)	N/A[5]
Topical Pilocarpine n (%)	0	2 (3.4%)	N/A[5]
Systemic Carbonic Anhydrase Inhibitor n (%)	0	5 (8.6%)	N/A[5]

ACG - angle-closure glaucoma, IOLMaster® - Optical Biometer Zeiss®, IOP - Intraocular pressure, iStent® - Trabecular Micro-Bypass Device, N/A - not applicable, NTG - normal-tension glaucoma, PG - pigmentary glaucoma, POAG - primary open-angle glaucoma, TE - trabeculectomy, XEN - XEN® Gel Stent, XFG - exfoliation glaucoma. Tests: [1]T-test, [2]Chi[2]-test, [3]Fisher-test, [4]Wilcoxon rank sum test, [5]No Test

3.2 OCT and OCT-A Parameters

When comparing the OCT parameters of the glaucomatous eyes with the control group, the GCC (p=<0.00001), the RNFL (p=<0.00001), the inferior RNFL (p=<0.00001), the superior RNFL (p=<0.00001) the rim area (p=<0.00001) and the cupvolume (p=<0.00001) were significantly reduced (Table 2). The CDR (p=<0.00001), the vertical CDR (p=<0.00001), the GLV (p=<0.00001) as well as the FLV (p=<0.00001) were significantly elevated.

When comparing the OCT-A parameters of the glaucomatous eye with the control group, the VD of the whole ONH (p=<0.00001), including all predefined segments and the VD of the whole macula in the SVP (p=<0.00001), as well as the VD of the PeriFovea average (p < 0.00001) including all segments in the SVP were significantly reduced (Table 2). The area of the FAZ and VD of the whole macula in the DVP and of the fovea in the SVP as well as DVP did not differ significantly.

Table 2 OCT and OCT-A parameters

Parameter	Control, mean ± SD or median with IQR	Glaucoma, mean ± SD or median with IQR	P-value
Ganglion Cell Complex (µm)	96.55 ± 8.41	76.00 [67.00 - 84.00]	< 0.00001[2]
Focal Loss Volume (%)	0.41 [0.21 - 0.80]	18.00 [15.00 - 21.25]	< 0.00001[2]
Global Loss Volume (%) (	2.10 [0.50 - 4.25]	19.24 ± 10.91	< 0.00001[2]
RNFL Thickness (µm)	96.79 ± 8.72	72.72 ± 13.10	< 0.00001[1]
RNFL Thickness Superior (µm)	116.55 ± 12.70	85.96 ± 19.35	< 0.00001[1]
RNFL Thickness Inferior (µm)	121.08 ± 14.79	85.00 ± 19.34	< 0.00001[1]
Cup/Disc Ratio Total	0.31 ± 0.15	0.68 [0.58 - 0.77]	< 0.00001[2]
Cup/Disc Ratio Vertical	0.52 [0.45 - 0.60]	0.82 [0.72 - 0.90]	< 0.00001[2]
Cup/Disc Ratio Horizontal	0.58 [0.46 - 0.65]	0.89 [0.75 - 0.94]	< 0.00001[2]
Disc Area (mm^2)	2.03 ± 0.32	2.05 ± 0.34	0.78[1]
Rim Area (mm^2)	1.37 ± 0.35	0.68 [0.49 - 0.91]	< 0.00001[2]
Cupvolume (mm^3)	0.11 [0.03 - 0.18]	0.38 [0.18 - 0.59]	< 0.00001[2]
VD ONH Whole (%)	47.00 ± 2.52	35.40 [30.17 - 38.90]	< 0.00001[2]
VD ONH Inside (%)	44.20 ± 4.06	41.74 ± 7.95	0.048[1]
VD PeriONH Average (%)	50.69 ± 2.82	36.72 ± 8.60	< 0.00001[1]
VD PeriONH NasSup (%)	47.86 ± 4.35	34.09 ± 9.04	< 0.00001[1]
VD PeriONH NasInf (%)	45.04 ± 5.42	33.73 ± 9.02	< 0.00001[1]
VD PeriONH InfNas (%)	50.14 ± 4.33	33.07 ± 10.49	< 0.00001[1]
VD PeriONH InfTemp (%)	55.54 ± 4.48	40.00 [26.80 - 50.85]	< 0.00001[2]

Parameter	Control, mean ± SD or median with IQR	Glaucoma, mean ± SD or median with IQR	P-value
VD PeriONH TempInf (%)	52.85 [51.08 - 56.23]	42.72 ± 8.06	< 0.00001[2]
VD PeriONH TempSup (%)	54.40 [53.05 - 58.08]	47.75 [38.73 - 52.42]	< 0.00001[2]
VD PeriONH SupTemp (%)	53.58 ± 4.87	36.90 ± 12.42	< 0.00001[1]
VD PeriONH SupNas (%)	49.92 ± 3.47	33.40 [23.78 - 41.28]	< 0.00001[1]
VD Macula SVP Whole (%)	41.90 ± 4.15	37.02 ± 4.28	< 0.00001[1]
VD Fovea SVP (%)	19.99 ± 6.69	17.30 [11.12 - 21.65]	0.06[2]
VD ParaFovea SVP Average (%)	41.94 ± 6.43	39.39 ± 4.69	0.031[1]
VD ParaFovea SVP Temp (%)	42.22 ± 6.86	38.71 ± 5.98	0.013[1]
VD ParaFovea SVP Sup (%)	42.30 [36.60 - 47.70]	40.06 ± 5.63	0.24[1]
VD ParaFovea SVP Nas (%)	40.47 ± 7.11	39.37 ± 5.99	0.44[1]
VD ParaFovea SVP Inf (%)	40.80 [38.20 - 49.00]	39.44 ± 5.84	0.047[2]
VD PeriFovea SVP Average (%)	42.47 ± 4.36	37.37 ± 4.65	< 0.00001[1]
VD PeriFovea SVP Temp (%)	38.51 ± 5.25	35.09 ± 4.46	0.001[1]
VD PeriFovea SVP Sup (%)	41.65 ± 5.11	36.60 ± 4.86	< 0.0001[1]
VD PeriFovea SVP Nas (%)	47.41 ± 4.33	41.27 ± 5.66	< 0.00001[1]
VD PeriFovea SVP Inf (%)	42.52 ± 4.41	36.40 ± 5.23	< 0.00001[1]
VD Macula DVP Whole (%)	39.96 ± 4.37	41.90 ± 4.83	0.06[1]
VD Fovea DVP (%)	34.28 ± 8.49	32.23 ± 7.99	0.26[1]
VD ParaFovea DVP Average (%)	48.03 ± 3.98	47.73 ± 4.67	0.77[1]
VD ParaFovea DVP Temp (%)	51.50 [48.00 - 52.70]	49.43 ± 5.34	0.45[2]
VD ParaFovea DVP Sup (%)	47.34 ± 5.65	46.81 ± 6.30	0.70[1]
VD ParaFovea DVP Nas (%)	51.20 [46.60 - 53.10]	49.15 ± 5.42	0.29[2]
VD ParaFovea DVP Inf (%)	44.94 ± 5.15	45.95 [42.53 - 48.83]	0.63[2]
VD PeriFovea DVP Average (%)	39.88 ± 5.46	42.47 ± 5.33	0.032[1]
VD PeriFovea DVP Temp (%)	43.91 ± 5.96	44.50 ± 5.92	0.65[1]
VD PeriFovea DVP Sup (%)	39.22 ± 6.54	41.76 ± 5.39	0.050[1]
VD PeriFovea DVP Nas (%)	39.61 ± 5.90	43.06 ± 6.15	0.012[1]
VD PeriFovea DVP Inf (%)	37.14 ± 6.80	40.49 ± 5.73	0.014[1]
FAZ (mm^2)	0.26 ± 0.10	0.26 [0.22 - 0.38]	0.29[2]

RNFL - retinal nerve fiber layer, VD – vessel density, ONH – optic nerve head, SVP – superficial vascular plexus, DVP - deep vascular plexus, FAZ - foveal avascular zone. Tests: [1]T-test, [2]Wilcoxon rank sum test

3.3 OCT-GSS Scores

The OCT-GSS score was calculated for every participant using the online tool by Brusini et al. (see 1.5.2 and 2.2.5.).

Of the control group including 30 patients, 23 patients were classified as healthy, five as borderline (Stage 0), one as early damage (Stage 1) and one as mild damage (Stage 2).

Of the glaucoma group, eleven of the 68 patients were classified as healthy, five as borderline (Stage 0), six as early damage (Stage 1), nine as mild damage (Stage 2), 17 as moderate damage (Stage 3), nine as advanced damage (Stage 4), and six as terminal damage (Stage 5) (Figure 2) .

Within the glaucoma group, the defect location (none, diffuse, superior or inferior) type differed significantly between OCT-GSS stages ($p<0.001$), with the diffuse defects dominating in higher OCT-GSS stages.

The change of important OCT and OCT-A parameters according to OCT-GSS Stage is graphically visualized in Figure 7.

The comparison of the OCT-GSS groups as ordinal variables with all parameters and their analysis of variance for the entire patient population can be found in table 3. While the significance of the RNFL and GCC thickness is to be expected as the OCT-GSS score is based on these values, it becomes apparent, that multiple OCT-A parameters, especially the VD of the PeriONH region and all its quadrants, as well as all PeriFovea quadrants in the SVP layer decrease significantly with increasing OCT-GSS stage (Table 4).

Following, a correlation analysis was performed where the ordinal OCT-GSS Stages were transformed into a continuous variable ranging from zero to approximately six (Healthy: 0 –<0.14, Borderline: 0.14 -<1, Stage 1: 1-<2, Stage 2: 2-<3, Stage 3: 3-<4, Stage 4: 4-<5, Stage 5: 5-<6). The correlation analysis revealed a significantly positive correlation of the ET-1 levels in plasma as well as AqH with the continuous OCT-GSS Score (Figure 8). Significant positive correlations were also found for the IOP, the cup volume, the vertical CDR, the FLV, the GLV and others (Table 3). Significantly negative correlations were found between the continuous OCT-GSS Score and the visual acuity (LogMAR), the RNFL, the VD ONH Whole, the VD of the whole-macula SVP as well as the rim area and several sub-quadrants (Table 3).

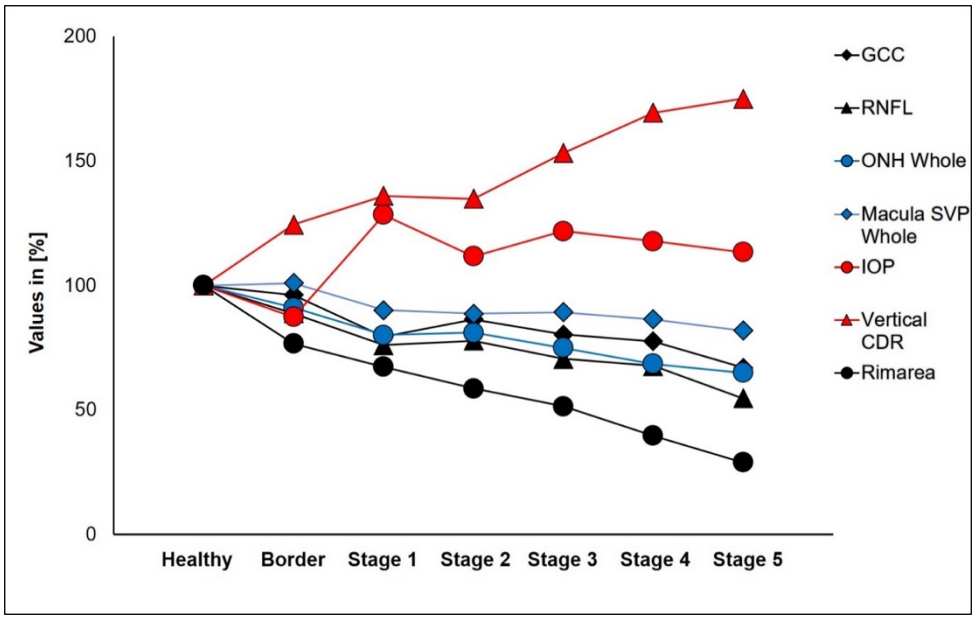

Figure 8 OCT and OCT-A parameters compared to OCT-GSS staging. Values from GCC, RNFL, IOP, vessel density of ONH Whole and Macula SVP Whole, vertical CDR and rim area for the healthy stage were set to 100%. Values for the other stages (borderline, stage 1–5) were normalized to the healthy stage and are displayed in %.

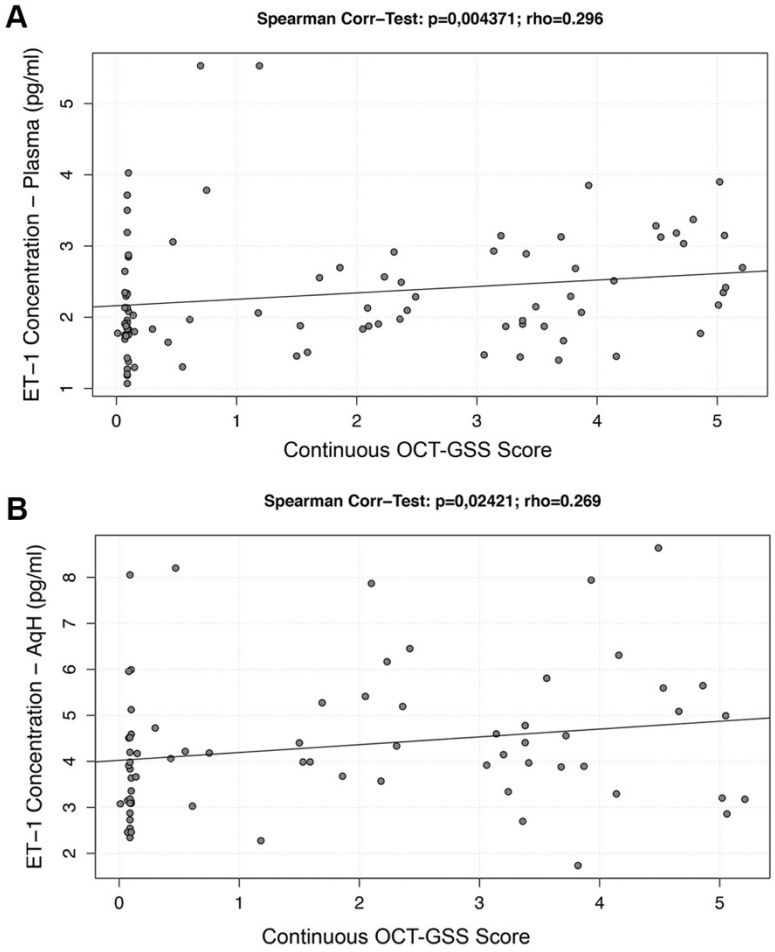

Figure 9 (A) Plasma and (B) AqH ET-1 level in pg/ml of entire study population compared to continuous OCT-GSS score. Healthy: 0 –<0.14; Borderline: 0.14 - <1; Stage 1: 1-<2; Stage 2: 2-<3; Stage 3: 3-<4; Stage 4: 4-<5, Stage 5: 5-<6

Table 3 Correlation analysis of clinical and OCT/OCT-A parameters with continuous OCT-GSS score of all patients

Parameter	Cont. OCT-GSS Score	
	All patients	
	Rho	P
ET-1 - AqH (pg/ml)	0.269	0.0242[1]
ET-1 - Plasma (pg/ml)	0.296	0.0044[1]
Protein - AqH (mg/ml)	0.194	0.0790[1]
Protein - Plasma (mg/ml)	0.227	0.0306[1]
Visual Acuity (LogMAR)	-0.321	0.0019[1]
IOP (mmHg)	0.379	0.0002[1]
Mean Arterial Pressure (mmHg)	-0.040	0.7304[1]
Ganglion Cell Complex (µm)	-0.723	<0.0001[1]
Focal Loss Volume (%)	0.665	<0.0001[1]
Global Loss Volume (%)	0.800	<0.0001[1]
RNFL Thickness (µm)	-0.912	<0.0001[1]
Cup/Disc Ratio Total	0.734	<0.0001[1]
Cup/Disc Ratio Vertical	0.775	<0.0001[1]
Cup/Disc Ratio Horizontal	0.656	<0.0001[1]
Rim Area (mm^2)	-0.764	<0.0001[1]
Disc Area (mm^2)	-0.027	0.8079[1]
Cupvolume (mm^3)	0.486	<0.0001[1]
VD ONH Whole (%)	-0.771	<0.0001[1]
VD ONH Inside (%)	-0.003	0.9807[1]
VD PeriONH Average (%)	-0.782	<0.0001[1]
VD PeriONH NasSup (%)	-0.712	<0.0001[1]
VD PeriONH NasInf (%)	-0.669	<0.0001[1]
VD PeriONHInfNas (%)	-0.780	<0.0001[1]
VD PeriONHInfTemp (%)	-0.743	<0.0001[1]
VD PeriONHTempInf (%)	-0.520	<0.0001[1]
VD PeriONHTempSup (%)	-0.531	<0.0001[1]
VD PeriONHSupTemp (%)	-0.734	<0.0001[1]
VD PeriONHSupNas (%)	-0.755	<0.0001[1]
VD Macula SVP Whole (%)	-0.545	<0.0001[1]
VD Macula DVP Whole (%)	0.079	0.4618[1]
VD Fovea SVP (%)	-0.210	0.0472[1]
VD Fovea DVP (%)	-0.156	0.1420[1]
VD ParaFoveaSVP Average (%)	-0.147	0.1657[1]
VD ParaFoveaDVP Average (%)	-0.074	0.4904[1]
VD PeriFoveaSVP Average (%)	-0.587	<0.0001[1]
VD PeriFovea DVP Average (%)	0.100	0.3491[1]
FAZ (mm^2)	0.061	0.5714[1]
Number Topical Antiglaucomatosa	0.138	0.2839[1]

AqH - aqueous humour, ET-1 - Endothelin-1, VD - vessel density, ONH - optic nerve head, SVP - superficial vascular plexus, DVP - deep vascular plexus, FAZ - foveal avascular zone, RNFL - retinal nerve fiber layer. Tests: [1]Spearman's Rank Correlation Test

Table 4 OCT-GSS staging comparisons for entire patient population

Parameter	Healthy	Border	Stage 1	Stage 2	Stage 3	Stage 4	Stage 5	P-Value
Group	Glaucoma:11 | Control:22	Glaucoma:5 | Control:5	Glaucoma:6 | Control:1	Glaucoma:9 | Control:1	Glaucoma:17 | Control:0	Glaucoma:8 | Control:0	Glaucoma:6 | Control:0	
Glaucoma Entity	POAG:6|XFG:3|NTG:0|PG:0|ACG:2	POAG:3|XFG:0|NTG:2|PG:0|ACG:0	POAG:4|XFG:2|NTG:0|PG:0|ACG:0	POAG:7|XFG:1|NTG:1|PG:0|ACG:0	POAG:13|XFG:1|NTG:1|PG:1|ACG:1	POAG:5|XFG:2|NTG:1|PG:0|ACG:0	POAG:6|XFG:0|NTG:0|PG:0|ACG:0	0.52[3]
OCT-GSS Defect Type	None:31| Inferior:2| Superior:0| Diffuse:0	None:0| Inferior:1| Superior:7| Diffuse:2	None:0Inferior:0| Superior:2| Diffuse:5	None:0|Inferior:3| Superior:2| Diffuse:5	None:0|Inferior:4| Superior:1| Diffuse:12	None:0| Inferior:0| Superior:0| Diffuse:8	None:0| Inferior:0| Superior:0| Diffuse:6	<0.001[3]
Operation Technique	TE:6|Canaloplasty:2|iStent:0|XEN:0| Cataract + iStent:0|Cataract:25	TE:1|Canaloplasty:2|iStent:0|XEN:0| Cataract + iStent:0|Cataract:7	TE:5|Canaloplasty:0|iStent:0|XEN:0| Cataract + iStent:0|Cataract:2	TE:4|Canaloplasty:2|iStent:0|XEN:1| Cataract + iStent:0|Cataract:3	TE:9|Canaloplasty:1|iStent:0|XEN:2| Cataract + iStent:2|Cataract:3	TE:6|Canaloplasty:1|iStent:0|XEN:0| Cataract + iStent:0|Cataract:1	TE:4|Canaloplasty:0|iStent:0|XEN:2| Cataract + iStent:0|Cataract:0	<0.001[3]
Pseudophakia	Phacic:33 | Pseudophacic:0	Phacic:10 | Pseudophacic:0	Phacic:6 | Pseudophacic:1	Phacic:7 | Pseudophacic:3	Phacic:15 | Pseudophacic:2	Phacic:6 | Pseudophacic:2	Phacic:4 | Pseudophacic:2	0.003[3]
Visual Acuity (LogMar)	0.36 ± 0.24	0.36 ± 0.31	0.20 [0.05-0.30]	0.05 [0.00-0.42]	0.20 [0.10-0.30]	0.18 ± 0.16	0.22 ± 0.19	0.17[4]
IOP (mmHg)	14.00 [12.00-16.00]	14.00 ± 2.79	20.57 ± 9.66	17.90 ± 3.93	19.53 ± 7.14	18.88 ± 6.13	18.17 ± 3.31	0.028[4]
MAP (mmHg)	95.00 [92.50 - 98.17]	90.00 [90.00-93.33]	91.00 ± 2.09	100.21 ± 4.52	98.84 ± 13.25	93.33 [92.92-97.17]	92.33 ± 7.70	0.13[4]
Protein - Plasma (mg/ml)	40.92 ± 5.58	42.50 ± 5.27	38.69 ± 4.09	42.18 [41.53 - 42.97]	45.34 ± 4.67	41.72 [40.97 - 45.90]	40.87 ± 8.81	0.07[5]
Protein - AqH (mg/ml)	0.75 ± 0.38	0.62 [0.50-0.98]	0.81 [0.75-0.90]	1.12 ± 0.44	0.81 [0.61-1.08]	1.04 ± 0.46	0.85 [0.78-0.85]	0.23[4]
ET-1 - Plasma (pg/ml)	1.92 [1.75-2.35]	1.90 [1.69-2.80]	2.06 [1.69-2.63]	2.21 ± 0.35	2.28 ± 0.71	2.72 ± 0.73	2.78 ± 0.65	0.20[4]
ET-1 - AqH (pg/ml)	3.36 [3.08-4.51]	4.18 [3.96-4.34]	3.93 ± 0.98	5.57 ± 1.42	4.26 ± 1.43	5.76 ± 1.74	3.56 ± 0.97	0.016[4]
GCC (µm)	94.15 ± 12.74	90.56 ± 6.25	74.71 ± 10.14	81.30 ± 9.03	73.00 [68.00-78.00]	73.00 ± 6.97	63.00 ± 6.66	<0.00001[4]
Focal Loss Volume (%)	0.49 [0.31-1.61]	2.15 ± 1.93	3.50 ± 3.92	5.02 ± 4.75	7.66 ± 4.02	6.31 ± 2.89	9.69 ± 2.36	<0.00001[4]
Global Loss Volume (%)	2.10 [0.56-6.29]	5.84 ± 4.39	17.56 ± 12.33	15.12 ± 7.34	21.30 ± 7.85	24.07 ± 5.75	33.64 ± 6.11	<0.00001[4]
RNFL (µm)	97.57 ± 7.80	86.56 ± 5.64	74.17 ± 5.53	75.90 ± 5.86	68.87 ± 7.57	66.00 ± 8.90	53.33 ± 9.07	<0.00001[5]
RNFL superior (µm)	118.37 ± 10.18	100.15 [96.40-101.13]	91.13 ± 4.83	90.02 ± 11.22	81.34 ± 15.18	69.82 ± 11.02	56.89 ± 5.61	<0.00001[4]
RNFL inferior (µm)	121.20 ± 12.07	109.71 ± 11.33	91.89 ± 5.16	86.39 [85.79-91.10]	75.40 ± 7.03	67.57 ± 4.74	58.22 ± 10.92	<0.00001[4]
Cup/Disc Ratio Total	0.35 ± 0.17	0.50 ± 0.20	0.54 ± 0.22	0.55 ± 0.17	0.64 ± 0.14	0.76 ± 0.12	0.81 ± 0.07	<0.00001[5]

Parameter	Healthy	Border	Stage 1	Stage 2	Stage 3	Stage 4	Stage 5	P-Value
Cup/Disc Ratio Vertical	0.56 [0.48-0.66]	0.66 ± 0.15	0.72 ± 0.16	0.71 ± 0.15	0.81 ± 0.12	0.90 ± 0.06	0.93 ± 0.05	<0.00001[4]
Cup/Disc Ratio Horizontal	0.61 [0.52-0.71]	0.73 ± 0.21	0.78 ± 0.18	0.74 ± 0.18	0.89 [0.77-0.91]	0.95 [0.93-0.96]	0.94 ± 0.04	<0.00001[4]
Rim Area (mm^2)	1.34 ± 0.36	1.03 ± 0.41	0.90 ± 0.42	0.78 ± 0.24	0.69 ± 0.24	0.53 ± 0.27	0.39 ± 0.11	<0.00001[5]
Disc Area (mm^2)	2.07 ± 0.33	2.19 ± 0.32	2.00 ± 0.20	1.73 [1.64-1.91]	1.96 ± 0.31	2.17 ± 0.55	2.12 ± 0.16	0.25[5]
Cupvolume (mm^3)	0.13 [0.03-0.26]	0.37 ± 0.31	0.22 ± 0.20	0.22 ± 0.16	0.45 ± 0.37	0.64 ± 0.34	0.55 ± 0.25	<0.001[4]
VD ONH Whole (%)	46.00 [44.20 - 47.70]	38.45 [37.55 - 45.82]	36.44 ± 8.08	36.90 ± 5.86	34.12 ± 4.79	31.21 ± 8.27	29.58 ± 3.98	<0.00001[5]
VD ONH Inside (%)	43.30 [40.10 - 47.80]	40.11 ± 6.37	44.57 ± 5.16	42.38 ± 7.40	43.40 ± 7.72	42.42 ± 5.82	43.43 ± 3.64	0.87[4]
VD PeriONH Average (%)	50.20 [47.00 - 51.70]	45.00 ± 6.97	37.86 ± 10.06	39.59 ± 7.08	34.68 ± 6.13	31.04 ± 9.53	29.28 ± 6.51	<0.00001[5]
VD PeriONH NasSup (%)	46.40 [44.40 - 50.10]	40.70 ± 9.33	35.40 ± 10.79	34.91 ± 9.23	33.19 ± 7.14	27.89 ± 10.07	28.75 ± 5.87	<0.00001[5]
VD PeriONH NasInf (%)	44.36 ± 6.03	38.36 ± 7.11	33.91 ± 9.48	35.05 ± 7.05	32.05 ± 7.83	28.24 ± 9.96	28.33 ± 8.19	<0.00001[5]
VD PeriONH InfNas (%)	48.20 [45.00 - 52.10]	47.30 ± 6.15	37.43 ± 10.97	33.58 ± 8.81	31.75 ± 7.67	24.69 ± 10.19	21.42 ± 4.43	<0.00001[4]
VD PeriONH InfTemp (%)	54.70 [50.80 - 57.70]	50.24 ± 9.18	40.90 ± 12.38	41.72 ± 10.70	38.20 ± 10.26	26.19 ± 11.64	23.50 ± 5.02	<0.00001[5]
VD PeriONH TempInf (%)	51.60 [48.10 - 53.60]	49.42 ± 13.33	45.20 ± 8.13	45.58 ± 7.34	42.71 ± 6.70	41.12 ± 6.92	38.77 ± 11.32	<0.001[5]
VD PeriONH TempSup (%)	53.80 [52.20 - 57.00]	54.58 ± 5.84	47.32 ± 8.83	47.42 ± 6.71	46.54 ± 8.27	44.84 ± 9.35	39.12 ± 7.77	<0.0001[5]
VD PeriONH SupTemp (%)	52.03 ± 6.18	48.81 ± 8.61	37.99 ± 13.15	40.43 ± 12.23	31.71 ± 10.01	32.95 ± 12.55	26.52 ± 8.92	<0.00001[5]
VD PeriONH SupNas (%)	49.20 [44.90 - 52.50]	40.08 ± 7.83	34.30 ± 13.18	42.90 [37.35-45.12]	29.56 ± 7.07	24.68 ± 11.60	25.90 ± 9.24	<0.00001[5]
VD Macula SVP Whole (%)	41.28 ± 4.49	41.67 ± 2.96	37.19 ± 4.46	36.61 ± 4.22	36.81 ± 3.42	35.65 ± 3.47	33.80 ± 3.64	<0.00001[5]
VD Fovea SVP (%)	19.07 ± 6.39	19.91 ± 11.26	17.66 ± 4.63	17.66 ± 4.51	18.39 ± 6.98	21.09 ± 8.92	8.20 ± 2.51	0.042[4]
VD ParaFovea SVP Average (%)	41.55 ± 6.21	40.38 ± 4.63	39.69 ± 4.41	39.00 [37.05-40.38]	39.90 ± 4.74	39.06 ± 4.42	38.92 ± 5.39	0.94[4]
VD PeriFovea SVP Average (%)	41.93 ± 4.68	42.42 ± 3.08	37.49 ± 4.88	36.53 ± 4.61	37.19 ± 3.43	35.79 ± 3.28	33.62 ± 3.36	<0.00001[5]
VD PeriFovea SVP Temp (%)	38.46 ± 5.33	38.03 ± 4.28	35.36 ± 4.64	33.58 ± 5.55	34.64 ± 3.49	34.15 ± 2.88	33.47 ± 3.99	0.010[5]

Parameter	Healthy	Border	Stage 1	Stage 2	Stage 3	Stage 4	Stage 5	P-Value
VD PeriFovea SVP Sup (%)	41.04 ± 5.33	41.10 ± 3.92	37.37 ± 4.35	35.34 ± 4.73	36.22 ± 3.70	36.21 ± 4.07	32.25 ± 3.01	<0.0001[5]
VD PeriFovea SVP Nas (%)	46.58 ± 4.80	47.07 ± 4.22	41.33 ± 6.88	41.07 ± 5.04	41.28 ± 4.81	42.00 [36.38-42.42]	36.45 ± 4.45	<0.00001[5]
VD PeriFovea SVP Inf (%)	41.54 ± 4.77	43.53 ± 2.90	35.94 ± 5.75	36.15 [35.28-36.72]	36.23 ± 3.62	33.84 ± 3.00	31.92 ± 4.57	<0.00001[5]
VD Macula DVP Whole (%)	41.29 ± 3.83	39.08 ± 5.30	40.96 ± 5.41	38.80 [37.62-40.10]	41.50 ± 4.68	42.69 ± 5.37	44.40 ± 6.69	0.39[5]
VD Fovea DVP (%)	34.07 ± 7.30	30.72 ± 13.26	35.13 ± 8.39	33.07 ± 3.03	33.78 ± 7.68	34.54 ± 8.55	23.73 ± 6.22	0.11[4]
VD ParaFovea DVP Average (%)	48.95 ± 3.19	45.57 ± 4.79	46.51 ± 4.48	47.08 ± 3.31	47.18 ± 5.14	47.80 ± 5.64	50.43 ± 6.58	0.43[4]
FAZ (mm²)	0.27 ± 0.09	0.39 ± 0.20	0.23 ± 0.10	0.28 ± 0.10	0.24 ± 0.09	0.25 ± 0.11	0.38 ± 0.03	0.027[4]
AI	1.08 [1.07-1.09]	1.11 [1.09-1.16]	1.10 ± 0.03	1.09 [1.08-1.16]	1.10 ± 0.05	1.09 ± 0.04	1.11 ± 0.03	0.11[4]
Topical Antiglaucomatosa	2.00 [1.00-4.00]	3.00 [1.00-3.00]	2.00 ± 1.90	2.56 ± 1.01	2.00 [2.00-4.00]	3.00 [3.00-3.25]	2.00 ± 1.41	0.57[4]
Topical Beta-Blocker n (%)	5 (45.5%)	1 (20.0%)	3 (50.0%)	7 (77.8%)	13 (76.5%)	7 (87.5%)	2 (33.3%)	0.07[3]
Topical Carbonic Anhydrase Inhibitor n (%)	7 (63.6%)	3 (60.0%)	4 (66.7%)	6 (66.7%)	11 (64.7%)	8 (100.0%)	3 (50.0%)	0.47[3]
Topical Prostaglandine Analogue n (%)	9 (81.8%)	4 (80.0%)	3 (50.0%)	5 (55.6%)	13 (76.5%)	8 (100.0%)	4 (66.7%)	0.29[3]
Topical Alpha Adrenergic Agonist n (%)	5 (45.5%)	2 (40.0%)	2 (33.3%)	2 (22.2%)	5 (29.4%)	3 (37.5%)	2 (33.3%)	0.97[3]
Topical Pilocarpine n (%)	0 (0.0%)	0 (0.0%)	0 (0.0%)	0 (0.0%)	1 (5.9%)	0 (0.0%)	1 (16.7%)	0.68[3]
Systemic Carbonic Anhydrase Inhibitor n (%)	2 (18.2%)	0 (0.0%)	1 (16.7%)	0 (0.0%)	0 (0.0%)	1 (12.5%)	1 (16.7%)	0.26[3]

ACG - angle-closure glaucoma, Adj - Adjusted, AqH-aqueous humour, Cont-Controls, DVP - deep vascular plexus, ET-1-Endothelin-1, FAZ-foveal avascular zone, Glauc - Glaucoma, IOP-Intraocular pressure, iStent® - Trabecular Micro-Bypass Device, NTG - normal-tension glaucoma, ONH-optic nerve head, PG - pigmentary glaucoma, POAG - primary open-angle glaucoma, RNFL-retinal nerve fiber layer, SVP - superficial vascular plexus, TE - trabeculectomy, XEN - XEN® Gel Stent, XFG - exfoliation glaucoma. Tests:[1]T-test, [2]Chi²-test, [3]Fisher-test, [4]Kruskal-Wallis Test, [5]ANOVA, [6]Tukey-Test, [7]Dunn-Test

3.4 Endothelin-1- and protein-level in plasma and AqH

The ET-1, Big ET-1 and protein levels were analysed. The ET-1 levels in plasma (p=<0.00001) and AqH (p=<0.001) of glaucoma patients were significantly elevated compared to the group of control patients (Table 3, Figure 1 A, B).

The ET-1 levels in the AqH of glaucoma patients were significantly higher than in the corresponding plasma samples of glaucoma patients ($p < 0.001$) but nevertheless no significant correlation between them was discovered (p=0.84, r=−0.029, Figure 2C). Likewise, no significant correlation between AqH and plasma ET-1 levels were found when looking at the control group (p=0.254, r=-0.254) or both groups together (p=0.434, r=0.092).

When analysing the levels of Big ET-1, no significant differences in the Big ET-1 level in neither plasma nor AqH between both groups were found, as the levels in all groups were almost undetectably low (Table 3).

The protein concentration in the plasma (p<0.001) and AqH (p=0.005) of the glaucoma group was significantly higher than in the control group (Table 3). The plasma protein concentration of the glaucoma group correlated significantly positively with the plasma ET-1 level (r=0.33, p=0.006), while the plasma protein and AqH ET-1 level did not (r=-0.067, p=0.63). Likewise, no correlation between the plasma and AqH proteins levels in the glaucoma group could be found (r=-0.012, p=0.924).

The correlation of the ET-1 levels in AqH and plasma of the glaucoma patients with clinical parameters and OCT measurements were analysed. It became apparent that increased plasma ET-1 in the glaucoma group correlated significantly positively with the patient's age (p=0.035), refraction (p=0.031), disc area (p<0.01) and vertical CDR (p=0.044) (Table 3).

There was a significant negative correlation of plasma ET-1 levels in glaucoma patients with increases in IOP (p=0.030) and superior hemisphere RNFL thickness (p=0.049). No significant correlations between glaucomatous plasma ET-1 and inferior hemisphere RNFL thickness, and between glaucomatous AqH ET-1 levels and RNFL thickness in either hemisphere were found (Table 3).

Looking at the VD and other OCT-A parameters in comparison with the glaucomatous plasma ET-1 levels, significant negative correlations were discovered

between the temporal superior sector in the peripapillary region (PeriONH TempSup) (p=0.007, r=-0.348) and the SVP (p=0.007, r=-0.323) and DVP (p=0.006, r=-0.331) layer of the fovea (Table 6). Additionally, there was a significant positive correlation of the plasma ET-1 level and the FAZ (p=0.035, r=0.256).

The AqH ET-1 level in glaucoma patients did not correlate with the lens status and IOP, but significant positive correlations with the amount of used topical antiglaucoma medications were found (p=0.006, r=0.374) (Table 6).

In order to investigate whether this correlation might be due to an increased amount of used antiglaucoma medication because of a more elevated IOP, a subgroup analysis (Group 1 IOP ≤18 mmHg Group 2 IOP 19–24 mmHg Group 3 IOP ≥25 mmHg) was performed. No significant differences in the number of different topical antiglaucoma drugs between the three IOP groups could be found (Kruskal Wallis p=0.494). Within the glaucoma group, Wilcoxon rank sum tests for AqH ET-1 level and the different topical antiglaucoma medications were performed. Of the glaucoma group (N=68), 39.7% (N=23) used topical alpha adrenergic agonists and there was no significant difference in AqH ET-1 level (4.16 [3.65-5.17] vs 5.20[±1.72] pg/ml; p=0.192); 74.1% (N=43) used topical beta blockers and the AqH ET-1 level was significantly higher within the beta blocker group (3.92 [3.14-4.68] vs. 4.59 [3.95-5.62] pg/ml; p=0.039); 81.0% (N=47) used topical CA inhibitors and the AqH ET-1 level was significantly higher in the CA inhibitor group (4,05 [±1.13] vs. 4.59 [3.88-5.88] pg/ml; p=0.032); 87.9% (N=51) used topical prostaglandin analogues and there was no significant difference in AqH ET-1 level (3.98 [3.66-4.38] vs. 4.85 [±1,59] pg/ml; p= 0.254). These tests did not take into account whether several topical medications were used simultaneously.

For the determination of the reference ranges of “normal” and “high” plasma levels of ET-1, in accordance with previous literature[70,71], we defined the “normal” range of plasma ET-1 by determining the inner 90% (1.645 SD under assumption of normal distribution) of the plasma ET-1 levels of the control group, resulting in a “normal” range of 1.01 to 2.49 pg/ml, ≤1.0 pg/ml and ≥2.5 pg/ml therefore being the limits for “low” and “high” respectively. The resulting mean for the “normal” plasma ET-1 group of the controls was 1.75 (± 0.33). When dividing the group of glaucomatous patients according to this definition, 37 patients of the glaucoma group were situated within the normal plasma ET-1 range (1.92±0.33 pg/ml), while

31 patients presented with high levels (3.13 [2.87–3.44] pg/ml; p<0.001). When comparing the “normal” with the “high” plasma ET-1 glaucoma group, numerous significant differences were identified (Table 7). The IOP in the plasma ET-1 “normal” glaucomatous group was significantly lower than in the “high” group (p=0.045), and the plasma protein concentration was significantly higher in the “high” group (p=0.021). Between the two glaucomatous groups there were no significant differences between age, the OCT and OCT-A parameters as well as the OCT-GSS score (Table 5).

When looking at AqH ET-1 levels in the control group with “normal” plasma ET-1 levels, the AqH ET-1 levels of the “normal” (p=0.001) as well as the “high” (p=0.021) plasma ET-1 group were significantly higher. There was no significant difference when only comparing the AqH ET-1 level of the two glaucoma groups.

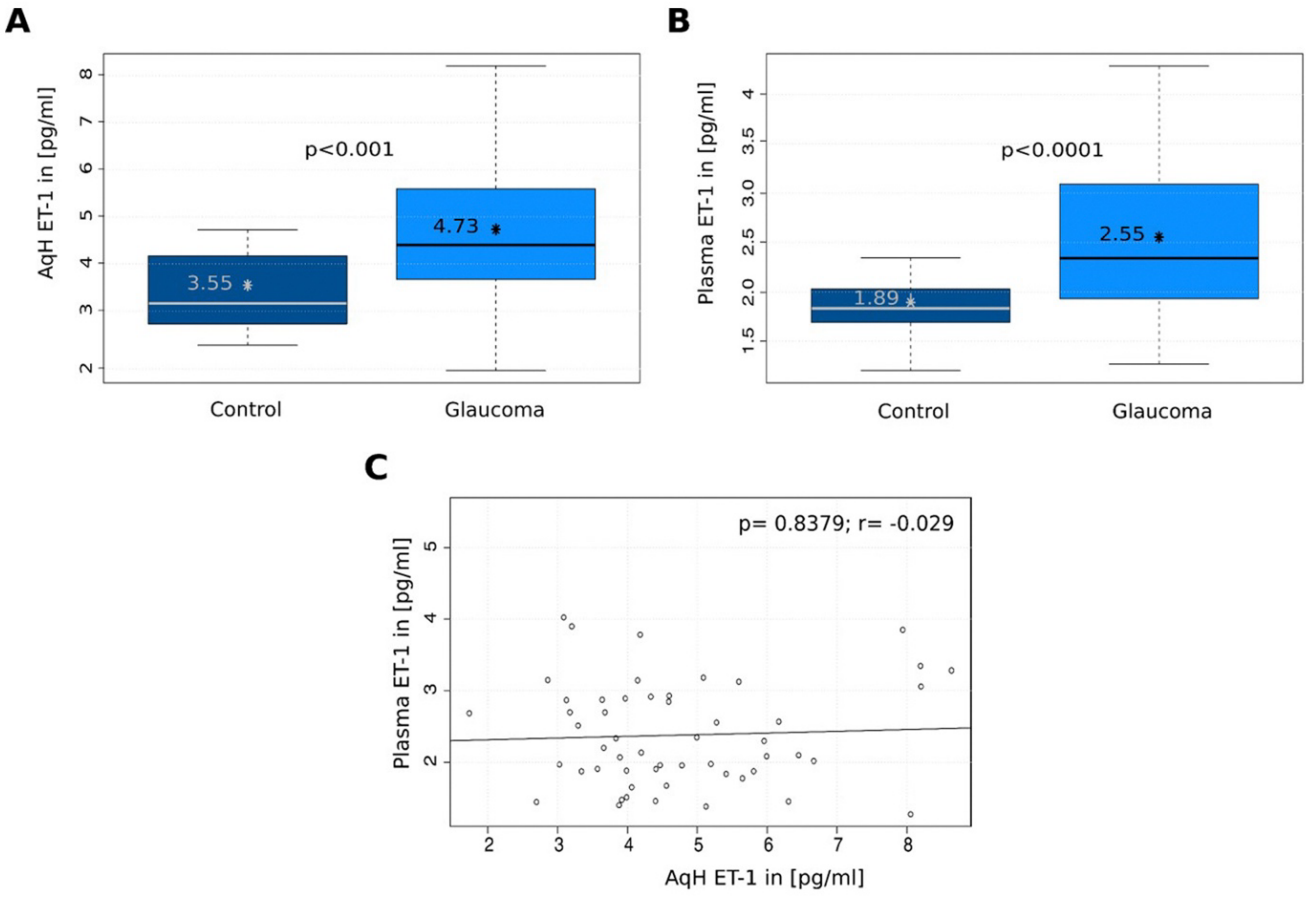

Figure 10 ET-1 level in pg/ml of (A) AqH and (B) plasma samples from cataract and glaucoma patients. (C) Spearman rank correlation of plasma ET-1 level with AqH ET-1 level in the glaucoma group.

Table 5 Plasma and AqH analysis

Parameter	Control, mean ± SD or median with IQR	Glaucoma, mean ± SD or median with IQR	P-value
Protein Concentration – Plasma (mg/ml)	40.21 [38.11 - 42.05]	43.50 ± 5.66	< 0.001[1]
Protein Concentration – AqH (mg/ml)	0.69 ± 0.37	0.85 [0.70 - 1.07]	0.005[1]
ET-1 Concentration – Plasma (pg/ml)	1.83 [1.70 - 2.01]	2.34 [1.94 - 3.07]	< 0.0001[1]
ET-1 Concentration – AqH (pg/ml)	3.16 [2.77 - 4.12]	4.40 [3.68 - 5.59]	< 0.001[1]
Big ET-1 Concentration – Plasma (pg/ml)	0.06 [0.00 – 4.44]	0.00 [0.00 – 3.44]	0.792[1]
Big ET-1 Concentration – AqH (pg/ml)	0.00 [0.00 - 0.00]	0.00 [0.00 - 0.00]	0.626[1]
AqH - aqueous humour, ET-1 - Endothelin-1, Big ET-1- Big Endothelin-1 Tests: [1]Wilcoxon rank sum test			

Table 6 Correlation of ET-1 level in plasma and AqH with clinical, OCT & OCT-A parameters in the glaucoma group

Parameter	ET-1-Plasma [pg/ml]		ET-1-AqH [pg/ml]	
	Glaucoma		Glaucoma	
	Rho	P	Rho	P
Age at OP (years)	0.256	0.035	-0.178	0.200
Refractive Error (dpt)	0.264	0.031	-0.088	0.530
Visual Acuity (LogMAR)	0.131	0.290	-0.060	0.670
IOP (mmHg)	-0.263	0.030	-0.020	0.890
Mean Arterial Pressure (mmHg)	0.020	0.880	0.230	0.130
Ganglion Cell Complex (µm)	-0.205	0.090	0.155	0.270
RNFL Thickness (µm)	-0.164	0.210	0.072	0.630
RNFL Thickness Sup. (µm)	-0.242	<0.050	-0.101	0.480
RNFL Thickness Inf. (µm)	-0.089	0.480	0.086	0.550
Focal Loss Volume (%)	0.210	0.090	-0.147	0.290
Global Loss Volume (%)	0.214	0.080	-0.063	0.660
Cup/Disc Ratio Total	0.192	0.140	-0.066	0.650
Cup/Disc Ratio Vertical	0.261	0.044	0.029	0.850
Cup/Disc Ratio Horizontal	0.119	0.370	-0.013	0.930
Rim Area (mm^2)	-0.091	0.490	0.081	0.580
Disc Area (mm^2)	0.370	0.004	0.024	0.870
Cupvolume (mm^3)	0.209	0.110	0.150	0.310
VD ONH Whole (%)	-0.080	0.520	0.066	0.640
VD PeriONH Average (%)	-0.097	0.430	0.050	0.720
VD PeriONH NasSup (%)	-0.106	0.390	-0.089	0.530
VD PeriONH NasInf (%)	-0.049	0.690	-0.038	0.790
VD PeriONHInfNas (%)	0.065	0.600	0.046	0.750
VD PeriONHInfTemp (%)	0.031	0.800	0.117	0.410
VD PeriONHTempInf (%)	-0.246	0.050	0.201	0.170
VD PeriONHTempSup (%)	-0.348	0.007	-0.001	1.0
VD PeriONHSupTemp (%)	-0.090	0.470	0.103	0.460
VD PeriONHSupNas (%)	-0.088	0.480	-0.032	0.820
VD Macula SVP Whole (%)	-0.012	0.920	-0.011	0.940
VD Macula DVP Whole (%)	-0.023	0.850	-0.037	0.790
VD Fovea SVP (%)	-0.323	0.007	0.177	0.200
VD Fovea DVP (%)	-0.331	0.006	0.204	0.140
VD ParaFoveaSVP Average (%)	-0.113	0.360	0.089	0.530
VD ParaFoveaDVP Average (%)	0.058	0.640	0.058	0.680
VD PeriFoveaSVP Average (%)	-0.006	0.960	-0.005	0.970
VD PeriFovea DVP Average (%)	-0.045	0.710	-0.032	0.820
FAZ (mm^2)	0.256	0.035	-0.110	0.430
OCT-GSS Continuous Score	0.112	(0.380	-0.042	0.780
Number Topical Antiglaucomatosa	-0.126	0.310	0.374	0.006
Systemic Carbonic Anhydrase Inhibitor		0.570		0.550

AqH - aqueous humour, ET-1 - Endothelin-1, VD - vessel density, ONH - optic nerve head, SVP - superficial vascular plexus, DVP - deep vascular plexus, FAZ - foveal avascular zone, RNFL - retinal nerve fiber layer. Tests: Spearman's Rank Correlation Test for all variables

Table 7 Normal vs. high plasma ET-1 within glaucoma group compared to controls

Parameter	Control ET-1 normal	Glaucoma ET-1normal	Glaucoma ET-1 high	P-value	Adj. P: Cont ET-1 norm vs. Glauc. ET-1 norm	Adj. P: Cont ET-1 norm vs. Glauc ET-1 high	Adj. P: Glauc ET-1 norm vs Glauc ET-1 high
Group	Glaucoma:0|Control:27	Glaucoma:37|Control:0	Glaucoma:31|Control:0	< 0.00001[2]			
OCT-GSS Staging	Healthy:19|Border:5|Stage 1:1|Stage 2:1|Stage 3:0|Stage 4:0|Stage 5:0	Healthy:6|Border:2|Stage 1:3|Stage 2:7|Stage 3:11|Stage 4:2|Stage 5:3	Healthy:5|Border:3|Stage 1:3|Stage 2:2|Stage 3:6|Stage 4:6|Stage 5:3	< 0.001[3]			
RNFL Thickness Sup. (µm)	116.04 ± 12.76	88.93 ± 19.84	82.17 ± 18.35	< 0.00001[5]	< 0.00001[6]	<0.00001[6]	0.27[6]
RNFL Thickness Inf. (µm)	120.31 ± 14.49	86.52 ± 18.93	83.06 ± 20.02	< 0.00001[5]	<0.00001[6]	< 0.00001[6]	0.72[6]
OCT GSS Score	0.09 [0.08 - 0.13]	2.46 [1.51 - 3.65]	3.17 [0.74 - 4.50]	< 0.00001[4]	<0.00001[7]	< 0.00001[7]	0.85[7]
Sex	Female:18|Male:9	Female:22|Male:15	Female:19|Male:12	0.84[2]			
Visual Acuity (LogMar)	0.40 [0.30 - 0.60]	0.10 [0.00 - 0.20]	0.20 [0.02 - 0.35]	< 0.00001[4]	<0.00001[7]	< 0.001[7]	0.37[7]
IOP (mmHg)	14.00 [12.00 - 14.00]	20.00 [17.00 - 24.00]	16.00 [13.00 - 18.00]	< 0.00001[4]	< 0.00001[7]	0.009[7]	0.045[7]
MAP (mmHg)	95.00 [93.33 - 100.50]	94.17 [93.33 - 100.42]	93.33 [91.00 - 103.67]	0.84[4]	1.00	0.84	1.00
Protein - Plasma (mg/ml)	40.21 [38.11 - 42.58]	42.02 ± 5.44	45.26 ± 5.48	< 0.001[4]	0.14[7]	< 0.001[7]	0.021[7]
Protein - AqH (mg/ml)	0.70 ± 0.38	0.85 [0.69 - 1.12]	0.88 [0.71 - 1.06]	0.043[4]	0.048[7]	0.032[7]	1.00[7]
ET-1 - Plasma (pg/ml)	1.75 ± 0.33	1.92 ± 0.33	3.13 [2.87 - 3.44]	< 0.00001[4]	0.21[7]	< 0.00001[7]	< 0.00001[7]
ET-1 - AqH (pg/ml)	3.18 [2.88 - 4.17]	4.74 ± 1.21	4.18 [3.25 - 5.43]	0.003[4]	0.001[7]	0.021[7]	0.69[7]
Ganglion Cell Complex (µm)	96.69 ± 8.77	76.00 [68.00 - 87.00]	74.39 ± 11.39	< 0.00001[4]	< 0.00001[7]	< 0.00001[7]	0.41[7]
RNFL (µm)	96.36 ± 8.58	74.51 ± 13.63	70.20 ± 12.13	< 0.00001[5]	< 0.00001[6]	< 0.00001[6]	0.35[6]
Focal Loss Volume (%)	0.40 [0.12 - 1.16]	4.97 [1.53 - 9.12]	7.02 ± 4.55	< 0.00001[4]	< 0.00001[7]	< 0.00001[7]	0.31[7]
Global Loss Volume (%)	2.18 [0.47 - 4.70]	17.61 ± 10.35	21.19 ± 11.41	< 0.00001[4]	< 0.00001[7]	< 0.00001[7]	0.47[7]
Cup/Disc Ratio Total	0.33 ± 0.14	0.62 ± 0.18	0.70 [0.61 - 0.79]	< 0.00001[4]	< 0.00001[7]	< 0.00001[7]	0.49[7]
Cup/Disc Ratio Vertical	0.54 [0.48 - 0.61]	0.76 ± 0.16	0.85 [0.80 - 0.91]	< 0.00001[4]	< 0.00001[7]	< 0.00001[7]	0.12[7]
Cup/Disc Ratio Horizontal	0.60 [0.47 - 0.66]	0.87 [0.72 - 0.92]	0.91 [0.76 - 0.96]	< 0.00001[4]	< 0.0001[7]	< 0.00001[7]	0.34[7]
Rim Area (mm²)	1.33 ± 0.35	0.76 ± 0.36	0.68 [0.47 - 0.87]	< 0.00001[5]	< 0.00001[6]	< 0.00001[6]	0.76[6]
Disc Area (mm²)	2.03 ± 0.34	1.96 ± 0.31	2.17 ± 0.35	0.049[5]	0.67[6]	0.29[6]	0.039[6]
Cupvolume (mm^3)	0.11 [0.05 - 0.20]	0.35 [0.14 - 0.56]	0.49 ± 0.31	< 0.0001[4]	0.003[7]	< 0.0001[7]	0.17[7]
VD ONH Whole (%)	46.84 ± 2.45	35.98 ± 6.45	34.69 ± 7.22	< 0.00001[4]	< 0.00001[7]	< 0.00001[7]	0.95[7]
VD ONH Inside (%)	44.03 ± 4.09	41.21 ± 7.36	45.20 [36.55 - 47.85]	0.22[4]	0.17[7]	1.00[7]	0.27[7]
VD PeriONH Average (%)	50.51 ± 2.73	37.71 ± 8.11	35.54 ± 9.14	< 0.00001[4]	< 0.00001[7]	< 0.00001[7]	0.61[7]
VD Macula SVP Whole (%)	41.39 ± 3.80	37.08 ± 4.04	36.95 ± 4.61	< 0.0001[5]	< 0.001[6]	< 0.001[6]	0.99[6]
VD Fovea SVP (%)	19.86 ± 7.05	17.82 ± 7.44	14.50 [9.05 - 21.30]	0.13[4]	0.39[7]	0.06[7]	0.46[7]
VD ParaFoveaSVP Average (%)	41.21 ± 5.83	39.20 [36.60 - 42.50]	38.70 ± 4.76	0.32[4]	0.70[7]	0.20[7]	0.57[7]
VD PeriFoveaSVP Average (%)	41.93 ± 4.00	37.48 ± 4.48	37.25 ± 4.91	< 0.001[5]	< 0.001[6]	< 0.001[6]	0.98[6]
VD Macula DVP Whole (%)	39.37 ± 3.90	42.08 ± 4.93	41.70 ± 4.78	0.06[5]	0.06[6]	0.15[6]	0.94[6]
VD Fovea DVP (%)	33.91 ± 8.75	33.48 ± 8.21	30.73 ± 7.58	0.26[5]	0.98[6]	0.31[6]	0.35[6]
VD ParaFovea DVP Average (%)	48.25 [47.10 - 49.35]	47.84 ± 4.37	47.61 ± 5.08	0.96[5]	0.97[6]	1.00[6]	0.98[6]
VD PeriFovea DVP Average (%)	39.17 ± 4.84	42.72 ± 5.54	42.18 ± 5.15	0.025[5]	0.025[6]	0.08[6]	0.91[6]
VD PeriFovea DVP Inf (%)	36.17 ± 6.18	40.45 ± 6.24	40.54 ± 5.15	0.008[5]	0.015[6]	0.017[6]	1.00[6]
FAZ (mm²)	0.26 ± 0.10	0.28 ± 0.11	0.26 [0.23 - 0.38]	0.51[4]	0.98[7]	0.39[7]	0.66[7]

Parameter	Control ET-1 normal	Glaucoma ET-1normal	Glaucoma ET-1 high	P-value	Adj. P: Cont ET-1 norm vs. Glauc ET-1 norm	Adj. P: Cont ET-1 norm vs. Glauc ET-1 high	Adj. P: Glauc ET-1 norm vs. Glauc ET-1 high
AI	1.08 [1.07 - 1.10]	1.09 [1.07 - 1.11]	1.11 [1.08 - 1.13]	0.023[4]	0.75[7]	0.016[7]	<0.05[7]
Topical Antiglaucomatosa		3.00 [2.00 - 4.00]	2.00 [1.00 - 3.00]	0.29[1]			
Topical Beta-Blocker (n [%])		26 (70.3%)	17 (54.8%)	0.29[2]			
Topical Carbonic Anhydrase Inhibitor (n [%])		27 (73.0%)	20 (64.5%)	0.63[2]			
Topical Prostaglandine Analogue (n [%])		27 (73.0%)	24 (77.4%)	0.89[2]			
Topical Alpha Adrenergic Agonist (n [%])		12 (32.4%)	11 (35.5%)	0.99[2]			
Topical Pilocarpine (n [%])		2 (5.4%)	0 (0.0%)	0.50[3]			
Systemic Carbonic Anhydrase Inhibitor (n [%])		3 (8.1%)	2 (6.5%)	1.00[3]			

Adj-Adjusted, AqH-aqueous humour, Cont-Controls, DVP-deep vascular plexus, ET-1-Endothelin-1, FAZ-foveal avascular zone, Glauc-Glaucoma, IOP-Intraocular pressure, ONH-optic nerve head, RNFL-retinal nerve fiber layer, SVP-superficial vascular plexus. Tests:[1]T-test, [2]Chi[2]-test, [3]Fisher-test, [4]Kruskal-Wallis Test, [5]ANOVA, [6]Tukey-Test, [7]Dunn-Test

3.5 Multivariable analysis

In accordance with the new findings that have been identified within this research project, multivariable linear regression analyses were conducted to assess the relationship between several independent variables and the OCT-A parameters.

There was special interest in endothelin levels in relation to OCT-A parameters, most notably the VD. Because of their known importance as risk factors for the development of glaucoma, the variables age, IOP and MAP were used together with the ET-1 plasma level as independent variables in the multivariable gaussian linear regression models and tested against the VD OCT-A variables, as well as FAZ, AI and the FD-300µm.

Separate analyses were performed for the entire group of patients with either plasma or AqH ET-1 level as well as for only the group of glaucoma patients with either the plasma ET-1 and AqH ET-1 (Table 8).

When assessing the entire group of patients with plasma ET-1, age, MAP and IOP as independent variables, it becomes apparent that, out of the four chosen independent variables, the IOP yields a significant p-value with the highest number of OCT-A variables (22 out of 38 significant), more than the plasma ET-1 levels (10 out of 38), age (10 out of 38) and MAP (3 out of 38) (Table 8). When exchanging the plasma ET-1 with AqH ET-1 in the analysis of the group of all patients, age yields a significant p-value with the highest number of OCT-A variables (14 out of 38 significant), more than the IOP (13 out of 38), the AqH ET-1 levels (9 out of 38) and the MAP (4 out of 38) (Table 5).

Given the primary focus on glaucoma patients, subgroup analyses were performed within this group using the three independent variables: either plasma or AqH ET-1 levels (analyzed separately), age, and IOP. MAP was excluded in the sub analysis due to the limited number of glaucomatous eyes (N=68), as the number of cases with four independent variables was insufficient to fulfil Cohen's two-step-rule (see 2.2.10). Since MAP had the fewest significant correlations in the previous analysis it was decided to exclude this variable.

In the analysis including plasma ET-1, age, and IOP, IOP was not significantly associated with any of the evaluated OCT-A parameters, while age showed significant associations with five DVP VD parameters and the FD-300µm. The

plasma ET-1 level was significant for the VD of the peripapillary temporal superior sector (PeriONH TempSup) (p=0.006), the VD of the foveal SVP (VD Fovea SVP) (p=0.008) and the VD of the foveal DVP (VD Fovea DVP) (p=0.008) (Table 8). In the sub analysis with AqH ET-1 levels, age and IOP, there were significant correlations for seven variables with age (7 out of 38), one for IOP (1 out of 38) and none for AqH ET-1 level (Table 8).

Table 8 Multivariable linear regression analysis of plasma and AqH ET-1 for all patients and glaucoma group

Parameter	P-Values Multivariable Regression (All Patients)								P-Values Multivariable Regression (Glaucoma Patients)					
	ET1-Plasma				ET-1 AqH				ET1-Plasma			ET-1 AqH		
	ET-1 Plasma	Age	MAP	IOP	ET-1 AqH	Age	MAP	IOP	ET-1 Plasma	Age	IOP	ET-1 AqH	Age	IOP
VD ONH Whole (%)	0.007	0.45	0.36	< 0.001	0.049	0.18	0.76	0.025	0.44	0.80	0.53	0.62	0.89	0.75
VD ONH Inside (%)	0.82	0.43	0.11	0.31	0.05	0.54	0.22	0.96	0.82	0.31	0.90	0.51	0.29	0.50
VD PeriONH Average (%)	0.007	0.49	0.47	< 0.001	0.07	0.23	0.90	0.039	0.44	0.83	0.54	0.55	1.00	0.74
VD PeriONH NasSup (%)	0.016	0.38	0.18	0.001	0.011	0.17	0.57	0.05	0.50	0.55	0.51	0.53	0.68	0.89
VD PeriONH NasInf (%)	0.025	0.11	0.22	< 0.001	0.049	0.030	0.64	0.006	0.53	0.18	0.13	0.97	0.22	0.35
VD PeriONHInfNas (%)	0.11	0.82	0.65	0.001	0.11	0.85	0.93	0.021	0.60	0.48	0.51	0.51	0.40	0.81
VD PeriONHInfTemp (%)	0.06	0.78	0.80	0.009	0.15	0.38	0.70	0.09	0.59	0.83	0.98	0.35	0.88	0.69
VD PeriONHTempInf (%)	0.002	0.73	0.56	0.046	0.34	0.46	0.81	0.60	0.07	0.72	0.71	0.30	0.47	0.08
VD PeriONHTempSup (%)	0.002	0.94	0.19	0.09	0.06	0.90	0.33	0.92	0.006	0.96	0.84	0.51	0.90	0.29
VD PeriONHSupTemp (%)	0.015	0.70	0.65	0.014	0.34	0.83	0.86	0.15	0.36	0.52	0.95	0.14	0.35	0.34
VD PeriONHSupNas (%)	0.007	0.48	0.81	< 0.001	0.044	0.32	0.82	0.033	0.51	0.71	0.46	0.94	0.99	0.98
VD Macula SVP Whole (%)	0.18	0.33	0.20	0.001	0.022	0.042	0.12	0.011	0.96	0.88	0.53	0.82	0.53	0.82
VD Fovea SVP (%)	0.006	0.79	0.10	0.47	1.00	0.62	0.17	0.75	0.008	0.84	0.64	0.63	0.57	0.82
VD ParaFoveaSVP Average (%)	0.42	0.17	0.22	0.020	0.44	0.026	0.09	0.07	0.37	0.46	0.24	0.84	0.19	0.49
VD ParaFoveaSVPTemp (%)	0.62	0.54	0.17	0.05	0.11	0.22	0.09	0.25	0.45	0.98	0.55	0.38	0.64	0.86
VD ParaFoveaSVPSup (%)	0.39	0.41	0.45	0.10	0.79	0.14	0.24	0.28	0.22	0.96	0.68	0.55	0.63	0.90
VD ParaFoveaSVPNas (%)	0.56	0.18	0.29	0.19	0.99	0.08	0.31	0.41	0.47	0.16	0.25	0.93	0.14	0.50
VD ParaFoveaSVPInf (%)	0.37	0.06	0.44	0.002	0.31	0.005	0.18	0.005	0.88	0.32	0.12	0.65	0.07	0.14
VD PeriFoveaSVP Average (%)	0.19	0.35	0.22	< 0.001	0.015	0.048	0.17	0.007	0.93	0.98	0.46	0.86	0.66	0.75
VD PeriFoveaSVP Temp (%)	0.55	0.74	0.13	0.018	0.034	0.18	0.09	0.06	0.78	0.84	0.77	0.26	0.70	0.83
VD PeriFoveaSVPSup (%)	0.28	0.43	0.26	0.003	0.031	0.09	0.22	0.020	0.82	0.89	0.69	0.67	0.91	0.79
VD PeriFovea SVPNas (%)	0.06	0.33	0.17	0.001	0.005	0.07	0.22	0.026	0.44	0.90	0.46	0.63	0.60	0.86
VD PeriFoveaSVPInf (%)	0.19	0.26	0.44	< 0.001	0.06	0.043	0.34	0.003	0.63	0.85	0.28	0.85	0.56	0.46
VD Macula DVP Whole (%)	0.37	0.004	0.23	0.10	0.68	0.010	0.12	0.16	0.76	0.028	0.27	0.26	0.024	0.18

Parameter	P-Values Multivariable Regression (All Patients)								P-Values Multivariable Regression (Glaucoma Patients)					
	ET1-Plasma				ET-1 AqH				ET1-Plasma			ET-1 AqH		
	ET-1 Plasma	Age	MAP	IOP	ET-1 AqH	Age	MAP	IOP	ET-1 Plasma	Age	IOP	ET-1 AqH	Age	IOP
VD Fovea DVP (%)	0.011	0.22	0.037	0.59	0.68	0.12	0.08	0.66	0.008	0.12	0.90	0.63	0.12	0.75
VD ParaFovea DVP Average (%)	0.52	0.003	0.06	0.005	0.56	0.006	0.036	0.032	0.53	0.016	0.12	0.27	0.016	0.14
VD ParaFovea DVP Temp (%)	0.54	0.05	0.005	0.043	0.79	0.08	0.006	0.10	0.74	0.05	0.13	0.31	0.06	0.22
VD ParaFovea DVP Sup (%)	0.56	0.012	0.72	0.023	0.68	0.027	0.75	0.11	0.33	0.08	0.42	0.98	0.15	0.66
VD ParaFovea DVP Nas (%)	0.83	0.18	0.69	0.24	0.71	0.32	0.63	0.40	0.59	0.10	0.32	0.27	0.14	0.28
VD ParaFovea DVP Inf (%)	0.44	0.008	0.08	0.011	0.30	0.006	0.035	0.030	0.54	0.022	0.07	0.12	0.007	0.046
VD PeriFovea DVP Average (%)	0.40	0.005	0.32	0.11	0.81	0.011	0.15	0.17	0.91	0.031	0.19	0.31	0.023	0.13
VD PeriFovea DVP Temp (%)	0.68	0.017	0.15	0.027	0.19	0.010	0.16	0.06	0.55	0.06	0.20	0.08	0.022	0.16
VD PeriFoveaDVP Sup (%)	0.32	0.005	0.69	0.08	0.54	0.012	0.40	0.17	0.68	0.07	0.28	0.60	0.08	0.29
VD PeriFovea DVP Nas (%)	0.34	0.028	0.79	0.45	0.99	0.09	0.42	0.49	0.94	0.031	0.22	0.29	0.023	0.11
VD PeriFovea DVP Inf (%)	0.20	0.034	0.31	0.22	0.62	0.06	0.13	0.26	0.61	0.13	0.21	0.59	0.11	0.10
FAZ (mm^2)	0.21	0.84	0.21	0.73	0.81	0.82	0.44	0.68	0.09	0.66	0.86	0.35	0.81	0.57
AI	0.52	0.34	0.26	0.54	0.68	0.51	0.52	0.86	0.39	0.20	0.82	0.55	0.49	0.68
FD300µm (%)	0.96	0.012	0.025	0.61	0.76	0.009	0.026	0.63	0.77	0.011	0.72	0.19	0.012	0.68

VD – vessel density, ONH – optic nerve head, SVP – superficial vascular plexus, DVP - deep vascular plexus, FAZ - foveal avascular zone, AI - acircularity index, FD300µm - foveal density 300µm

4. Discussion

4.1 OCT-A in glaucoma

To date, the pathogenesis of glaucoma, particularly POAG, remains incompletely elucidated. Traditionally, elevated IOP exceeding 21 mmHg has been recognized as the predominant and most critical risk factor for the onset and advancement of OAG. Consequently, pharmacological or surgical reduction of IOP constitutes the sole modifiable risk factor in the majority of cases[10,23]. Furthermore, it becomes increasingly evident that a substantial subset of individuals with POAG manifests NTG, despite never exhibiting a clinically defined elevation in IOP[12–15]. One may therefore raise the question of IOP monitoring consistently represents the most appropriate diagnostic and surveillance tool for POAG and NTG. Moreover, given that pharmacological reduction of IOP remains among the limited therapeutic choices, patients who receive a diagnosis typically undergo medication administration, often leading to normalized IOP levels. Although this approach has been demonstrated to significantly delay disease progression, it does not completely arrest its course[112].

Computer-assisted visual field measurement (perimetry) is an important tool for the diagnosis of glaucoma and for monitoring the progression of damage. As previously discussed, severe limitations arise because 30% to 50% of RGCs are already irreversibly lost before subjective changes during perimetry can be detected, combined with a high test-retest variability[22,23,25,27,81]. As the loss of RGCs is irreversible, it is of great importance to diagnose glaucomatous damage at the pre-perimetric stage of disease in order to stop or slow progression even before significant perimetric changes occur. In many cases, this can lead to an improvement of quality of life and a reduction of socio-economic burden.

Until today, the European Glaucoma Association's Guidelines (5th Edition, 2021) name the combination of Goldmann applanation tonometry, visual acuity, perimetry and ophthalmoscopy the gold standard for diagnosis and follow-up of glaucoma[113]. As elaborated, this modality unfortunately makes early cases of glaucoma, especially POAG and NTG, very difficult to detect.

Since its clinical introduction in 2006 the OCT has been rapidly evolved and widely implemented in diagnosing and monitoring of glaucoma and other retinal diseases.

Contemporary ophthalmology relies heavily on this technology, which has become indispensable for early disease detection and meticulous patient follow-up[114]. Even though it is acknowledged that glaucoma diagnosis should not be reduced to OCT only, but used it in conjunction with IOP, perimetry and ophthalmoscopy, the author does not agree with the restraint of using OCT technologies in the current European Glaucoma Society Guidelines[113]. Since the value and potential of SD-OCT has been well established, this research focused on the further development of this technology, the OCT-A, which is clinically in use since 2014 and not yet widely implemented[85,89]. The principle of OCT-A has been described in section (1.5). OCT-A represents an intriguing advancement, as accumulating evidence indicates that quantification of the VD can discern alterations at earlier disease stages and continue to be informative even in more advanced phases, surpassing the limitations imposed by the floor effect encountered with SD-OCT[115]. The floor effect describes the situation where SD-OCT measurements can no longer detect further thinning of the RNFL, while clinical and visual field deteriorations continue. The floor effect is thought to be caused by residual material like vessels and glial cells, as well as limitations of software and imaging hardware[115]. It commonly ranges from around 45-60µm, depending on the dynamic range of the used OCT machine and the proprietary software used[115].

This dissertation has demonstrated that in the group of glaucoma patients, next to the RNFL and GCC, the VD of the ONH whole area, as well as all PeriONH quadrants are significantly reduced as compared to the control group. These findings confirm the results of several prior investigations, which have consistently demonstrated favourable performance in terms of area under the receiver operating characteristics (AUROC) when assessing VD using OCT-A, in contrast to measurements of RNFL obtained via SD-OCT[76,116–119]. In the context of macular VD, the present study identified statistically significant differences between the groups in whole macular VD within the superficial vascular plexus (SVP). However, no such differences were observed in the deep vascular plexus (DVP). These findings align with a recently published study that reported similar results[120]. Likewise, the VD of perifoveal sectors was significantly lower in the SVP and to a lesser extend in the DVP (Table 2). These findings correspond to other recently published studies[77,120].

Consistent with these research findings, accumulating evidence indicates that decreases in OCT-A derived VD parameters may occur prior to reductions in RNFL thickness as measured by SD-OCT. Consequently, this suggests that OCT-A could potentially facilitate the earlier detection of glaucoma[76,116–128].

For instance, Chen et al. established that in patients with POAG, including NTG, who exhibited visual field defects in one hemisphere but not yet in the other, RNFL thinning was only detectable by SD-OCT in the affected hemisphere. Interestingly, VD reduction was detectable in the affected hemisphere and, to a lesser degree, in the yet unaffected hemisphere[124]. However, not all similar studies can confirm that VD reduction precedes RNFL thinning in perimetrically unaffected sectors at this point of time[128].

While it remains uncertain whether a reduction in VD consistently precedes RNFL thinning, additional confirmation is necessary. Nevertheless, the current findings are promising.

Additionally, the previously mentioned lack of a floor effect in OCT-A as described by for example Mwanza et al. and Moghimi et al. suggest that OCT-A is superior in monitoring late-stage glaucomatous progression[115,129].

In the context of the vascular theory of glaucoma pathophysiology, which is increasingly gaining attention over the traditional mechanical theory (see chapter 1.4.1 & 1.4.4), the visualization of retinal vasculature and blood supply are becoming more important than ever before. The results of this research therefore point to the assumption that OCT-A imaging presents the most promising technology for this objective and will become gradually more implemented in everyday use.

These findings further emphasize that VD measured by OCT-A is a valuable tool in glaucoma diagnosis and presumably also the follow-up of the disease. It is evident that further longitudinal research is necessary to validate the hypothesis that VD measurements obtained via OCT-A outperform RNFL and GCL measurements for early glaucoma detection and late-stage follow-up. If this hypothesis can be substantiated, OCT-A has the potential to emerge as a pivotal non-invasive tool for glaucoma diagnosis and longitudinal monitoring. Its utilization could facilitate early implementation of treatment strategies and preventive measures, thereby

enhancing patients' quality of life and mitigating the socioeconomic burden associated with advanced-stage glaucoma.

4.2 OCT-GSS with OCT-A and ET-1

To the current knowledge, this study is the first study to investigate the usability of Brusini's OCT-GSS with OCT as well as OCT-A parameters[95]. While the predecessor, the GSS 2 has been implemented as one of the most commonly used glaucoma staging systems for many years, its value is severely constrained by the fact that the GSS 2 is only based on perimetry results[94]. In a recent study conducted by Zhen et al., significant correlations were observed between the older GSS 1 score based on perimetry and the macular and peripapillary VD measured using OCT-A[118]. The VD measurements were further segmented into central, inner, outer, and full sectors.

Because of the previously discussed limitations of glaucoma staging systems based on perimetry, there was great interest whether these results could be reproduced when comparing with an OCT-based staging system. Classification based on OCT values bears several advantages, because, as previously mentioned, at least 30-50% of RGCs are irreversibly lost before perimetry changes are detected. The OCT-GSS uses RNFL measurements of the superior and inferior quadrant to classify the eye as either healthy, borderline or stage one to five and is being implemented into the clinical practice since 2018 (see 1.5.2). While larger confirmation studies are currently lacking, a recent comparative study conducted by Mossa et al. comparing the GSS 2 with the OCT-GSS indicates that the OCT-GSS is likely more sensitive than the GSS 2[130].

A study by De Jesus et al. has analysed peripapillary VD in several sectors and layers and developed three different machine learning models for the classification of glaucoma severity in POAG and NTG patients[131]. All three models reached slightly higher AUROCs than RNFL thickness in differentiating healthy from glaucomatous eyes, the vascular models were also better in classifying glaucoma severity than the RNFL model. Interestingly, the inferotemporal sector in the superficial layer was the single most discriminant feature for severity classification, but when combining the data of all measured layers into one model, added value

for classification was noted[131]. These results are interesting and in line with the results of this dissertation. Even though it will be interesting to investigate whether these models can be confirmed with larger sample sizes and be implemented in user friendly software, the study of De Jesus et al. has several limitations. In the severity classification, only four grades were employed: healthy, mild, moderate, and severe. Also, a substantial volume of data points needs to be gathered and integrated within sophisticated software.

Therefore, a system that is based on a commonly known and widely used classification system like the GSS 2 and uses the same severity grades, combined with a simple to use online-interface, might be preferable in the clinical practice. These features could reduce the inhibition threshold of using the classification system and using the same grades would make comparing results easier on an everyday basis. Finer grades, including the borderline stage also allow earlier diagnosis and more specific classification.

While the classification of the OCT-GSS is based on the SD-OCT measurements of the RNFL, the current research was able to demonstrate significant correlations with the VD of the whole ONH region, as well as the VDs of all subdivided PeriONH areas. Additionally, significant correlations of the OCT GSS score with VD of the whole macula in the SVP layer, the foveal SVP layer and all perifoveal sectors in the SVP layer were found. The fact that the fovea and most parafoveal sectors in both layers are not significantly related to the OCT-GSS can likely be explained by the anatomy of the retina in the foveal area, as the RGCs are absent at the macula and progressively gain thickness towards the peripheral regions, i.e. the peri-foveal sectors.

Even though significant differences of most perifoveal sectors in the DVP when comparing healthy patients with glaucoma patients were demonstrated, the VD of the perifoveal DVP layers was not significantly correlated to the OCT-GSS, while the VD of the SVP sectors was. These interesting outcomes indicate that the close relations of VD and RNFL in glaucoma, that have been discussed in the previous section, appear to be transferable to the OCT GSS. Naturally, further confirmation studies are required and an adaption of the original OCT GSS's software by the author would be needed to reach consensus on cut-off values for OCT-A parameters. Should one succeed in updating the OCT GSS to include OCT-A

values, an already powerful glaucoma staging tool could become even more powerful and efficient. As previously discussed, under certain circumstances, VD decreases can be detectable before RNFL changes and implementation of these values could therefore help to increase the sensitivity for early glaucomatous damage even further. Since the OCT-A, unlike the OCT, presumably has no lower limit of measurement if the dynamic range is sufficient, the implementation of VD values in the OCT-GSS could also classify and track late-stage changes more accurately in an updated version of the OCT-GSS[129]. Even though the current study did not include the perimetry results, a significant positive correlation of the LogMar and OCT-GSS could be detected.

To the most recent knowledge, for the first time, this study detected a significantly positive correlation of the OCT-GSS with plasma ET-1 levels, which leads to several interesting conclusions and assumptions about the pathophysiology that will be addressed in detail in the following section.

The study results support the assertion that the OCT-GSS serves as a valuable instrument for early glaucoma diagnosis and long-term monitoring. When used in conjunction with OCT-A, its versatility and sensitivity seem to be further enhanced. For a comprehensive assessment, it is ideal to combine the findings from the OCT-GSS with relevant clinical parameters such as IOP and frequent perimetry measurements. This holistic approach ensures a more thorough understanding of the patient's condition.

4.3 AqH ET-1 and plasma ET-1

Within the vascular theory of glaucomatous pathophysiology (see 1.4.4), ET-1 is increasingly gaining attention as a potential contributor and new biomarker[132].

In the years after the initial discovery of ET-1 and the endothelin receptors in the ocular tissues including the retina, several research groups, including Yorio et al. have strengthened the hypothesis that ET-1 plays a role in the pathogenesis of glaucoma[133]. It has been demonstrated that ET-1 is part of the physiologic autoregulatory mechanisms of ocular and retinal blood flow and, in healthy conditions, stays tightly balanced with endogenous vasodilatory substances like NO (see 1.4.4.3 and 1.4.4.4). As described earlier, the retinal RGCs have a very

high rate of metabolism and are therefore extremely susceptible to ischemic damage. The vasoconstrictive effects of ET-1 may play a pivotal role in elucidating the pathophysiology of OAG. Notably, in patients with NTG, the occurrence of severe optic neuropathy despite the absence of elevated IOP remains an intriguing phenomenon. Besides evidence of elevated systemic ET-1 levels in POAG and NTG patients, Henry et al. have demonstrated that POAG patients with normal plasma ET-1 levels present with abnormal systemic vasoreactivity that appears to be in part based on ET-A-R overactivation and reduced ET-B-R mediated vasodilatation[71,75]. For example, even with similar basal plasma ET-1 levels, POAG patients that were given exogenous ET-1, showed reduced systemic ET-B-R mediated vasodilatation after administration of ET-A-R antagonists than did healthy controls[75]. Many of these findings indicate that OAG might be rather part of a systemic vascular disorder than of just a local ocular disease. Several other studies demonstrated reduced retinal blood flow at the ONH and macula region with elevated plasma ET-1 levels[72,73,133–135]. Other research has shown that systemically administered ET-1 in humans leads to reduced blood flow of the ONH and macula region[136–138].

The rationale behind the current study lies in the need to explore the role of ET-1 and its direct precursor, Big ET-1, in the context of OAG. Specifically, it was aimed to investigate their associations with OCT-A parameters and disease stage. Given the limited existing research on ET-1 levels and optic nerve head ONH perfusion, it was sought to contribute to this relatively sparse field[70,71,75–77].

This present research project found significantly elevated levels of plasma and AqH ET-1 in the glaucoma group as compared to the control group. These findings are interesting and in line with the expectations, as various earlier research reports significantly elevated plasma ET-1 in POAG and NTG patients[70,71,139]. While plasma as well as AqH ET-1 levels were significantly elevated in the glaucoma group, no significant relationship between the AqH and plasma ET-1 levels could be found in the regression analysis. This points to the conclusion that elevated AqH ET-1 levels are not necessarily a result of diffused systemic ET-1 but that the ET-1 in the AqH is rather locally synthesized. This conclusion is substantiated by the widely acknowledged belief that ET-1 does not permeate the BRB and BBB[140]. Interestingly, there was no significant correlation of AqH ET-1 level with the IOP in

the patient population. This is in contrast with other studies from for example Choritz et al., that found correlations of increased AqH ET-1 with elevated IOP. Nevertheless, the IOP among glaucoma patients in that investigation surpassed that observed in the current study, potentially attributable to a reduced utilization of topical medications[141]. It has been suggested that ET-1 in AqH might induce contraction of smooth muscle cells in the TM, leading to increased AqH outflow resistance, contributing to a gradual build-up of IOP[141,142]. In opposition, in vitro research has demonstrated that ET-1 reduces the activity of the sodium–potassium pump in the ciliary body, which theoretically leads to reduced AqH production[143].

Conversely, both human and animal studies have demonstrated a dose-dependent effect on IOP. Additionally, intravitreal injections in animal models have been observed to induce an initial elevation in IOP, succeeded by a sustained decrease[144]. Other animal studies have shown that intravitreal ET-1 injection causes reduced retinal perfusion and subsequent RGC damage[145]. The knowledge and evidence about AqH ET-1 levels on IOP therefore remains inconclusive and the present findings do not show a significant correlation with elevated IOP levels[142].

Nevertheless, examination of the findings from this investigation unveiled a noteworthy association between heightened AqH ET-1 levels and the quantity of employed topical glaucoma medications. This prompts an inquiry into whether specific topical medications may play a role in the upregulation of local ET-1 synthesis in AqH. To further evaluate this finding, the group of the glaucoma patients was sub-divided into three IOP groups (Group 1 IOP ≤18 mmHg Group 2 IOP 19–24 mmHg Group 3 IOP ≥25 mmHg – See 3.4). Subsequently, an examination was conducted to ascertain the presence of substantial variations in the utilization of topical medications among the IOP groups. This was undertaken to eliminate the possibility that the correlation with AqH ET-1 levels stemmed from the necessity for patients with higher IOP to employ a greater diversity of topical medications to achieve an acceptable IOP. The sub-analyses negated this correlation, prompting the assertion that this novel discovery warrants further investigation in future research. As previously discussed, it is known that the vasoconstrictive effects of ET-1 in plasma as well as AqH lead to progressive optic neuropathy most likely because delicate RGCs undergo ischemic damage. If the

administration of certain topical glaucoma medications indeed results in a decline in IOP while concurrently causing heightened levels of AqH ET-1, potentially exacerbating optic neuropathy through mechanisms discussed earlier, it may be postulated that certain topical medications are not as effective in impeding the progression of glaucoma as previously thought. It is apparent, that for decennia, the mainstay of glaucoma treatment has been regulation of IOP, but new substances like ET-1 and VD visualisation using OCT-A might provide new insights into these treatments and might warrant their re-evaluation.

This current study found significantly elevated levels of AqH ET-1 in patients using topical beta blockers as well as topical CA inhibitors. However, it is difficult to draw conclusions from these findings, because the calculations did not consider whether multiple topical medications were used simultaneously, because of the small sample size and because of the design of the study. Interestingly, some previous studies have registered similar findings, especially regarding topical beta blockers but also regarding CA inhibitors and reduced retinal blood flow[146–148]. For example, Takusagawa et al. found a significant decrease of 3.3% in macular SVD VD ($p=0.043$) in patients using topical beta blockers in a small study[149].

On the other hand, this study identified significantly elevated AqH ET-1 levels in the glaucoma group as compared to the control group, but no significant relations of AqH ET-1 level and VD parameters or RNFL thickness were found. The importance of this novel finding is therefore not certain. This is behind the scopes and design of this research, but these results should initiate further research into this topic with larger cohorts. Within this context, it would be valuable to know about the diffusion of ET-1 from the AqH to the vitreous body and subsequently to the retina. It is known that specific substances diffuse from the AqH to the vitreous body, but research into the diffusion of ET-1 is very limited[150].

Suggesting direct effects on the retina by topical medications, a recent study by Samaha et al. investigated the effect of short-term administration of the topical prostaglandin analogue latanoprostene bunod in healthy volunteers and found a significant increase in blood volume at the ONH as well as significantly increased capillary oxygen saturation measured by multichannel spectroscopic reflectometry[151]. In that study however, no ET-1 levels were measured, and the

participants were healthy volunteers that only temporarily received one single topical glaucoma medication.

4.4 Systemic Big ET-1, ET-1 and protein levels

Interestingly, the present study detected no significant differences in Big ET-1 levels between the control and the glaucoma group. In fact, the levels in both groups were almost undetectably low. Literature suggests that Big ET-1 has a longer half-life than ET-1 and is therefore a more suitable biomarker[66,67,69]. Accordingly, it was expected to find significant differences between the groups.

While it has been shown that under normal circumstances ET-1 is quickly removed from the circulation, it has also been shown that its mainly ET-A-R mediated vasoconstrictive effects last remarkably long, with some initial studies even suggesting irreversible ET-A-R binding. More recent research has shown that binding is not irreversible but that dissociation from the receptor is slow, explaining its long-lasting effects[64,66,68]. Under normal circumstances, certain amounts of ET-1 are continuously synthesized and released to preserve the physiologic vascular tone[64]. It becomes apparent, that the normal function of ET-1 is based on a fragile balance that can become deranged by various pathologies and long-term imbalances can even lead to vascular remodelling[75]. Given the existing evidence, it is unsurprising that elevated levels of ET-1 play a contributory role in the pathogenesis of various vascular diseases such as cerebral vasospasms, cardiac vasospasms, subarachnoid bleedings as well as Raynaud's disease[75].

Different investigations have shown in healthy patients that ET-1 as well as Big ET-1 clearance from the circulation is efficient and occurs in two phases. The half-life of the first and rapid phase was reported to be around four minutes for ET-1 and around seven minutes for Big ET-1, while the half-life of the following slower phase was more than one hour and more than 23 minutes to reach basal level respectively[64,66,68]. It is important to realize that the half-life and clearance of the circulation do not directly depict the substance's clinical effect, as discussed above. Binding of ET-1 to ET-A-R is mainly responsible for vasoconstrictive effects, while ET-B-R binding leads to NO mediated vasodilating effects and to the lysosomal degradation of ET-1. The lungs, liver and kidneys appear to accommodate the

highest densities of ET-1 receptors[64,66]. However, Big ET-1 is also rapidly cleared from circulation, in animal models mainly by the liver and lungs for conversion to ET-1 by endothelin-converting enzyme 1 (ECE-1), which is widely expressed throughout the human body[64]. The current findings imply discordant data regarding the detectable duration of Big ET-1 and ET-1 in the circulation. Moreover, it is not definitively established that Big ET-1 represents a superior method for monitoring endothelins compared to the direct measurement of ET-1. A study by Kostov et al. found similar results when comparing plasma Big ET-1 and ET-1 in healthy and hypertensive patients[152].

Although not conclusively established, it can be hypothesised that in patients with systemic illnesses, an imbalance between ET-1 production and degradation, induced by pathological processes, could eventually result in the saturation of ET-1 receptors. Because of the long duration of binding to ET-A-R, the vasoconstrictive and RGC damaging effects could maximize because of saturation of ET-A-R, while the amount of freely circulating ET-1 gradually increases with only limited new binding, leading to detectable increased plasma ET-1 levels. The reason for normal Big ET-1 levels could be that the aforementioned ET-1 inducing pathology might not impair ECE-1 function, causing similar Big-ET-1 conversion times in both groups. Hence, it is plausible that OAG within the eye represents a manifestation of systemic disease rather than an isolated ocular disorder. This is supported by the finding that plasma ET-1 had significant correlations with VD in several ONH and macula regions, while AqH ET-1 did not.

ET-1 is, next to its potent vasoconstrictive effects, known to possess several proinflammatory actions that result in cytokine release, generation of reactive oxygen species (ROS) and eventually promotes vascular fibrosis[63]. Additionally, a strong proinflammatory cascade is activated, that leads to release of tissue necrosis factor alpha (TNF-α), interleukin 1 (IL-1) and IL-6 among others, and activates different types of leucocytes, which in turn causes additional production of ET-1[63]. Several ET-A-R blocking agents have demonstrated a significant reduction of oxidative damage in for example ischemic myocardium and in neurodegenerative disorders[63,153]. Several studies have shown that in the context of glaucoma, ET-1 also exerts important effects on astrocytes in the retina and optic nerve, resulting in abnormal activation and proliferation, eventually disrupting RGC

homeostasis and causing cell loss[133,135,154]. A previously mentioned study by Kiyota et al. showed that reductions in peripapillary blood flow measured by laser speckle flowgraphy (LSFG) preceded measurable RNFL reductions in OAG an found correlations with age, as well as cardiovascular disease including tachycardia, hyper- and hypo-tension[122]. The findings of this current study find a strong correlation with age and the VD of several PeriONH quadrants, most of all the PeriONH TempSup. Interestingly, as opposed to Kiyota's study, this present research excluded patients with cardiac disease or an abnormal cardiac physical examination during intake but nevertheless found similar correlations. Considering OAG as a component of a systemic disease, it is conceivable that ocular manifestations, such as RGC damage, represent an early indication of the systemic disease, with additional symptoms emerging later in its progression. This systemic theory is further supported by this dissertation's finding of a significant positive correlation of the plasma protein concentration of the glaucoma group with the plasma ET-1 level, as proinflammatory processes are known to increase plasma protein concentration[63].

Within these findings, the demonstrated importance of ET-1 in glaucoma and its apparent systemic, rather than local pathologic character, the previously identified primary vascular dysregulation syndrome (PVD), which is also known as Flammer Syndrome (FS) might play a role[52,155]. PVD or FS is of growing interest within glaucoma research as it incorporates several of the previously mentioned vascular considerations of POAG pathophysiology. It is more prevalent in women than in men and has a strong hereditary component[52]. In FS there are temporarily inappropriate arterial constrictions or dilatations, leading to inadequate blood supply and causing symptoms in different organs, often the eye and extremeties[52]. FS patients are predisposed to react with vascular dysregulation to stimuli like for example temperature changes, mechanical manipulation or emotional stress or pain. The syndrome often occurs simultaneously with weakening of the BRB and BBB. The exact pathophysiology is still unknown but appears to partly involve autonomous dysregulation, but since for example the uninnervated retinal vasculature is also affected, it cannot be the only explanation. More evidence is pointing towards a possible disbalance between NO and ET-1 levels in FS[52]. Due to the ocular vasospasms in FS and resulting fluctuations in OBF, FS is known to

be an important contributor to the development of glaucoma. Imaging in FS patients has for example shown rapid OBF decrease after cold provocation of the extremities and cases of permanent visual field defects after exposure to temporary cold are known[52].

In light of the discussed findings from this research, which highlight the substantial impact of plasma ET-1 levels on VD in specific retinal regions and its systemic nature, several potential implications for future research and clinical applications become evident.

To further investigate the assumptions, it would be beneficial to expand prospective research to not only the plasma and AqH levels but to also find a way to determine the fraction of saturated ET-1 receptors, as well as measuring the blood flow or VD of other peripheral tissues or vascular organs in relation to plasma ET-1 levels. For example, it has been established that significant correlations between the prevalence of chronic kidney disease and glaucoma exist[156]. Additionally, research into the significance of ET-2 in glaucoma appears to be valuable. While studies about this topic are still extremely sparse, it is known that ET-2 is also a potent vasoconstrictor binding to the same ET-A-R and ET-B-R, but circulating in different proportions and being synthesized by somewhat different pathways and tissues[140].

It seems worthwhile to conduct further research into the group of endothelin receptor blockers for the treatment of glaucoma, counteracting the discussed detrimental effects of elevated ET-1. First promising results for neuroprotection in glaucoma have been found using the ET-A-R and ET-B-R antagonist bosentan, which is used in pulmonary hypertension, and the selective ET-A-R blocker BQ-123, which have both shown to improve OBF[157–159].

4.5 Limitations

This study has several limitations that need to be addressed.

Firstly, as this study mainly included patients with early stages of glaucoma, it was decided to focus on OCT measurements of the RNFL and did not perform separate perimetry measurements simultaneously. This is in part due to the previously discussed pathophysiological characteristics of glaucoma, stating that up to 40% of all RGC will be inevitably lost before perimetry changes can be detected. Since early stages of glaucoma were to be included, OCT measurements were deemed more sensitive. Since at this point, perimetry remains the gold standard of glaucoma monitoring, it would nevertheless have been beneficial to include perimetry in this study, also for comparability with other studies. Secondly, as explained earlier, due to the low numbers of NTG and XFG patients, no separate sub-analyses for these groups were performed. It would be desirable to perform longitudinal follow-up measurements of the patients and to increase the patient population and to examine a boarder glaucoma cohort with and without further systemic diseases. This is required to prove the suspected biomarker quality of plasma ET-1 for prediction of ONH blood flow and to perform sub-analyses for the different types of glaucoma. Thirdly, the examinations and measurements were performed at one point of time only. A follow-up and reassessment at a later moment would allow to investigate the sensitivity and specificity of variables like ET-1 as a prognostic marker in glaucoma. Fourthly, inclusion of NO and ET-2 measurements might have been beneficial in interpreting the current findings, but insufficient material for these analyses was available. Fifthly, the topical glaucoma medications of the glaucoma patients were not discontinued peri-operatively, which theoretically might have had some influence on the ET-1 concentrations. Sixthly, the blood and AqH samples were obtained while patients were under general anaesthesia. It is known that different stressors of an operation can lead to a gradual increase of ET-1 levels intra-operatively[160]. However, all samples were obtained within the first 10 minutes after induction of general anaesthesia and these effects were therefore deemed minimal.

5. Summary / Zusammenfassung

English

Introduction:
This dissertation aimed to investigate the correlation between optical coherence tomography angiography (OCT-A) parameters, specifically vessel density (VD) in the optic nerve head (ONH) and foveal regions of glaucoma patients with the levels of the potent vasoconstrictor endothelin 1 (ET-1) and its precursor big ET-1 in both plasma and aqueous humour (AqH). Furthermore, the compatibility of OCT-A parameters with the optical coherence tomography (OCT) glaucoma staging system (OCT-GSS), previously validated only for OCT measurements, was explored.

Materials and Methods:
This prospective monocenter study included adult patients undergoing elective cataract or glaucoma surgery. Intraoperatively gathered AqH and plasma were collected from glaucoma patients and control patients. Glaucoma diagnosis was confirmed or excluded through medical history, intraocular pressure assessment, fundoscopy and spectral domain (SD) OCT imaging. Exclusion criteria encompassed low-quality imaging, systemic disease, vasoactive medication usage, as well as previous ophthalmologic surgery, except posterior chamber lens implantation, laser trabeculoplasty or laser iridotomy more than six months ago. ET-1 and big ET-1 levels were quantified using Enzyme-Linked-Immunosorbent-Assay (ELISA) and multiplex immunoassays, respectively. Protein levels were determined using the Bradford protein assay. Descriptive statistics were applied for dataset exploration, followed by linear correlation analysis. A multivariable regression analysis was subsequently conducted with appropriate variables.

Results:
Significantly elevated levels of ET-1 in both plasma and AqH were observed in glaucoma patients compared to the control group. Significant correlations were identified between plasma ET-1 levels and various OCT-A VD parameters in the ONH and foveal regions. No correlations were found for Big ET-1 levels. The OCT-GSS exhibited significant correlations with several OCT-A VD parameters, including the VD of the entire ONH and the VD of the entire macula superficial vascular plexus (SVP).

Discussion:

The detected correlations between plasma ET-1 levels and OCT-A parameters suggest a potential novel diagnostic criterion for early detection and assessment of glaucomatous damage, potentially surpassing the capabilities of SD-OCT. The findings support the theory of a systemic pathology in primary open-angle glaucoma (POAG), rather than the concept of a local disease.

The correlation of OCT-A parameters with the OCT-GSS suggests that integrating OCT-A analysis into this staging system could potentially enable enhanced early detection and greater sensitivity.

Deutsch

Einleitung:

Diese Dissertation hatte zum Ziel, die Korrelation zwischen den Parametern der optischen Kohärenztomographie-Angiographie (OCT-A), insbesondere der Gefäßdichte (VD) im Bereich des Sehnervenkopfs (ONH) und der Fovea bei Glaukom-Patienten zu untersuchen, sowie die Konzentrationen des potenten Vasokonstriktors Endothelin 1 (ET-1) und seines Vorläufers Big ET-1 sowohl im Plasma als auch in der Kammerflüssigkeit (AqH). Darüber hinaus wurde die Kompatibilität der OCT-A-Parameter mit dem Glaukom-Stadiensystem der optischen Kohärenztomographie (OCT-GSS), das bisher nur für OCT-Messungen validiert wurde, erforscht.

Material und Methoden:

In diese prospektive monozentrische Studie wurden erwachsene Patienten aufgenommen, die sich einer elektiven Katarakt- oder Glaukom-Operation unterzogen. Intraoperativ wurden AqH und Plasma von Glaukom-Patienten und Kontrollpatienten abgenommen. Die Glaukom-Diagnose wurde durch die Anamnese, die Bewertung des Augeninnendrucks, die Fundoskopie und die spectral-domain (SD) OCT-Bildgebung bestätigt oder ausgeschlossen. Die Ausschlusskriterien umfassten Bildgebung von niedriger Qualität, systemische Erkrankungen, Verwendung vasoaktiver Medikamente sowie frühere ophthalmologische Eingriffe, mit Ausnahme der Implantation einer Hinterkammerlinse, Lasertrabekuloplastie oder Laseriridotomie, die vor mehr als

sechs Monaten durchgeführt wurden. ET-1- und Big ET-1-Spiegel wurden mittels Enzyme-Linked-Immunosorbent-Assay (ELISA) bzw. Multiplex-Immunassays quantifiziert, während die Proteinspiegel mittels des Bradford-Proteinassays bestimmt wurden. Zur Datenerkundung wurden deskriptive Statistiken angewendet, gefolgt von einer linearen Korrelationsanalyse. Schließlich wurde eine multivariable Regressionsanalyse mit geeigneten Variablen durchgeführt.

Ergebnisse:

Signifikant erhöhte ET-1-Spiegel sowohl im Plasma als auch in AqH wurden bei Glaukom-Patienten im Vergleich zur Kontrollgruppe beobachtet. Signifikante Korrelationen wurden zwischen den Plasma-ET-1-Spiegeln und verschiedenen OCT-A-VD-Parametern im ONH- und Fovea-Bereich identifiziert. Keine Korrelationen konnten für die Big ET-1-Spiegel gefunden werden. Das OCT-GSS zeigte signifikante Korrelationen mit verschiedenen OCT-A-VD-Parametern, einschließlich der VD des gesamten ONH und der VD des gesamten oberflächlichen vaskulären Plexus der Makula (SVP).

Diskussion:

Die festgestellten Zusammenhänge zwischen den Plasma-ET-1-Spiegeln und den OCT-A-Parametern deuten auf ein potenziell neues diagnostisches Kriterium für die Früherkennung und Bewertung glaukomatöser Schäden hin, welches möglicherweise über die Möglichkeiten von SD-OCT hinausgeht. Die Befunde stützen die Hypothese einer systemischen Pathologie beim primären Offenwinkelglaukom (POAG), anstatt der Theorie einer lokalen Erkrankung. Die Korrelation der OCT-A-Parameter mit dem OCT-GSS legt nahe, dass die OCT-A-Analyse möglicherweise in dieses Stadiensystem integriert werden kann, was unter Umständen eine verbesserte Früherkennung und höhere Sensitivität ermöglichen würde.

Deutsch - Ausführlich

Einleitung

Glaukom ist eine Gruppe heterogener Augenerkrankungen, die zu Schäden an den retinalen Ganglienzellen (RGC) und am Sehnervenkopf (ONH) führen. Unbehandelt führt die Krankheit zu einem fortschreitenden Verlust des Gesichtsfeldes und kann im Endstadium zu irreversibler Erblindung führen.

Epidemiologie

Glaukom ist die weltweit führende Ursache für irreversible Erblindung. Etwa 3,55% der Bevölkerung im Alter von 40 bis 80 Jahren sind betroffen, wobei das primäre Offenwinkelglaukom (POAG) und das primäre Winkelblockglaukom (PACG) die häufigsten Formen sind. Männer haben eine höhere Wahrscheinlichkeit, an POAG zu erkranken als Frauen, und Menschen afrikanischer Abstammung weisen die höchste Prävalenz auf. Die globale Anzahl der Glaukompatienten stieg von 64,3 Millionen im Jahr 2013 auf 76 Millionen im Jahr 2020 und wird bis 2040 voraussichtlich 112 Millionen erreichen. Besonders besorgniserregend ist das Normaldruckglaukom (NTG), das etwa 30-50% der POAG-Fälle ausmacht und weltweit stark variiert.

Klinische Präsentation

Das POAG entwickelt sich meist langsam und schmerzlos. Symptome treten oft erst im fortgeschrittenen Stadium auf, wenn bereits irreversible Schäden an den RGCs eingetreten sind. Typische Gesichtsfeldausfälle beginnen peripher und betreffen meist den unteren Quadranten. Das PACG kann akut oder chronisch verlaufen. Die akute Form äußert sich durch starke Augenschmerzen, während die chronische Form schleichend und oft schmerzlos verläuft.

Pathophysiologie

Der Hauptmechanismus, der zur Erblindung führt, ist die Schädigung der RGCs, was zu einer Abnahme der retinalen Nervenfaserschicht (RNFL) und Veränderungen des ONH führt. Die RGCs sind spezialisierte Nervenzellen, die visuelle Informationen von den Photorezeptoren zu den visuellen Zentren des Gehirns übertragen. Der Verlust von RGCs führt zur Ausdünnung der RNFL und zur Vertiefung der Papille. Der Schaden an den RGCs ist irreversibel.

Die Grundlage der mechanischen Theorie des Glaukoms ist ein Druckunterschied

zwischen dem Auge und dem retrobulbären Kompartiment, dem Raum hinter dem Auge, der mit dem Gehirn verbunden ist. Diese Drücke wirken von entgegengesetzten Seiten auf die dünne Lamina cribrosa, welche die Axone der RGCs stützt. Bei einem Glaukom ist der Druckunterschied aus verschiedenen Gründen verändert, was zu Scherbelastung der Nervenzellen und Schädigung der RGCs führt.

Die vaskuläre Theorie beschreibt die vom IOP unabhängigen Prozesse, welche zum Beispiel das NTG erklären könnten. Ein wesentlicher Faktor in der Pathophysiologie des Glaukoms ist Endothelin-1 (ET-1), ein potenter Vasokonstriktor, der in höheren Konzentrationen bei Glaukompatienten gefunden wurde. ET-1 kann eine direkte neurotoxische Wirkung auf RGCs haben und die Durchblutung des ONH beeinträchtigen, was zur Ischämie und zum Zelltod führen kann. Die erhöhte ET-1-Konzentration könnte somit eine zentrale Rolle bei der Glaukompathogenese spielen, insbesondere beim NTG, wo der erhöhte Augeninnendruck nicht der Hauptfaktor ist. Zusätzlich zu ET-1 sind oxidative Stressmechanismen und Entzündungsprozesse von großer Bedeutung, welche die Mitochondrienfunktion der RGCs beeinträchtigen und zur Apoptose führen können. Die Dysfunktion der Mikrozirkulation im ONH und die resultierende Hypoxie sind zentrale Elemente der Pathophysiologie des Glaukoms.

Diagnostik und Bildgebung

Die optische Kohärenztomographie (OCT) hat sich als unverzichtbares Werkzeug in der Diagnose und Überwachung des Glaukoms etabliert. Die OCT ermöglicht eine hochauflösende Querschnittsdarstellung der retinalen Schichten und bietet präzise Messungen der RNFL-Dicke und der ONH-Morphologie. Diese Technologie erlaubt es, strukturelle Schäden frühzeitig zu erkennen und den Krankheitsverlauf zu überwachen. Eine neuere Entwicklung in der Bildgebungstechnologie ist die OCT-Angiographie (OCT-A), die die Durchblutung der Netzhaut und des ONH ohne die Notwendigkeit von Farbstoffinjektionen visualisiert. Dies ist besonders nützlich zur Untersuchung der vaskulären Veränderungen beim Glaukom. Die OCT-A bietet detaillierte Bilder der retinalen und choroidalen Mikrogefäße und kann helfen, die vaskulären Komponenten der Glaukompathogenese besser zu verstehen. Die Kombination von OCT und OCT-A bietet eine umfassende Bewertung sowohl der strukturellen als auch der funktionellen Aspekte des Glaukoms.

Das OCT-Glaukom-Staging-System (OCT-GSS) wurde von Brusini et al. entwickelt, um die Schädigung der RNFL bei Glaukom zu klassifizieren. Es basiert auf Messungen der SD-OCT und ermöglicht eine integrierte Bewertung von strukturellen und funktionellen Schäden. Hierbei werden die RNFL-Dicke im oberen Quadranten und im unteren Quadranten berücksichtigt. Das OCT-GSS bietet eine Sensitivität von 95% und eine Spezifität von 92% bei der Unterscheidung zwischen normalen und glaukomatösen Augen.

Forschungsziel

Diese Dissertation erforscht die vaskuläre Pathogenese des POAG mit besonderem Fokus auf ET-1. Es werden potenzielle Korrelationen von ET-1 mit der retinalen Gefäßdichte am ONH und der Makula sowie anderen OCT-A-Parametern untersucht. Analysiert werden ET-1 in Plasma und Kammerwasser, Big ET-1 und Proteinkonzentrationen bei gesunden Kontrollen und Glaukompatienten verschiedener Stadien. Die Erkenntnisse könnten neue Informationen zur Diagnose und Pathophysiologie der Krankheit liefern. Zudem wird die potenzielle Nützlichkeit der OCT-A im Vergleich zur SD-OCT für die Früherkennung und Stadieneinteilung des POAG, insbesondere hinsichtlich der Erweiterung bestehender Staging-Tools wie dem OCT-GSS, untersucht.

Methoden

Diese Studie wurde als prospektive Single-Center-Studie am St. Franziskus Krankenhaus in Münster, Deutschland, durchgeführt. Die Teilnehmer wurden zwischen 2018 und 2020 identifiziert und eingeschlossen. Alle Teilnehmer waren für eine Katarakt- oder Glaukomoperation vorgesehen. Zwei Gruppen von Patienten wurden eingeschlossen: Glaukompatienten und eine Kontrollgruppe. Die Diagnose des Glaukoms in der Glaukomgruppe musste mindestens zwei oder mehr der folgenden Kriterien erfüllen: Erhöhtes vertikales Cup-to-Disc-Verhältnis (VCDR; ≥0,5), CDR-Asymmetrie zwischen beiden Augen >0,2, glaukomatöse Reduktion der peripapillären RNFL-Dicke und/oder GCC-Dicke am hinteren Pol. Für die OCT- und OCT-A-Messungen wurde das SD-OCT-Gerät RTVue-XR von Optovue verwendet. Jeder Teilnehmer wurde mit OCT-A auf einem 6 mm x 6 mm großen Bereich zentriert an der Fovea und auf einem 4,5 mm x 4,5 mm großen Bereich zentriert am ONH untersucht.

Die OCT-GSS von Brusini et al. wurde für jeden Teilnehmer dieser Studie

berechnet. Jeder Teilnehmer wurde daher innerhalb der sieben Klassen des OCT-GSS entsprechend der oberen und unteren RNFL-Dicke und korrigiert für das Alter klassifiziert.

Während der ophthalmologischen Operation wurden von jedem Teilnehmer insgesamt 7 ml Blut und zwischen 100 bis 150 Mikroliter (µl) Kammerwasser (AqH) entnommen. Für die Quantifizierung von ET-1 in dieser Studie wurde ein Enzyme-linked-immunosorbent-Assay (ELISA) mit dem Plasma und AqH durchgeführt, wobei das kommerziell erhältliche ET-1-Testsystem "Quantikine® ELISA Endothelin-1 Immunoassay" von Bio-Techne® verwendet wurde.

Die statistischen Analysen wurden mit der Software R (Version 4.0.2; Dormagen, Deutschland) durchgeführt. Für den Vergleich von zwei Gruppen und mehr als zwei Gruppen wurde ein geeigneter T-Test oder ANOVA gefolgt von einer Tukey-Post-hoc-Analyse verwendet.

Ergebnisse

Die Patientenpopulation bestand aus insgesamt 98 Augen, davon 30 Kontrollen und 68 glaukomatöse Augen. Signifikant erhöhte ET-1-Spiegel sowohl im Plasma als auch in AqH wurden bei Glaukom-Patienten im Vergleich zur Kontrollgruppe beobachtet. Signifikante Korrelationen wurden zwischen den Plasma-ET-1-Spiegeln und verschiedenen OCT-A-VD-Parametern im ONH- und Fovea-Bereich identifiziert. Keine Korrelationen konnten für die Big ET-1-Spiegel gefunden werden. Das OCT-GSS zeigte signifikante Korrelationen mit verschiedenen OCT-A-VD-Parametern, einschließlich der Gefäßdichte (VD) des gesamten ONH und der VD des gesamten oberflächlichen vaskulären Plexus der Makula (SVP).

Der OCT-GSS-Score wurde für jeden Teilnehmer mithilfe des Online-Tools von Brusini et al. berechnet. In der Kontrollgruppe mit 30 Patienten wurden 23 Patienten als gesund, fünf als grenzwertig (Stadium 0), einer als Frühschaden (Stadium 1) und einer als leichter Schaden (Stadium 2) klassifiziert. In der Glaukomgruppe wurden elf der 68 Patienten als gesund, fünf als grenzwertig (Stadium 0), sechs als Frühschaden (Stadium 1), neun als leichter Schaden (Stadium 2), 17 als mäßiger Schaden (Stadium 3), neun als fortgeschrittener Schaden (Stadium 4) und sechs als terminaler Schaden (Stadium 5) eingestuft. Innerhalb der Glaukomgruppe unterschied sich der Defektort signifikant zwischen den OCT-GSS-Stadien, wobei diffuse Defekte in höheren OCT-GSS-Stadien dominierten. Mit höheren Stadien

sinken die RNFL und verschiedene OCT-A Parameter der ONH und Macula Region signifikant. Während die Signifikanz der RNFL-Dicke zu erwarten ist, da der OCT-GSS-Score auf diesen Werten basiert, wird deutlich, dass mehrere OCT-A-Parameter, insbesondere die VD der PeriONH-Region und aller Quadranten sowie alle PeriFovea-Quadranten in der SVP-Schicht, mit zunehmendem OCT-GSS-Stadium signifikant abnehmen.

In einer multivariablen linearen Regressionsanalyse wurde der Zusammenhang zwischen mehreren unabhängigen Variablen und den OCT-A-Parametern untersucht. Besonderes Interesse galt den Endothelinspiegeln in Bezug auf die OCT-A-Parameter. Die Analyse ergab signifikante Korrelationen zwischen dem Plasmaspiegel ET-1 und bestimmten VD-Werten (PeriONH TempSup, VD Fovea SVP und VD Fovea DVP [tiefer vaskulärer Plexus der Makula]).

Diskussion

Diese Dissertation hat gezeigt, dass in der Gruppe der Glaukompatienten neben der retinalen RNFL und der Ganglienzellschicht (GCC) die VD des gesamten ONH sowie aller PeriONH-Quadranten im Vergleich zur Kontrollgruppe signifikant reduziert ist. Es wird immer deutlicher, dass Abnahmen der OCT-A abgeleiteten VD-Parameter möglicherweise vor Reduktionen der RNFL-Dicke auftreten, wie sie durch SD-OCT gemessen werden. Dies legt nahe, dass OCT-A möglicherweise die frühere Erkennung von Glaukom erleichtern könnte. Es ist offensichtlich, dass weitere Längsschnittstudien notwendig sind, um die Hypothese zu bestätigen, dass VD-Messungen, die über OCT-A erhalten wurden, RNFL- und GCL-Messungen für die frühe Glaukomerkennung und die Verlaufskontrolle im Spätstadium übertreffen. Wenn diese Hypothese bestätigt werden kann, hat OCT-A das Potenzial, sich als entscheidendes nicht-invasives Werkzeug für die Glaukomdiagnose und die Längsschnittüberwachung zu etablieren. Seine Nutzung könnte die frühzeitige Umsetzung von Behandlungsstrategien und präventiven Maßnahmen erleichtern, wodurch die Lebensqualität der Patienten verbessert und die sozioökonomische Belastung, die mit fortgeschrittenem Glaukom verbunden ist, gemindert wird. Es wurden signifikant erhöhte Werte von ET-1 im Plasma und im Kammerwasser in der Glaukomgruppe im Vergleich zur Kontrollgruppe gefunden. Diese Ergebnisse sind interessant und stimmen mit den Erwartungen überein, da verschiedene frühere Forschungsberichte signifikant erhöhte Plasma-ET-1-Werte bei POAG- und NTG-

Patienten festgestellt haben. Es scheint lohnend, weitere Forschungen zur Gruppe der Endothelin-Rezeptor-Blocker für die Behandlung von Glaukom durchzuführen, um die diskutierten schädlichen Auswirkungen von erhöhtem ET-1 entgegenzuwirken. Erste vielversprechende Ergebnisse für die Neuroprotektion bei Glaukom wurden mit verschiedenen ET-A-R (Endothelin-A-Rezeptor)- und ET-B-R-Antagonisten erzielt. Die Ergebnisse unterstützten die Hypothese, dass das Offenwinkelglaukom (OAG) im Auge eher eine Manifestation einer systemischen Erkrankung als eine isolierte Augenerkrankung darstellt. Dies wird durch den Befund dieser Dissertation unterstützt, der eine signifikante positive Korrelation der Plasmaprotein-Konzentration der Glaukomgruppe mit dem Plasmaspiegel von ET-1 zeigt, da proinflammatorische Prozesse bekanntermaßen die Plasmaprotein-Konzentration erhöhen.

Während die Klassifikation des OCT-GSS auf den SD-OCT-Messungen der RNFL basiert, zeigte die aktuelle Forschung signifikante Korrelationen mit der VD der gesamten ONH-Region und allen PeriONH-Bereichen. Auch wurden Korrelationen mit der VD der gesamten Makula und perifovealen Sektoren in der SVP-Schicht gefunden. Die fehlende Signifikanz in der Fovea und den meisten parafovealen Sektoren kann durch die dortige Netzhaut-Anatomie erklärt werden, da RGCs in der Makula fehlen und in perifovealen Sektoren dicker werden. Diese Ergebnisse deuten darauf hin, dass die Beziehung zwischen VD und RNFL beim Glaukom auf das OCT-GSS übertragbar ist. Weitere Studien und Anpassungen der OCT-GSS-Software sind jedoch erforderlich, um Konsens über Cut-off-Werte für OCT-A-Parameter zu erzielen. Die Einbeziehung von OCT-A-Werten könnte das OCT-GSS zu einem noch leistungsfähigeren Tool machen, insbesondere da VD-Abnahmen vor RNFL-Veränderungen detektiert werden können. Erstmals wurde eine signifikante positive Korrelation des OCT-GSS mit Plasma-ET-1-Spiegeln festgestellt, was neue Einblicke in die Pathophysiologie liefert.

6. References

1. Lommatzsch C, Rothaus K, Schopmeyer L, et al. Elevated endothelin-1 levels as risk factor for an impaired ocular blood flow measured by OCT-A in glaucoma. *Scientific Reports*. 2022;12(1):11801. doi:10.1038/s41598-022-15401-5
2. Quigley H, Broman AT. The number of people with glaucoma worldwide in 2010 and 2020. *British Journal of Ophthalmology*. 2006;90(3):262-267. doi:10.1136/bjo.2005.081224
3. Tham YC, Li X, Wong TY, Quigley HA, Aung T, Cheng CY. Global prevalence of glaucoma and projections of glaucoma burden through 2040: A systematic review and meta-analysis. *Ophthalmology*. 2014;121(11):2081-2090. doi:10.1016/j.ophtha.2014.05.013
4. Jonas JB, Aung T, Bourne RR, Bron AM, Ritch R, Panda-Jonas S. Glaucoma. *The Lancet*. 2017;390(10108):2183-2193. doi:10.1016/S0140-6736(17)31469-1
5. Kyari F, Entekume G, Rabiu M, et al. A Population-based survey of the prevalence and types of glaucoma in Nigeria: Results from the Nigeria National Blindness and Visual Impairment Survey. *BMC Ophthalmology*. 2015;15(1). doi:10.1186/s12886-015-0160-6
6. Foster PJ, Aung T, Nolan WP, et al. Defining “occludable” angles in population surveys: Drainage angle width, peripheral anterior synechiae, and glaucomatous optic neuropathy in east Asian people. *British Journal of Ophthalmology*. 2004;88(4):486-490. doi:10.1136/bjo.2003.020016
7. Cheng JW, Zong Y, Zeng YY, Wei RL. The prevalence of primary angle closure glaucoma in adult Asians: A systematic review and meta-analysis. *PLoS One*. 2014;9(7). doi:10.1371/journal.pone.0103222
8. Mishima K, Tomidokoro A, Suramethakul P, et al. Iridotrabecular contact observed using anterior segment three-dimensional OCT in eyes with a shallow peripheral anterior chamber. *Investigative Ophthalmology & Visual Science*. 2013;54(7):4628-4635. doi:10.1167/iovs.12-11230
9. Kang JM, Tanna AP. Glaucoma. *Medical Clinics of North America*. 2021;105(3):493-510. doi:10.1016/j.mcna.2021.01.004
10. Weinreb RN, Leung CKS, Crowston JG, et al. Primary open-angle glaucoma. *Nature Reviews Disease Primers*. 2016;2(1):16067. doi: 10.1038/nrdp.2016.67
11. Vajaranant TS, Wu S, Torres M, Varma R. The changing face of primary open-angle glaucoma in the United States: Demographic and geographic changes from 2011 to 2050. *American Journal of Ophthalmology*. 2012;154(2). doi:10.1016/j.ajo.2012.02.024
12. Killer HE, Pircher A. Normal tension glaucoma: Review of current understanding and mechanisms of the pathogenesis /692/699/3161/3169/3170 /692/699/3161 review-article. *Eye*. 2018;32(5):924-930. doi:10.1038/s41433-018-0042-2
13. Lee JWY, Chan PP, Zhang X, Chen LJ, Jonas JB. Latest Developments in Normal-Pressure Glaucoma: Diagnosis, Epidemiology, Genetics, Etiology, Causes and Mechanisms to Management. *Asia-Pacific Journal of*

Ophthalmology.2019;8(6):457-468. doi:10.1097/01.APO.0000605096.48529.9c
14. Iwase A, Suzuki Y, Araie M, et al. The prevalence of primary open-angle glaucoma in Japanese: The Tajimi Study. *Ophthalmology*. 2004;111(9):1641-1648. doi:10.1016/j.ophtha.2004.03.029
15. Budenz DL, Barton K, Whiteside-De Vos J, et al. Prevalence of glaucoma in an urban west african population: The tema eye survey. *JAMA Ophthalmology*. 2013;131(5):651-658. doi: 10.1001/ jamaophthalmol. 2013.1686
16. Leite MT, Sakata LM, Medeiros FA. Managing glaucoma in developing countries. *Arquivos Brasileiros de Oftalmologia*. 2011;74(2):83-84. doi: 10.1590/s0004-27492011000200001
17. Susanna R, de Moraes CG, Cioffi GA, Ritch R. Why Do People (Still) Go Blind from Glaucoma? *Translational Vision Science & Technology*. 2015;4(2):1. doi:10.1167/tvst.4.2.1
18. Lee PP. A Multicenter, Retrospective Pilot Study of Resource Use and Costs Associated With Severity of Disease in Glaucoma. *Archives of Ophthalmology*. 2006;124(1):12. doi:10.1001/archopht.124.1.12
19. Rahman MQ, Beard SM, Discombe R, Sharma R, Montgomery DMI. Direct healthcare costs of glaucoma treatment. *British Journal of Ophthalmology*. 2013;97(6):720-724. doi:10.1136/bjophthalmol-2012-302525
20. Huang W, Gao K, Liu Y, Liang M, Zhang X. The Adverse Impact of Glaucoma on Psychological Function and Daily Physical Activity. *Journal of Ophthalmology*. 2020;2020. doi:10.1155/2020/9606420
21. Newman-Casey PA, Salman M, Lee PP, Gatwood JD. Cost-Utility Analysis of Glaucoma Medication Adherence. *Ophthalmology*. 2020;127(5):589-598. doi:10.1016/j.ophtha.2019.09.041
22. Harwerth RS, Wheat JL, Fredette MJ, Anderson DR. Linking structure and function in glaucoma. *Progress in Retinal and Eye Research*. 2010;29(4):249-271. doi:10.1016/j.preteyeres.2010.02.001
23. Weinreb RN, Aung T, Medeiros FA. The pathophysiology and treatment of glaucoma: A review. *JAMA - Journal of the American Medical Association*. 2014;311(18):1901-1911. doi:10.1001/jama.2014.3192
24. Weinreb RN, Khaw PT. Primary open-angle glaucoma. *The Lancet*. 2004;363(9422):1711-1720. doi:10.1016/S0140-6736(04)16257-0
25. Schiefer U, Papageorgiou E, Sample PA, et al. Spatial pattern of glaucomatous visual field loss obtained with regionally condensed stimulus arrangements. *Investigative Ophthalmology & Visual Science*. 2010;51(11): 5685-5689. doi:10.1167/iovs.09-5067
26. Broadway DC. Visual field testing for glaucoma - a practical guide. *Community Eye Health*. 2012;25(79-80):66-70. http://www.ncbi.nlm.nih.gov/pubmed/23520423
27. Boden C. The Structure-Function Relationship in Eyes With Glaucomatous Visual Field Loss That Crosses the Horizontal Meridian. *Archives of Ophthalmology*. 2002;120(7):907. doi:10.1001/archopht.120.7.907
28. Hu CX, Zangalli C, Hsieh M, et al. What do patients with glaucoma see? Visual symptoms reported by patients with glaucoma. *American Journal of the Medical Sciences*. 2014;348(5):403-409. doi: 10.1097/ MAJ.0000000000000319

29. Sun X, Dai Y, Chen Y, et al. Primary angle closure glaucoma: What we know and what we don't know. *Progress in Retinal and Eye Research*. 2017;57:26-45. doi:10.1016/j.preteyeres.2016.12.003
30. Kim US, Mahroo OA, Mollon JD, Yu-Wai-Man P. Retinal Ganglion Cells—Diversity of Cell Types and Clinical Relevance. *Frontiers in Neurology*. 2021;12. doi:10.3389/fneur.2021.661938
31. Watson AB. A formula for human retinal ganglion cell receptive field density as a function of visual field location. *Journal of Vision*. 2014;14(7). doi: 10.1167/14.7.15
32. Hood DC, Raza AS, de Moraes CG v., Liebmann JM, Ritch R. Glaucomatous damage of the macula. *Progress in Retinal and Eye Research*. 2013;32(1):1-21. doi:10.1016/j.preteyeres.2012.08.003
33. Baneke AJ, Aubry J, Viswanathan AC, Plant GT. The role of intracranial pressure in glaucoma and therapeutic implications. *Eye*. 2020;34(1):178-191. doi:10.1038/s41433-019-0681-y
34. Fechtner RD, Weinreb RN. Mechanisms of optic nerve damage in primary open angle glaucoma. *Survey of Ophthalmology*. 1994;39(1):23-42. doi:10.1016/S0039-6257(05)80042-6
35. Buffault J, Labbé A, Hamard P, Brignole-Baudouin F, Baudouin C. The trabecular meshwork: Structure, function and clinical implications. A review of the literature. *Journal Français d'Ophtalmologie*. 2020;43(7):e217-e230. doi:10.1016/j.jfo.2020.05.002
36. To CH, Kong CW, Chan CY, Shahidullah M, Do CW. The mechanism of aqueous humour formation. *Clinical and Experimental Optometry*. 2002;85(6):335-349. doi:10.1111/j.1444-0938.2002.tb02384.x
37. Wright C, Tawfik MA, Waisbourd M, Katz LJ. Primary angle-closure glaucoma: An update. *Acta Ophthalmologica*. 2016;94(3):217-225. doi: 10.1111/aos.12784
38. Pedrigi RM, Simon D, Reed A, Stamer WD, Overby DR. A model of giant vacuole dynamics in human Schlemm's canal endothelial cells. *Experimental Eye Research*. 2011;92(1):57-66. doi:10.1016/j.exer.2010.11.003
39. Shields MB. Normal-tension glaucoma: is it different from primary open-angle glaucoma? *Current Opinion in Ophthalmology*. 2008;19(2):85-88. doi:10.1097/ICU.0b013e3282f3919b
40. Aboobakar IF, Allingham RR. Genetics of Exfoliation Syndrome and Glaucoma. *International Ophthalmology Clinics*. 2014;54(4):43-56. doi: 10.1097/IIO.0000000000000042
41. Plateroti P, Plateroti AM, Abdolrahimzadeh S, Scuderi G. Pseudoexfoliation Syndrome and Pseudoexfoliation Glaucoma: A Review of the Literature with Updates on Surgical Management. *Journal of Ophthalmology*. 2015;2015:1-9. doi:10.1155/2015/370371
42. Küchle M, Iliff W, Green W. Kombinierte „Feuerlamelle" und Pseudoexfoliation der vorderen Linsenkapsel*. *Klinische Monatsblätter für Augenheilkunde*. 1996;208(02):127-129. doi:10.1055/s-2008-1035184
43. Scuderi G, Contestabile MT, Scuderi L, Librando A, Fenicia V, Rahimi S. Pigment dispersion syndrome and pigmentary glaucoma: a review and update. *International Ophthalmology*. 2019;39(7):1651-1662. doi: 10.1007/s10792-018-0938-7

44. Naylor A, Hopkins A, Hudson N, Campbell M. Tight Junctions of the Outer Blood Retina Barrier. *International Journal of Molecular Sciences*. 2019;21(1):211. doi:10.3390/ijms21010211
45. Michalinos A, Zogana S, Kotsiomitis E, Mazarakis A, Troupis T. Anatomy of the Ophthalmic Artery: A Review concerning Its Modern Surgical and Clinical Applications. *Anatomy Research International*. 2015;2015:1-8. doi:10.1155/2015/591961
46. Flammer J, Orgül S, Costa VP, et al. The impact of ocular blood flow in glaucoma. *Progress in Retinal and Eye Research*. 2002;21(4):359-393. doi:10.1016/S1350-9462(02)00008-3
47. Schneider M, Molnar A, Angeli O, et al. Prevalence of Cilioretinal Arteries: A systematic review and a prospective cross-sectional observational study. *Acta Ophthalmologica*. 2021;99(3):e310-e318. doi:10.1111/aos.14592
48. Pournaras CJ, Rungger-Brändle E, Riva CE, Hardarson SH, Stefansson E. Regulation of retinal blood flow in health and disease. *Progress in Retinal and Eye Research*. 2008;27(3):284-330. doi:10.1016/j.preteyeres.2008.02.002
49. Shiihara H, Terasaki H, Sonoda S, et al. Objective evaluation of size and shape of superficial foveal avascular zone in normal subjects by optical coherence tomography angiography. *Scientific Reports*. 2018;8(1). doi:10.1038/s41598-018-28530-7
50. Yang X, Yu XW, Zhang DD, Fan ZG. Blood-retinal barrier as a converging pivot in understanding the initiation and development of retinal diseases. *Chinese Medical Journal*. 2020;133(21):2586-2594. doi:10.1097/CM9.0000000000001015
51. García-Bermúdez MY, Freude KK, Mouhammad ZA, van Wijngaarden P, Martin KK, Kolko M. Glial Cells in Glaucoma: Friends, Foes, and Potential Therapeutic Targets. *Frontiers in Neurology*. 2021;12. doi:10.3389/fneur.2021.624983
52. Flammer J, Konieczka K, Flammer AJ. The primary vascular dysregulation syndrome: implications for eye diseases. *EPMA Journal*. 2013;4(1):14. doi:10.1186/1878-5085-4-14
53. Harris A. Regulation of Retinal and Optic Nerve Blood Flow. *Archives of Ophthalmology*. 1998;116(11):1491. doi:10.1001/archopht.116.11.1491
54. Leske MC. Ocular perfusion pressure and glaucoma: Clinical trial and epidemiologic findings. *Current Opinion in Ophthalmology*. 2009;20(2):73-78. doi:10.1097/ICU.0b013e32831eef82
55. Luo X, Shen YM, Jiang MN, Lou XF, Shen Y. Ocular Blood Flow Autoregulation Mechanisms and Methods. *Journal of Ophthalmology*. 2015;2015. doi:10.1155/2015/864871
56. Duffin J, Mikulis DJ, Fisher JA. Control of Cerebral Blood Flow by Blood Gases. *Frontiers in Physiology*. 2021;12. doi:10.3389/fphys.2021.640075
57. Chen K, Pittman RN, Popel AS. Nitric Oxide in the Vasculature: Where Does It Come From and Where Does It Go? A Quantitative Perspective. *Antioxidants & Redox Signaling*. 2008;10(7):1185-1198. doi:10.1089/ars.2007.1959
58. Denninger JW, Marletta MA. Guanylate cyclase and the ·NO/cGMP signaling pathway. *Biochimica et Biophysica Acta (BBA) - Bioenergetics*. 1999;1411(2-3):334-350. doi:10.1016/S0005-2728(99)00024-9

59. Meng L, Gelb AW. Regulation of Cerebral Autoregulation by Carbon Dioxide. *Anesthesiology*. 2015;122(1):196-205. doi:10.1097/ALN.0000000000000506
60. Bor-Seng-Shu E, Kita WS, Figueiredo EG, et al. Cerebral hemodynamics: concepts of clinical importance. *Arquivos de Neuro-Psiquiatria*. 2012;70(5):357-365. doi:10.1590/S0004-282X2012000500010
61. Horinouchi T, Terada K, Higashi T, Miwa S. Endothelin receptor signaling: New insight into its regulatory mechanisms. *Journal of Pharmacological Sciences*. 2013;123(2):85-101. doi:10.1254/jphs.13R02CR
62. Doucette LP, Walter MA. Prostaglandins in the eye: Function, expression, and roles in glaucoma. *Ophthalmic Genetics*. 2017;38(2):108-116. doi:10.3109/13816810.2016.1164193
63. Kowalczyk A, Kleniewska P, Kolodziejczyk M, Skibska B, Goraca A. The Role of Endothelin-1 and Endothelin Receptor Antagonists in Inflammatory Response and Sepsis. *Archivum Immunologiae et Therapiae Experimentalis*. 2015;63(1):41-52. doi:10.1007/s00005-014-0310-1
64. Davenport AP, Hyndman KA, Dhaun N, et al. Endothelin. *Pharmacological Reviews*. 2016;68(2):357-418. doi:10.1124/pr.115.011833
65. Haefliger IO, Flammer J, Luscher TF. *Nitric Oxide and Endothelin-1 Ore Important Regulators of Human Ophthalmic Artery*. Vol 33.; 1992.
66. Houde M, Desbiens L, D'Orléans-Juste P. Endothelin-1. In: *Advances in Pharmacology*. Vol 77. Academic Press Inc.; 2016:143-175. doi:10.1016/bs.apha.2016.05.002
67. Rubanyi GM, Polokoff MA. Endothelins: molecular biology, biochemistry, pharmacology, physiology, and pathophysiology. *Pharmacological Reviews*. 1994;46(3):325-415.
68. Fecteau MH, Honoré JC, Plante M, Labonté J, Rae GA, D'Orléans-Juste P. Endothelin-1 (1-31) is an intermediate in the production of endothelin-1 after big endothelin-1 administration in vivo. *Hypertension*. 2005;46(1):87-92. doi:10.1161/01.HYP.0000170460.24604.23
69. Mo R, Yang Y min, Yu L tian, Tan H qiong, Zhu J. Elevated Plasma Big Endothelin-1 at Admission Is Associated With Poor Short-Term Outcomes in Patients With Acute Decompensated Heart Failure. *Frontiers in Cardiovascular Medicine*. 2021;8. doi:10.3389/fcvm.2021.629268
70. Emre M, Orgül S, Haufschild T, Shaw SG, Flammer J. Increased plasma endothelin-1 levels in patients with progressive open angle glaucoma. *British Journal of Ophthalmology*. 2005;89(1):60-63. doi:10.1136/bjo.2004.046755
71. Cellini M, Strobbe E, Gizzi C, Balducci N, Toschi PG, Campos EC. Endothelin-1 plasma levels and vascular endothelial dysfunction in primary open angle glaucoma. In: *Life Sciences*. Vol 91; 2012:699-702. doi:10.1016/j.lfs.2012.02.013
72. Cioffi GA, Orgül S, Onda E, Bacon DR, Van Buskirk EM. An in vivo model of chronic optic nerve ischemia: The dose-dependent effects of endothelin-l on the optic nerve microvasculature. *Current Eye Research*. 1995;14(12):1147-1153. doi:10.3109/02713689508995821
73. Orgiil S, Doffi GA, Wilson DJ, Bacon DR, Michael E, Buskirk V. *An Endothelin-1 Induced Model of Optic Nerve Ischemia in the Rabbit*. Vol 37.; 1996.
74. McGrady NR, Minton AZ, Stankowska DL, He S, Jefferies HB, Krishnamoorthy RR. Upregulation of the endothelin A (ETA) receptor and its

association with neurodegeneration in a rodent model of glaucoma. *BMC Neuroscience*. 2017;18(1). doi:10.1186/s12868-017-0346-3
75. Henry E, Newby DE, Webb DJ, Hadoke PWF, O'Brien CJ. Altered Endothelin-1 Vasoreactivity in Patients with Untreated Normal-Pressure Glaucoma. *Investigative Opthalmology & Visual Science*. 2006;47(6):2528. doi:10.1167/iovs.05-0240
76. Lommatzsch C, Rothaus K, Koch JM, Heinz C, Grisanti S. Vessel density in oct angiography permits differentiation between normal and glaucomatous optic nerve heads. *International Journal of Ophthalmology*. 2018;11(5):835-843. doi:10.18240/ijo.2018.05.20
77. Lommatzsch C, Rothaus K, Koch JM, Heinz C, Grisanti S. OCTA vessel density changes in the macular zone in glaucomatous eyes. *Graefe's Archive for Clinical and Experimental Ophthalmology*. 2018;256(8):1499-1508. doi:10.1007/s00417-018-3965-1
78. Shoji T, Zangwill LM, Akagi T, et al. Progressive Macula Vessel Density Loss in Primary Open-Angle Glaucoma: A Longitudinal Study. *American Journal of Ophthalmology*. 2017;182:107-117. doi:10.1016/j.ajo.2017.07.011
79. Leske MC, Wu SY, Hennis A, Honkanen R, Nemesure B. Risk Factors for Incident Open-angle Glaucoma. The Barbados Eye Studies. *Ophthalmology*. 2008;115(1):85-93. doi:10.1016/j.ophtha.2007.03.017
80. Rangel-Castillo L, Gopinath S, Robertson CS. Management of Intracranial Hypertension. *Neurologic Clinics*. 2008;26(2):521-541. doi:10.1016/j.ncl.2008.02.003
81. Heijl A, Lindgren A, Lindgren G. Test-Retest Variability in Glaucomatous Visual Fields. *American Journal of Ophthalmology*. 1989;108(2):130-135. doi:10.1016/0002-9394(89)90006-8
82. Veena HN, Muruganandham A, Kumaran TS. A Review on the optic disc and optic cup segmentation and classification approaches over retinal fundus images for detection of glaucoma. *Discover Applied Sciences*. 2020;2(9):1476. doi:10.1007/s42452-020-03221-z
83. Harizman N. The ISNT Rule and Differentiation of Normal From Glaucomatous Eyes. *Archives of Ophthalmology*. 2006;124(11):1579. doi:10.1001/archopht.124.11.1579
84. Bechetoille A, Aouchiche M, Hartani D. L'Etude de Touggourt: Une Proposition Pour Le Depistage De Masse Des Glaucomes Chroniques Par L'Examen Du Disque Optique. *Journal Français d'Ophtalmologie*. 1980;3(8):495-500.
85. Hell SW, Weinreb RN, Bille Editor JF. *High Resolution Imaging in Microscopy and Ophthalmology*. (Bille JF, ed.). Springer International Publishing; 2019. doi:10.1007/978-3-030-16638-0
86. Everett M, Magazzeni S, Schmoll T, Kempe M. Optical coherence tomography: From technology to applications in ophthalmology. *Translational Biophotonics*. 2021;3(1). doi:10.1002/tbio.202000012
87. Yaqoob Z, Wu J, Yang C. Spectral domain optical coherence tomography: a better OCT imaging strategy. *Biotechniques*. 2005;39(6S):S6-S13. doi:10.2144/000112090
88. Kishi S. Impact of swept source optical coherence tomography on ophthalmology. *Taiwan Journal of Ophthalmology*. 2016;6(2):58-68. doi:10.1016/j.tjo.2015.09.002

89. de Carlo TE, Romano A, Waheed NK, Duker JS. A review of optical coherence tomography angiography (OCTA). *International Journal of Retina and Vitreous*. 2015;1(1):5. doi:10.1186/s40942-015-0005-8
90. Brusini P, Johnson CA. Staging Functional Damage in Glaucoma: Review of Different Classification Methods. *Survey of Ophthalmology*. 2007;52(2):156-179. doi:10.1016/j.survophthal.2006.12.008
91. Susanna Jr. R. Staging Glaucoma Patient: Why and How? *The Open Journal of Ophthalmology*. 2009;3(1):59-64. doi:10.2174/1874364100903010059
92. Valente C, D'Alessandro E, Iester M. Classification and Statistical Trend Analysis in Detecting Glaucomatous Visual Field Progression. *Journal of Ophthalmology*. 2019;2019. doi:10.1155/2019/1583260
93. Brusini P. Clinical use of a New Method for Visual Field Damage Classification in Glaucoma. *European Journal of Ophthalmology*. 1996;6(4):402-407. doi:10.1177/112067219600600411
94. Brusini P, Filacorda S. Enhanced Glaucoma Staging System (GSS 2) for Classifying Functional Damage in Glaucoma. *Journal of Glaucoma*. 2006;15(1):40-46. doi:10.1097/01.ijg.0000195932.48288.97
95. Brusini P. OCT Glaucoma Staging System: A new method for retinal nerve fiber layer damage classification using spectral-domain OCT. *Eye*. 2018;32(1):113-119. doi:10.1038/eye.2017.159
96. Gandolfi SA, Cimino L. Beta-Adrenergic Antagonists in the Treatment of Glaucoma. *European Journal of Ophthalmology*. 2001;11(2_suppl):63-66. doi:10.1177/112067210101102S08
97. Arthur S, Cantor LB. Update on the role of alpha-agonists in glaucoma management. *Experimental Eye Research*. 2011;93(3):271-283. doi:10.1016/j.exer.2011.04.002
98. Shahidullah M, To CH, Pelis RM, Delamere NA. Studies on bicarbonate transporters and carbonic anhydrase in porcine nonpigmented ciliary epithelium. *Investigative Ophthalmology & Visual Science*. 2009;50(4):1791-1800. doi:10.1167/iovs.08-2487
99. Tanna AP, Johnson M. Rho Kinase Inhibitors as a Novel Treatment for Glaucoma and Ocular Hypertension. *Ophthalmology*. 2018;125(11):1741-1756. doi:10.1016/j.ophtha.2018.04.040
100. Riva I, Brusini P, Oddone F, Michelessi M, Weinreb RN, Quaranta L. Canaloplasty in the Treatment of Open-Angle Glaucoma: A Review of Patient Selection and Outcomes. *Advances in Therapy*. 2019;36(1):31-43. doi:10.1007/s12325-018-0842-6
101. Shalaby WS, Jia J, Katz LJ, Lee D. iStent inject: comprehensive review. *J Journal of Cataract & Refractive Surgery*. 2021;47(3):385-399. doi:10.1097/j.jcrs.0000000000000325
102. Optovue®. *Avanti® Widefield OCT with AngioVue®OCT Angiography Brochure*.; 2017.
103. Ashraf M, Sampani K, Abu-Qamar O, et al. Optical coherence tomography angiography projection artifact removal: Impact on capillary density and interaction with diabetic retinopathy severity. *Translational Vision Science & Technology*. 2020;9(7):1-13. doi:10.1167/tvst.9.7.10
104. Juncal VR, Abadeh A, Koushan K, Berger AR, Chow DR. Does Projection Artifact Removal Improve Visualization of Images in Optical Coherence

Tomography Angiography? *Journal of VitreoRetinal Diseases*. 2019;3(5):289-296. doi:10.1177/2474126419867631
105. Czakó C, István L, Ecsedy M, et al. The effect of image quality on the reliability of OCT angiography measurements in patients with diabetes. *International Journal of Retina and Vitreous*. 2019;5(1). doi:10.1186/s40942-019-0197-4
106. Mase T, Ishibazawa A, Nagaoka T, Yokota H, Yoshida A. Radial peripapillary capillary network visualized using wide-field montage optical coherence tomography angiography. *Investigative Ophthalmology & Visual Science*. 2016;57(9):504-510. doi:10.1167/iovs.15-18877
107. Aydin S. A short history, principles, and types of ELISA, and our laboratory experience with peptide/protein analyses using ELISA. *Peptides*. 2015;72:4-15. doi:10.1016/j.peptides.2015.04.012
108. Tighe PJ, Ryder RR, Todd I, Fairclough LC. ELISA in the multiplex era: Potentials and pitfalls. *Proteomics - Clinical Applications*. 2015;9(3-4):406-422. doi:10.1002/prca.201400130
109. Bradford M. A Rapid and Sensitive Method for the Quantitation of Microgram Quantities of Protein Utilizing the Principle of Protein-Dye Binding. *Analytical Biochemistry*. 1976;72(1-2):248-254. doi:10.1006/abio.1976.9999
110. Green SB. How Many Subjects Does It Take To Do A Regression Analysis. *Multivariate Behavioral Research*. 1991;26(3):499-510. doi:10.1207/s15327906mbr2603_7
111. Hemmerich W. StatistikGuru: Poweranalyse und Stichprobenberechnung für Regression. StatistikGuru. Published September 23, 2022. Accessed September 23, 2022. https://statistikguru.de/rechner/poweranalyse-regression.html
112. Heijl A. Reduction of Intraocular Pressure and Glaucoma Progression. *Archives of Ophthalmology*. 2002;120(10):1268. doi:10.1001/archopht.120.10.1268
113. European Glaucoma Society. European Glaucoma Society Terminology and Guidelines for Glaucoma, 5th Edition. *British Journal of Ophthalmology*. 2021;105(Suppl 1):1-169. doi:10.1136/bjophthalmol-2021-egsguidelines
114. Dong ZM, Wollstein G, Schuman JS. Clinical utility of optical coherence tomography in glaucoma. *Investigative Ophthalmology & Visual Science*. 2016;57(9Special Issue):OCT556-OCT567. doi:10.1167/iovs.16-19933
115. Mwanza JC, Kim HY, Budenz DL, et al. Residual and dynamic range of retinal nerve fiber layer thickness in glaucoma: Comparison of three OCT platforms. *Investigative Ophthalmology & Visual Science*. 2015;56(11):6344-6351. doi:10.1167/iovs.15-17248
116. Yarmohammadi A, Zangwill LM, Diniz-Filho A, et al. Optical coherence tomography angiography vessel density in healthy, glaucoma suspect, and glaucoma eyes. *Investigative Ophthalmology & Visual Science*. 2016;57(9):OCT451-OCT459. doi:10.1167/iovs.15-18944
117. Aghsaei Fard M, Ritch R. Optical coherence tomography angiography in glaucoma. *Annals of Translational Medicine*. 2020;8(18):1204-1204. doi:10.21037/atm-20-2828
118. Li Z, Xu Z, Liu Q, Chen X, Li L. Comparisons of retinal vessel density and glaucomatous parameters in optical coherence tomography angiography. *PLoS One*. 2020;15(6). doi:10.1371/journal.pone.0234816

119. Ghahari E, Bowd C, Zangwill LM, et al. Association of Macular and Circumpapillary Microvasculature with Visual Field Sensitivity in Advanced Glaucoma. *American Journal of Ophthalmology*. 2019;204:51-61. doi:10.1016/j.ajo.2019.03.004
120. Hohberger B, Lucio M, Schlick S, Wollborn A, Hosari S, Mardin C. OCT-angiography: Regional reduced macula microcirculation in ocular hypertensive and pre-perimetric glaucoma patients. *PLoS One*. 2021;16(2 February). doi:10.1371/journal.pone.0246469
121. Holló G. Vessel Density Calculated from OCT Angiography in 3 Peripapillary Sectors in Normal, Ocular Hypertensive, and Glaucoma Eyes. *European Journal of Ophthalmology*. 2016;26(3):e42-e45. doi:10.5301/ejo.5000717
122. Kiyota N, Shiga Y, Omodaka K, Pak K, Nakazawa T. Time-Course Changes in Optic Nerve Head Blood Flow and Retinal Nerve Fiber Layer Thickness in Eyes with Open-angle Glaucoma. *Ophthalmology*. 2021;128(5):663-671. doi:10.1016/j.ophtha.2020.10.010
123. Kiyota N, Shiga Y, Yasuda M, et al. Sectoral differences in the association of optic nerve head blood flow and glaucomatous visual field defect severity and progression. *Investigative Ophthalmology & Visual Science*. 2019;60(7):2650-2658. doi:10.1167/iovs.19-27230
124. Chen CL, Bojikian KD, Wen JC, et al. Peripapillary retinal nerve fiber layer vascular microcirculation in eyes with glaucoma and single-hemifield visual field loss. *JAMA Ophthalmology*. 2017;135(5):461-468. doi:10.1001/jamaophthalmol.2017.0261
125. Chen HSL, Liu CH, Wu WC, Tseng HJ, Lee YS. Optical coherence tomography angiography of the superficial microvasculature in the macular and peripapillary areas in glaucomatous and healthy eyes. *Investigative Ophthalmology & Visual Science*. 2017;58(9):3637-3645. doi:10.1167/iovs.17-21846
126. Rao HL, Pradhan ZS, Weinreb RN, et al. A comparison of the diagnostic ability of vessel density and structural measurements of optical coherence tomography in primary open angle glaucoma. *PLoS One*. 2017;12(3). doi:10.1371/journal.pone.0173930
127. Rao HL, Pradhan ZS, Weinreb RN, et al. Vessel Density and Structural Measurements of Optical Coherence Tomography in Primary Angle Closure and Primary Angle Closure Glaucoma. *American Journal of Ophthalmology*. 2017;177:106-115. doi:10.1016/j.ajo.2017.02.020
128. Pradhan ZS, Dixit S, Sreenivasaiah S, et al. A Sectoral Analysis of Vessel Density Measurements in Perimetrically Intact Regions of Glaucomatous Eyes: An Optical Coherence Tomography Angiography Study. *Journal of Glaucoma*. 2018;27(6):525-531. doi:10.1097/IJG.0000000000000950
129. Moghimi S, Bowd C, Zangwill LM, et al. Measurement Floors and Dynamic Ranges of OCT and OCT Angiography in Glaucoma. *Ophthalmology*. 2019;126(7):980-988. doi:10.1016/j.ophtha.2019.03.003
130. Mossa EAM, Khallaf H, Sayed KM. Agreement between the newly developed OCT glaucoma staging system and the standardized visual field glaucoma staging system 2. *European Journal of Ophthalmology*. 2022;32(2):1009-1015. doi:10.1177/11206721211014378
131. Andrade De Jesus D, Sánchez Brea L, Barbosa Breda J, et al. OCTA multilayer and multisector peripapillary microvascular modeling for diagnosing

and staging of glaucoma. *Translational Vision Science & Technology*. 2020;9(2):1-22. doi:10.1167/tvst.9.2.58
132. Gugleta K. Significance of Endothelin-1 in Glaucoma - A Short Overview. *Klinische Monatsblätter für Augenheilkunde*. 2018;235(2):140-145. doi:10.1055/s-0043-124084
133. Yorio T, Krishnamoorthy R, Prasanna G. Endothelin: Is It a Contributor to Glaucoma Pathophysiology? *Journal of Glaucoma*. 2002;11(3):259-270. doi:10.1097/00061198-200206000-00016
134. Cellini M, Strobbe E, Gizzi C, Campos EC. ET-1 plasma levels and ocular blood flow in retinitis pigmentosa. *Canadian Journal of Physiology and Pharmacology*. 2010;88(6):630-635. doi:10.1139/Y10-036
135. Prasanna G, Krishnamoorthy R, Yorio T. Endothelin, astrocytes and glaucoma. *Experimental Eye Research*. 2011;93(2):170-177. doi:10.1016/j.exer.2010.09.006
136. Polak K, Petternel V, Luksch A, et al. *Effect of Endothelin and BQ123 on Ocular Blood Flow Parameters in Healthy Subjects*. Vol 42.; 2001.
137. Polak K, Luksch A, Frank B, Jandrasits K, Polska E, Schmetterer L. Regulation of human retinal blood flow by endothelin-1. *Experimental Eye Research*. 2003;76(5):633-640. doi:10.1016/S0014-4835(02)00312-3
138. Schmetterer L, Findl O, Strenn K, et al. Effects of endothelin-1 (ET-1) on ocular hemodynamics. *Current Eye Research*. 1997;16(7):687-692. doi:10.1076/ceyr.16.7.687.5065
139. Li S, Zhang A, Cao W, Sun X. Elevated Plasma Endothelin-1 Levels in Normal Tension Glaucoma and Primary Open-Angle Glaucoma: A Meta-Analysis. *Journal of Ophthalmology*. 2016;2016. doi:10.1155/2016/2678017
140. Ling L, Maguire JJ, Davenport AP. Endothelin-2, the forgotten isoform: emerging role in the cardiovascular system, ovarian development, immunology and cancer. *British Journal of Pharmacology*. 2013;168(2):283-295. doi:10.1111/j.1476-5381.2011.01786.x
141. Choritz L, Machert M, Thieme H. Correlation of endothelin-1 concentration in aqueous humor with intraocular pressure in primary open angle and pseudoexfoliation glaucoma. *Investigative Ophthalmology & Visual Science*. 2012;53(11):7336-7342. doi:10.1167/iovs.12-10216
142. Choritz L, Mahmoodi B, Thieme H. Influence of endothelin-1 in aqueous humor on intermediate-term trabeculectomy outcomes. *Journal of Ophthalmology*. 2016;2016. doi:10.1155/2016/2401976
143. Prasanna G, Dibas A, Hulet C, Yorio T. Inhibition of Na(+)/K(+)-atpase by endothelin-1 in human nonpigmented ciliary epithelial cells. *Journal of Pharmacology and Experimental Therapeutics*. 2001;296(3):966-971. http://www.ncbi.nlm.nih.gov/pubmed/11181930
144. Taniguchi T, Okada K, Haque MSR, Sugiyama K, Kitazawa Y. Effects of endothelin-1 on intraocular pressure and aqueous humor dynamics in the rabbit eye. *Current Eye Research*. 1994;13(6):461-464. doi:10.3109/02713689408999874
145. Sasaoka M, Taniguchi T, Shimazawa M, Ishida N, Shimazaki A, Hara H. Intravitreal injection of endothelin-1 caused optic nerve damage following to ocular hypoperfusion in rabbits. *Experimental Eye Research*. 2006;83(3):629-637. doi:10.1016/j.exer.2006.03.007

146. Fuchsjäger-Mayrl G, Wally B, Rainer G, et al. Effect of dorzolamide and timolol on ocular blood flow in patients with primary open angle glaucoma and ocular hypertension. *British Journal of Ophthalmology*. 2005;89(10):1293-1297. doi:10.1136/bjo.2005.067637
147. Pillunat LE, Böhm AG, Köller AU, Schmidt KG, Klemm M, Richard G. Effect of topical dorzolamide on optic nerve head blood flow. *Graefe's Archive for Clinical and Experimental Ophthalmology*. 1999;237(6):495-500. doi:10.1007/s004170050268
148. Yoon J, Lee A, Song WK, Kim KE, Kook MS. Association of superficial macular vessel density with visual field progression in open-angle glaucoma with central visual field damage. *Scientific Reports*. 2023;13(1). doi:10.1038/s41598-023-34000-6
149. Takusagawa HL, Liu L, Ma KN, et al. Projection-Resolved Optical Coherence Tomography Angiography of Macular Retinal Circulation in Glaucoma. In: *Ophthalmology*. Vol 124. Elsevier Inc.; 2017:1589-1599. doi:10.1016/j.ophtha.2017.06.002
150. Käsdorf BT, Arends F, Lieleg O. Diffusion Regulation in the Vitreous Humor. *Biophysical Journal*. 2015;109(10):2171-2181. doi:10.1016/j.bpj.2015.10.002
151. Samaha D, Diaconu V, Bouchard JF, Desalliers C, Dupont A. Effect of Latanoprostene Bunod on Optic Nerve Head Blood Flow. *Optometry and Vision Science*. Published online December 9, 2021. doi:10.1097/OPX.0000000000001842
152. Kostov K, Blazhev A. Circulating levels of endothelin-1 and big endothelin-1 in patients with essential hypertension. *Pathophysiology*. 2021;28(4):489-495. doi:10.3390/pathophysiology28040031
153. Briyal S, Philip T, Gulati A. Endothelin-a receptor antagonists prevent amyloid-β-induced increase in ETA receptor expression, oxidative stress, and cognitive impairment. *Journal of Alzheimer's Disease*. 2011;23(3):491-503. doi:10.3233/JAD-2010-101245
154. Narayan S, Prasanna G, Krishnamoorthy RR, Zhang X, Yorio T. Endothelin-1 Synthesis and Secretion in Human Retinal Pigment Epithelial Cells (ARPE-19): Differential Regulation by Cholinergics and TNF-α. *Investigative Ophthalmology & Visual Sciencei*. 2003;44(11):4885-4894. doi:10.1167/iovs.03-0387
155. Flammer J, Konieczka K. The discovery of the Flammer syndrome: A historical and personal perspective. *EPMA Journal*. 2017;8(2):75-97. doi:10.1007/s13167-017-0090-x
156. Liu W, Guo R, Huang D, et al. Co-occurrence of chronic kidney disease and glaucoma: Epidemiology and etiological mechanisms. *Survey of Ophthalmology*. 2023;68(1):1-16. doi:10.1016/j.survophthal.2022.09.001
157. Howell GR, Macalinao DG, Sousa GL, et al. Molecular clustering identifies complement and endothelin induction as early events in a mouse model of glaucoma. *Journal of Clinical Investigation*. 2011;121(4):1429-1444. doi:10.1172/JCI44646
158. Gabbay E, Fraser J, McNeil K. Review of bosentan in the management of pulmonary arterial hypertension. *Vascular Health and Risk Management*. 2007;3(6):887-900. http://www.ncbi.nlm.nih.gov/pubmed/18200808

159. Rosenthal R, Fromm M. Endothelin antagonism as an active principle for glaucoma therapy. *British Journal of Pharmacology*. 2011;162(4):806-816. doi:10.1111/j.1476-5381.2010.01103.x
160. Hirata Y, Itoh K, Ando K, Endo M, Marumo F. Plasma endothelin levels during surgery. *The New England Journal of Medicine*. 1989;321(24):1686. doi:10.1056/NEJM198912143212420

7. Appendices

Contributing authors (in alphabetical order)

- Dr. rer. nat. Dirk **Bauer**
  Department of Ophthalmology and Ophtha Lab at St. Franziskus Hospital, Münster, Germany
- Maria **Feldmann**
  Department of Ophthalmology, Klinikum Braunschweig, Braunschweig, Germany
- Prof. Dr. med. Swaantje **Grisanti**
  Department of Ophthalmology, University of Lübeck, Lübeck, Germany
- Prof. Dr. med. Carsten **Heinz**
  Department of Ophthalmology and Ophtha Lab at St. Franziskus Hospital, Münster, Germany and Department of Ophthalmology, University of Essen, Essen, Germany
- Dr. rer. nat. Maren **Kasper**
  Department of Ophthalmology and Ophtha Lab at St. Franziskus Hospital, Münster, Germany
- Prof. Dr. med. Harald **Langer**
  Medical Clinic II –Cardiology, Angiology, Intensive Care Medicine, University of Lübeck, Lübeck, Germany
- PD Dr. med. Claudia **Lommatzsch**
  Department of Ophthalmology and Ophtha Lab at St. Franziskus Hospital, Münster, Germany and Department of Ophthalmology, University of Lübeck, Lübeck, Germany
- Kai **Rothaus**
  Department of Ophthalmology and Ophtha Lab at St. Franziskus Hospital, Münster, Germany

Funding

The study was supported by Novartis Pharma GmbH. The funders had no role in study design, data collection and analysis, or preparation of the manuscript.

Ethics committee approval

The study was approved by the ethics committee of the Medical Association of Westfalen-Lippe, Germany (reference number 2018-331-f-S).

Publications of the author

Important results of the dissertation have been previously published:

- C. Lommatzsch[1], K. Rothaus[1], **L. Schopmeyer**[2], M. Feldmann, D. Bauer, S. Grisanti, C. Heinz, M. Kasper. Elevated endothelin-1 levels as risk factor for an impaired ONH ocular blood flow measured by OCT-A in glaucoma. *Scientific Reports* 2022; 12:11801. *Doi: 10.1038/s41598-022-15401-5*

Other publications of the author:

- **L. Schopmeyer**, P.B. Sindhunata, I. Drogt- Bilaseschi, D. D. Lubbers. Fatal postoperative intracranial hypotension-associated venous congestion after elective laminectomy – Case Report. *Anaesthesia Reports* 2021; 9:44-47. *Doi:10.1002/anr3.12103*

- E. E. Quint, **L. Schopmeyer**, L. B. D. Banning, C. Moers, M. El-Moumni, G. J. Nieuwenhuijs-Moeke, S. P. Berger, S. J. L. Bakker, R. A. Pol. Transitions in frailty state after kidney transplantation. *Langenbeck's Archives of Surgery* 2020; 405:843–850. *Doi: 10.1007/s00423-020-01936-6*

- **L. Schopmeyer**, M. El-Moumni, G. J. Nieuwenhuijs-Moeke, S. P. Berger, S. J. L. Bakker, R. A. Pol. Frailty has a significant influence on postoperative complications after kidney transplantation - a prospective study on short-term outcomes. *Transplant International* 2019; 32:66–74. *Doi: 10.1111/tri.13330*

Ongoing studies:

- **L. Schopmeyer**, T. G. Cherpanath, M. J. Schultz et al. PRoVENT-Donor (PRactice of VENTilation in Organ Donors) - *ongoing study – Intensive Care Department, Academic Medical Center Amsterdam*

- **L. Schopmeyer**, C. Tigchelaar, A.R. Absalom et al. Levels of CSF kynurenic acid and CSF noradrenaline have significant influence on sensory block level in spinal anaesthesia - The Biobank of Cerebrospinal Fluid - *ongoing study – Anesthesiology Department, University Medical Center Groningen*

8. Acknowledgements

PD Dr. med. Claudia Lommatzsch, I want to express my sincere gratitude for your unwavering support, insightful supervision, and invaluable guidance throughout the course of this project over the years. Your expertise and experience have played a pivotal role in my academic growth and have expanded my medical horizons. While this dissertation ignited my enthusiasm for ophthalmology and the rapidly advancing fields of glaucoma and OCT-A research, I eventually discovered my true passion in a different realm of medicine. Nevertheless, the knowledge and inspiration gained under your mentorship have been instrumental in shaping my professional journey. Thank you for your enduring impact.

Dr. rer. nat. Maren Kasper, I would like to thank you for your supervision and expertise in the Ophtha Lab and for teaching essential techniques like the ELISA and multiplex immunoassays in the Ophtha Lab. Your profound scientific experience as well as your long-term passion for the glaucoma research lines were a valuable contribution to this dissertation.

Kai Rothaus, your statistical and mathematical skills were essential for the complex statistical analyses of this dissertation and their verification. Thank you for your supervision and advice.

Prof. Dr. med. Harald Langer, I would like to thank for the co-supervision of this dissertation.

I thank Dr. med. Jörg Koch, Dr. med. Suphi Taneri, and Prof. Dr. med. Arnd Heiligenhaus and Prof. Dr. med. Carsten Heinz for supporting the patient recruitment process.

I would like thank Dr. med. Paolo Brusini for his kind invitation to use the OCT staging tool in the current study.

Thanks to Novartis Pharma GmbH for supporting this research.

A special thanks to my parents Kati and Stefan for their support during my medical studies, research period and thereafter, you made everything possible.

Puck, dank voor jouw support en geduld tijdens al mijn onderzoeksdagen en voor alles wat wij gedurende de afgelopen bijna 8 jaar samen hebben mogen beleven.

Dr. med. JP en Dr. med. Michiel, gezien onze traditie moet ik de Marcus' Angels hier ook nog even noemen. Het is prachtig dat wij drieën op onze eigen manier de promoties hebben afgerond. Dank voor alle mooie momenten gedurende de afgelopen jaren.